Exploring the Function of a Novel Chronic Pain Player

Dissertation

for the award of the degree

“Doctor rerum naturalium”

of the Georg-August-University Göttingen

within the doctoral program *Sensory and Motor Neuroscience* of the Göttingen Graduate School for Neurosciences, Biophysics, and Molecular Biosciences (GGNB)

of the Georg-August-University School of Science (GAUSS)

submitted by

Meike Hütte

from Holzminden, Germany

Göttingen, 2019

Thesis Committee

Prof. Dr. Manuela Schmidt	Somatosensory Signaling and Systems Biology Group, Max Planck Institute of Experimental Medicine, Göttingen
Prof. Dr. Tobias Moser	Institute of Auditory Neuroscience and InnerEarLab, University Medical Center, Göttingen
Prof. Dr. Ralf Heinrich	Department of Cellular Neurobiology, Schwann-Schleiden Research Center, Göttingen

Members of the Examination Board

Referee: Prof. Dr. Manuela Schmidt	Somatosensory Signaling and Systems Biology Group, Max Planck Institute of Experimental Medicine, Göttingen
2nd Referee: Prof. Dr. Tobias Moser	Institute of Auditory Neuroscience and InnerEarLab, University Medical Center, Göttingen

Further Members of the Examination Board

Prof. Dr. Ralf Heinrich	Department of Cellular Neurobiology, Schwann-Schleiden Research Center, Göttingen
Prof. Dr. Dr. Hannelore Ehrenreich	Department of Clinical Neurosciences, Max Planck Institute of Experimental Medicine, Göttingen
Prof. Dr. Thomas Dresbach	Institute of Anatomy and Embryology, Synaptogenesis Group, University Medical Center, Göttingen
Prof. Dr. Tiago F. Outeiro	Department of Experimental Neurodegeneration, University Medical Center, Göttingen

Date of oral examination: June 13th, 2019

AFFIDAVIT

I hereby declare that my doctoral thesis entitled “Exploring the Function of a Novel Chronic Pain Player” has been written independently with no other sources and aids than quoted.

Meike Hütte

Göttingen, April 2019

Nichts gelingt gut, außer man vollbringt es mit Freude. *Thomas von Aquin*

Für all meine Lieben, besonders aber meine Eltern

CONTENTS

ACKNOWLEDGEMENTS ..... **I**

ABSTRACT ..... **IV**

LIST OF FIGURES ..... **V**

LIST OF TABLES ..... **VI**

1. INTRODUCTION **1**

1.1 Somatosensation and Pain **1**
1.2 The Molecular Basis for Nociception **3**
1.3 Pathophysiological Pain **4**
1.3.1 Inflammatory Pain 4
1.3.2 Neuropathic Pain 5
1.3 Mitochondrial Dysfunction in Chronic Pain **11**
1.4 Inadequate Pain Medication **13**
1.5 Aim of the Study **15**

2. MATERIALS AND METHODS **16**

2.1 Materials **16**
2.2 Mouse Models **23**
2.2.1 Animal Care and Conditions 23
2.2.2 Generation of Knock Out (KO) Mice 23
2.2.3 Validation of KO Mice 28
2.3 Murine Pain Models **33**
2.3.1 Inflammatory Pain Model: CFA 33
2.3.2 Neuropathic Pain Model: SNI 33
2.4 Phenotyping of Mice **34**
2.4.1 Assessment of Motor Performance 34
2.4.2 Evoked Pain Paradigms 34
2.4.3 Non-Evoked Pain Paradigms 35
2.4.4 Acute Pain Behavior 36
2.5 Cell Culture **36**
2.5.1 DRG Culture and Nucleofection 36
2.5.2 Schwann Cell (SC) Culture and Nucleofection 37
2.5.3 SC DRG Co-Culture 38
2.5.4 HEK293T Cell Culture and Transfection 39
2.6 Histology **39**
2.6.1 Cryo-Embedding 39
2.6.2 Paraffin-Embedding 39
2.6.3 Deparaffinization and Rehydration of Paraffin Sections 40
2.7 Fluorescence Staining **40**
2.7.1 Immunocytochemistry (ICC) 40
2.7.2 Immunohistochemistry (IHC) 40
2.7.3 Image Acquisition: ICC & IHC 43

2.7.4 Image Analysis: IHC 43
2.8 Live Imaging 43
2.8.1 Mitosox Imaging 43
2.8.2 TMRM Imaging 43
2.9 Ca^{2+}-Imaging 44
2.9.1 Ca^{2+}-Imaging upon TNFα Stimulation 44
3.0 Electrophysiology 45
3.1 Electron Microscopy (EM) 45
3.2 Molecular Cloning 47
3.3 Mitochondrial Assays 49
3.3.1 Enzyme Activity Dipstick (Complex IV) 49
3.3.2 Isolation of Mitochondria 49
3.3.3 Seahorse Respiration of Isolated Mitochondria 50
3.3.4 Blue Native PAGE of Electron Transport Chain Complexes 52
3.3.5 Activity Staining of Electron Transport Chain Complexes 52
3.4 Statistics 53

3. RESULTS 54

3.1 Functional Characterization of TM in Regard to Somatosensation and Chronic Pain 54
3.1.1 Differential TM Expression during Chronic Pain 54
3.1.2 Localization of TM in Mitochondria 55
3.1.3 Successful Generation of TM KO Mice 57
3.1.4 No Myelination Deficit in Consequence of TM Removal 60
3.1.5 TM Deletion results in Pain Modality specific Analgesia 62
3.1.6 Study of Neuronal Expression/ Excitability after TM Elimination 70
3.1.7 Screen for Molecular Changes upon TM Deletion 76
3.1.8 Investigation of Mitochondrial Function Upon TM Deletion 79
3.1.9 Oxidative Stress Response Compared Between Genotypes 85
3.1.10 Altered Inflammatory Signaling Pathways in TM KO mice 87

4. DISCUSSION 92

4.1 Characterization of TM as Novel Pain Modality-specific Mitochondrial Protein 92
4.1.1 No overt Mitochondrial Dysfunction upon TM Deletion 93
4.1.2 The Need for an extended Pain Paradigm Portfolio 95
4.1.3 Decreased Neuronal Subpopulation Excitability after TM Elimination 96
4.1.4 Modulatory Role for TM in Inflammatory Pain Signaling 97
4.1.5 Conclusion and Outlook 100

5. BIBLIOGRAPHY 103

CURRICULUM VITAE 115

ACKNOWLEDGEMENTS

First and foremost, I would like to thank my dear supervisor, Prof. Dr. Manuela Schmidt. Thank you so much for giving me the opportunity to work in your lab! I am very grateful for this fantastic and exciting project I was allowed to work on. Your door was always open for discussions and future experimental planning. The structured way of teaching was the ideal basis for a fruitful and efficient way of working. I learned a lot about myself and also for life! Thank you so much!

David Gómez-Varela, Ph.D., you are one of the most intelligent people I know! Thank you so much for asking the "nasty" questions. You encouraged me to think more profoundly about my project.

Dear Prof. Dr. Tobias Moser, dear Prof. Dr. Ralf Heinrich, I would like to express my gratitude for being part of my thesis committee. Thank you for your valuable input throughout my PhD.

Furthermore, I want to thank Prof. Dr. Dr. Hannelore Ehrenreich, Prof. Dr. Thomas Dresbach and Prof. Dr. Tiago F. Outeiro for your participation in my extended thesis committee. Especially, I want to thank Hannelore. You gave me the chance to prepare my Bachelor's thesis in your lab, in addition to a subsequent position as a student and later on graduate assistant. I will never forget this first lab experience, where I recognized my passion for science.

Many thanks to the Göttingen Graduate School for Neurosciences, Biophysics, and Molecular Biosciences (GGNB) who financially supported my project for one year via a junior group stipend. You also generously provided several travel grants, which made it possible to present my work at diverse conferences allowing for excellent input from other scientists.

***

Thanks to my colleague Dr. Julia Sondermann, for teaching all the required methods and careful proofreading of my thesis. You are a very talented scientist.

Dr. Pratibha Narayanan, it is a pity that the research community lost you, because you are brilliant, hard working and always willing to help. However, your decision to teach children in your home country is fantastic and honorable.

Niklas Michel, we started our PhD together. It was nice not being the only new one ;-) You are one of the most helpful and social people I know. You are a committed and smart colleague, who stands up for his believes. I wish you all the best for your future.

Sergej Zeiter, you are a very skillful technician. Thanks a lot for all your help in daily lab procedures and your accurate way of working.

Tanja Nilsson, meine liebe Kollegin! Ich möchte mich auf diesem Wege ganz herzlich für deine tolle Unterstützung im Labor bedanken. Dein Einstieg in unsere AG war das Beste was mir passieren konnte! Du hast von Anfang an gute Laune und frischen Wind mitgebracht. Das hat mir und meinem Projekt sehr gut getan. Du denkst immer ein paar Schritte voraus und bist sehr hilfsbereit. Ich werde dich vermissen!

Christin Kappert, I liked you from day one you joined our lab. You are a strong woman who knows what she wants. No matter which topic, you always have a story to tell. I am glad I got to know you. I wish you all the best!

I also want to thank Hanna Kristina Fischer for all the help in favor of my project. It was fun having you around.

Thanks to all former lab members, Dr. Luca Avenali, Reham Abdelaziz, Elena Cirrdaeva and Allison M. Barry for creating such a nice and friendly atmosphere.

***

Dear Prof. Dr. Esther Pogatzki-Zahn and Dr. Daniel Segelcke, I am very grateful for your agreement in collaborating with us. It was very fruitful and productive from the beginning. Thank you so much! You are both outstanding and hard working personalities.

I would also like to thank additional collaboration partners, Prof. Dr. Peter Rehling, Dr. Sven Dennerlein and Dr. David Pacheu Grau. It was a pleasure working with you. You helped us so much in figuring out the underlying work mechanism of our protein of interest.

Dr. Katrin Willig and Dr. Joris van Dorth, thanks a lot for all the time you invested in our collaboration.

Dear Dr. Susanne Quintes, our Schwann cell expert, I want to express my gratitude for your agreement in collaborating with us. Thank you for sharing the required expertise in regard to the exciting glial cells of the PNS.

Dear Dr. Sarah Flatters, it was fantastic to meet you during the poster session at the world congress on pain in Boston. Thanks for your ideas, interest and the help you offered.

Liebe Annette Fahrenholz, ich möchte mich herzlich bei dir bedanken. All die Paraffin-Histoarbeit hast du mir ganz geduldig gezeigt und warst für jede Frage offen. Danke!

Vielen lieben Dank an alle Tierhausmitarbeiter für die Hilfsbereitschaft. Besonders bedanken möchte ich mich bei Frau Dr. Schraepler für die tolle Beratung und Unterstützung vor allem während der Allergiezeit.

Ein großer Dank gilt auch Dr. Ursula Fünfschilling, sowie Nicole Weber und dem AGCT-Team für die Generierung und Validierung unserer KO Linie.

***

Beate, aus einer Zwischenmiete ist Freundschaft geworden. Wie schön, dass wir uns kennengelernt haben.

Maddy, mein kleiner kreativer Chaot. Wir zwei waren von Tag eins im Studium unzertrennlich und vertraut. Du bist immer da und hast mich so manches Mal gerettet. Ich werde unsere schönen Kochabende und das nächtliche Lernen nie vergessen. Danke für alles, meine Liebe!

Meine liebe Freundin Melli, du gehörst zu den liebenswertesten Menschen die ich kenne. Ich bewundere dich für dein großes Herz, dein Einfühlvermögen und deine Zielstrebigkeit. Man kann alles schaffen, wenn man es wirklich will. Ich wünsche dir alles Glück der Welt!

Joi, meine Beste! Über ein halbes Leben kennen wir uns nun schon, ist das zu fassen?! Du kennst mich wohl so gut wie kaum ein anderer und verstehst mich daher auch so gut. Man kann sich auf dich voll und ganz verlassen und du bist immer zur Stelle wenn man dich braucht. 1000 Dank! Ich wünsche dir alles, alles Liebe!

Lisa, du bist die Vierte im Bunde. Nie werde ich unsere Mädelsabende vergessen in denen alle Neuigkeiten, Sorgen, Probleme und Freuden ausführlich durchgesprochen wurden. Halt die Stellung in Göttingen! Ich werde dich und deine erfrischend ehrliche Art sehr vermissen!

Leni, Rile, Lea, Kerstin, meine lieben Schulfreunde. Es ist unbezahlbar, wenn man auf eine fast 20-jährige bzw. sogar längere Freundschaft zurückblicken kann. Leider treffen wir uns viel zu selten und doch ist es so vertraut wie früher, wenn wir uns sehen. Eure Freundschaft möchte ich niemals missen.

Meine liebe Raulsi, das Leben ist nicht fair…
Du musstest schon ganz schön viel durchmachen und hast es mit viel Stärke ertragen und die Lebensfreude trotz allem nicht verloren. Wenn du in einen Raum kommst geht die Sonne auf. Ich bin sehr froh dich zu kennen!

***

Ganz besonders möchte ich meinen lieben Eltern, Regine und Burkhard danken. Worte sind nicht genug um auszudrücken, wie dankbar ich für eure Kraft und Unterstützung bin. Ihr habt mein Leben lang alles möglich gemacht und an mich geglaubt. Ihr werdet immer meine Heimat sein!

Lennart, mein lieber Schatz, manchmal ist eine Umarmung alles was man braucht. Danke, dass du immer an meiner Seite bist! Bis zum Mond und zurück…

Vielen Dank an meine lieben Großeltern, Oma Marga und Opa Rolf (†), sowie Oma Ursel und Opa Alfred (†)! Ihr habt mich mit großgezogen und euch um mich gekümmert. Besonderer Dank gilt meiner geliebten Oma Marga, was würde ich nur ohne dich machen!

Mein lieber Cousin Marci, du warst schon immer wie ein Bruder für mich! Danke für deine unendliche Hilfsbereitschaft und die Unterstützung zu Hause!

Melanie, Rolf und Lena, danke für euer Interesse und die aufmunternden Worte!

Herzlichen Dank an meine zweite Familie Karin, Andreas und Nils mit Elisabeth und Ulrich. Ihr habt mich von vornherein so liebevoll aufgenommen, dass ich mich nur wohlfühlen konnte.

ABSTRACT

As currently available chronic pain medication is associated with undesirable side effects and suboptimal efficacy, the improvement of treatment options is a major task in the pain research community. The basis for the latter is an advanced understanding of the molecular mechanisms underlying chronic pain states. The approach to target molecules that are specifically involved in the pathological form of pain is highly important in order to maintain an individual's ability to process acute nociceptive pain. Such a strategy ideally allows for novel drug target identification, and thereby decreased side effects and enhanced therapeutic outcomes. Here, an uncharacterized mitochondrial transmembrane protein (TM) was investigated with regard to its role in chronic inflammatory and neuropathic pain. In a previous quantitative proteomics study, TM and other mitochondrial proteins showed differential expression in two mouse models of chronic pain. This finding was in line with the growing evidence for the connection between mitochondrial dysfunction and diverse chronic pain conditions.

TM was characterized *in vivo* by generating knock out (KO) mice with the CRISPR/Cas9 technology. Effective gene ablation was confirmed by, genomic sequencing, quantitative RT-PCR and *in situ* hybridization. Neuropathic pain was induced by a spared nerve injury (SNI-model) and the intraplantar injection of CFA (Complete Freund's Adjuvant) that causes inflammatory pain. Sham operated/vehicle injected mice served as controls. Subsequently, a battery of behavioral paradigms including measures of stimulus-evoked and spontaneous pain was performed. Strikingly, a specific attenuation of mechanical hypersensitivity upon induction of inflammatory pain and in the initial stage of neuropathic pain (7 days post surgery, marked by pronounced inflammation) was shown in TM KO mice. However, later neuropathic pain phases were not affected. Moreover, other investigated pain modalities such as heat hypersensitivity, NEP and movement-evoked pain were unaltered in TM-deficient mice. Besides, several *in vitro* techniques were applied to study the molecular basis for the behavioral phenotype. They revealed altered mRNA levels of several prototypic inflammatory mediators and components implicated in mitochondrial function in dorsal root ganglia (DRG) and sciatic nerves (SN) of TM KO mice. Mitochondrial dysfunction and potential alteration of neuronal excitability could not be approved with the applied methods. However, decreased activation of a specific nociceptor subpopulation was shown in sensory neurons upon TM ablation, which could be rescued by application of the cytokine TNFα (downregulated mRNA level).

Further research is needed to understand the molecular mechanism underlying the specific alleviation of mechanical hypersensitivity during the early inflammatory stage of neuropathic pain and CFA-evoked inflammatory pain in TM KO mice. Yet, these results propose a novel and pivotal implication for TM in modality-specific pain signaling.

LIST OF FIGURES

Figure 1: *The Ascending Pain Pathway* *2*
Figure 2: *Immune and Glial Cell Reactions at Site of Nerve Injury* *8*
Figure 3: *Immune and Glial Cell Reactions in DRG & Spinal Cord upon Nerve Injury* *10*
Figure 4*: Dysfunctional Mitochondria & Chronic Pain* *13*
Figure 5*: TM Expression Levels during Inflammatory Pain* *54*
Figure 6: *Ubiquitous TM Expression in Mitochondria* *56*
Figure 7: *Successful Generation and Validation of TM Deletion in KO Mice* *59*
Figure 8: *No Hint for Myelination Deficit in TM KO Mice* *61*
Figure 9: *Pain-Modality Specific Phenotype after TM Deletion in Vivo* *66*
Figure 10: *Diminished Mechanical Hypersensitivity upon TM Elimination* *68*
Figure 11: *Capsaicin-evoked Acute Pain unchanged among Genotypes* *69*
Figure 12: *Sensory Neuron-specific TM KO sufficient to evoke impaired CFA-mediated Mechanical Hypersensitivity* *69*
Figure 13: *No Difference in Expression of Neuronal Populations in DRG of naive TM KO Mice* *71*
Figure 14: *Similar Neuronal Population Expression in DRG of CFA-treated TM KO Mice* *72*
Figure 15: *Electrophysiological Investigation revealed no Major Changes in Neuronal Excitability after TM Removal* *73*
Figure 16: *TM Deletion caused no Change in Neuronal Excitability as examined by Ratiometric Calcium Imaging* *75*
Figure 17: *Altered Mitochondrial and Inflammatory Gene Expression in TM KO Mice* *78*
Figure 18: *No Major Protein Abundance Change in ETC Subunits of TM KO Brain, Heart and Liver* *80*
Figure 19: *ETC Activity Staining revealed no definite Difference among Genotypes* *81*
Figure 20: *Similar Complex IV Activity in TM KO Mice* *81*
Figure 21: *Seahorse Experiments revealed unaltered Oxygen Consumption Rate in TM KO* *83*
Figure 22: *TM KO DRG exhibited a normal Mitochondrial Membrane Potential* *84*
Figure 23: *Slightly increased Mitosox Signal in DRG of TM KO Mice* *86*
Figure 24: *Unchanged 4-HNE Intensity in TM-deficient CFA-treated Mice* *87*
Figure 25: *Macrophage Staining in DRG of TM KO and WT Mice under Inflammatory Pain Conditions* *88*
Figure 26: *TNFα Stimulation compensated lower Amount of TRPA1 Responders in TM KO Neurons* *90*

LIST OF TABLES

Table 1: *Lists of Reagents and Kits* *16*
Table 2: *PCR Master Mix Genotyping* *28*
Table 3: *PCR Cycle Genotyping* *29*
Table 4: *List of Primers* *30*
Table 5: *Primary Antibodies* *41*
Table 6: *Secondary Antibodies* *42*
Table 7: *Tissue Fixation for EM* *46*
Table 8: *Epoxy Resin Embedding for EM* *46*
Table 9: *PCR Master Mix Cloning* *47*
Table 10: *PCR Cycle Cloning* *48*
Table 11: *Mitochondrial Assay Solution* *50*
Table 12: *Mitochondrial Assay Compounds* *50*
Table 13: *MAS Complex II* *51*
Table 14: *MAS Complex IV* *51*
Table 15: *Seahorse Program* *51*

1. INTRODUCTION

1.1 Somatosensation and Pain

The skin is the largest sensory organ in our body. It protects us and constitutes the basis for somatosensation, as it is innervated by peripheral axons of pseudo-unipolar primary sensory neurons. These neurons have their somata located within dorsal root ganglia (DRG, trunk and limb innervation; **Figure 1**), trigeminal ganglia (TG, cephalic innervation) or nodose and jugular ganglia (vagal innervation of viscera and head) (Kollarik et al., 2010). They communicate to the central nervous system (CNS) via central axons projecting to the spinal cord (for DRG neurons; **Figure 1**) or the trigeminal subnucleus caudalis (for TG neurons) (Basbaum et al., 2009; Dubin and Patapoutian, 2010). A high threshold subpopulation of primary sensory neurons, the so called nociceptors, are able to detect extreme thermal, mechanical and chemical signals (e.g. a hot object or an intense pinch). Hence, nociceptors are able to detect potentially damaging noxious stimuli and thereby fulfill their most important function, namely the guarding of our physical integrity (Woolf and Ma, 2007). This significance for nociceptive signaling is demonstrated by individuals suffering from the congenital insensitivity to pain (CIP) (Cox et al., 2006; Indo, 2001), which results in self-mutilation by repeated unnoticed injuries. However, if healthy individuals are harmed the healing process is accompanied by hypersensitivity of the affected tissue in order to promote guarding (e.g. sunburn). As a consequence usually innocuous stimuli as light touch elicit pain (allodynia) or painful stimuli are perceived more intensely (hyperalgesia).

Moreover, noxious stimuli detectors are divided into subclasses that mediate the “first” well-localized and the “second” poorly-localized pain. The former is conducted by thinly-myelinated Aδ fibers that possess a relatively slow conduction velocity (CV) of 12-30 m/s, a medium diameter of 2-5 µm and a cell body size of 30-40 µm. The latter is conveyed via unmyelinated slow conducting C afferents (CV 0.5–2 m/s) that have thin axons of 0.4-1.2 µm and small somata (< 25 µm). Light touch, i.e. innocuous mechanical stimulation, on the other hand, is rapidly transmitted (CV of 70-130 m/s) by myelinated large caliber (5-20 µm) Aβ sensory neurons (cell bodies > 40 µm) (**Figure 1**).

Furthermore, Aδ nociceptors project to the spinal dorsal horn lamina I as well as to lamina V, whereas C fibers synapse to second order neurons in the superficial laminae I and II. By contrast, low threshold Aβ afferents project to the deep laminae III, IV and V within the dorsal horn of the spinal cord. The spinal dorsal horn is an important hub of the pain axis as it connects the periphery to the brain. Inputs from peripheral nociceptors, local interneurons and descending projections are integrated and processed signals are transmitted to the brain pain network (Todd, 2010; **Figure 1**). (Basbaum et al., 2009; Bourinet et al., 2014; Costigan et al., 2009; Patapoutian et al., 2009).

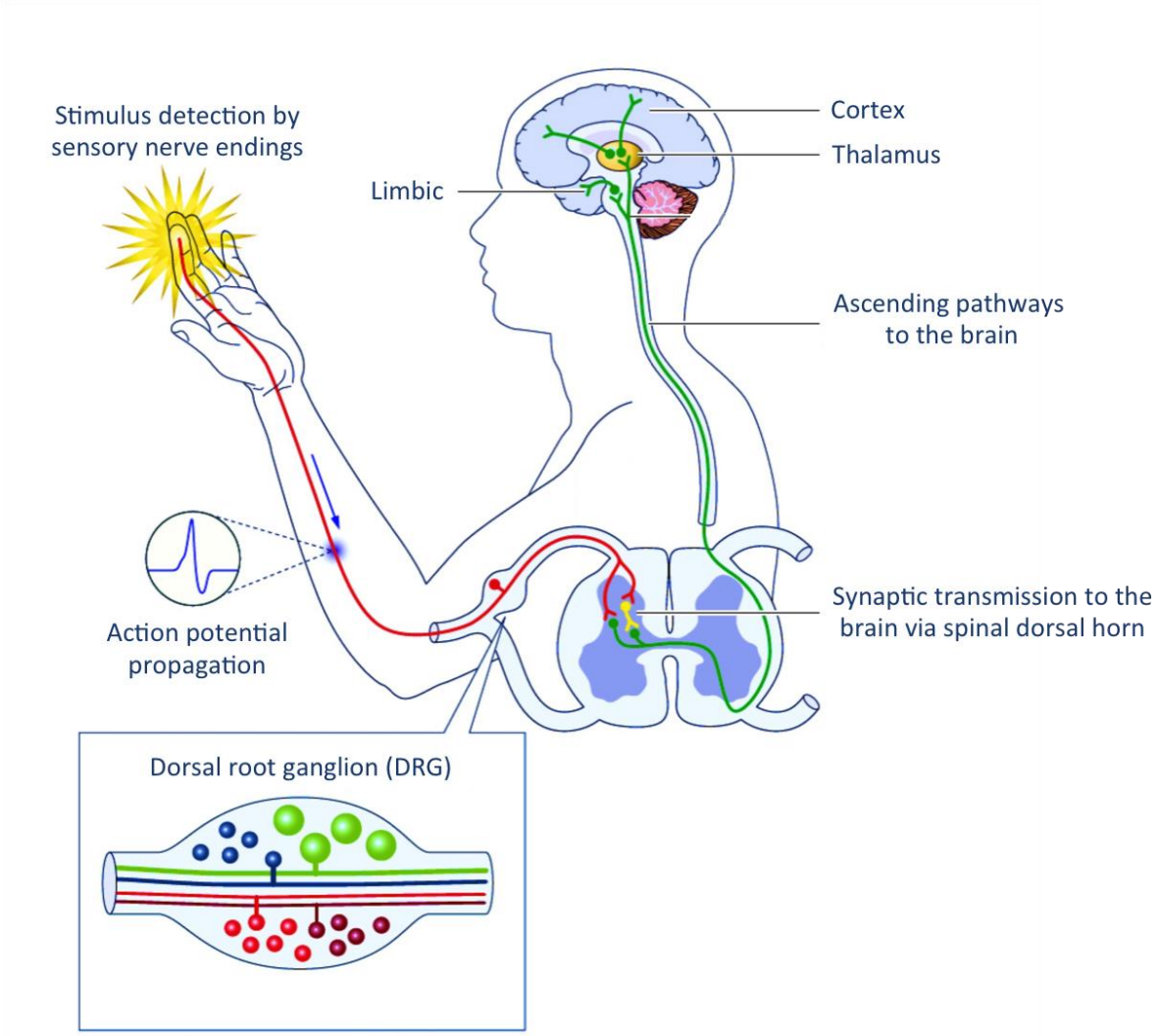

Figure 1: The Ascending Pain Pathway

Primary sensory neurons are composed of somata located in dorsal root ganglia (DRG), in addition to peripherally and centrally projecting axons. These neurons can be divided into several subtypes such as small non-myelinated C fibers and medium-sized slightly myelinated Aδ fibers that are primarily responsible for thermosensation and nociception. Large-diameter Aβ fibers mainly convey touch perception (neuronal subtypes are illustrated in the DRG magnification). Upon noxious stimulation of the sensory nerve ending the signal is propagated as an action potential along the peripheral axon that synapse to second order spinal dorsal horn neurons. In the dorsal horn the sensory information is integrated and sent to the thalamus and higher cortical brain structures where the sensation of pain is generated. Modified from (Bourinet et al., 2014).

1.2 The Molecular Basis for Nociception

The expression of specialized transducer ion channel receptors, mainly transient receptor potential (TRP) channels by high threshold primary sensory neurons constitutes the molecular basis for nociception. Channels like the transient receptor potential vanilloid receptor 1 (TRPV1) and transient receptor potential ankyrin 1 (TRPA1) are tuned to respond to polymodal stimuli and therefore allow nociceptors the reaction to excessive thermal, chemical or mechanical stimuli (Dhaka et al., 2006). Sodium and calcium influx through these channels transform stimuli into spreading membrane depolarizations, propagating action potentials to higher brain centers enabled via the spinal cord (Talavera et al., 2008). The involvement of TRP channels in thermosensation and pain was first suggested in 1997 by Caterina and colleagues. It was found that TRPV1 is activated by capsaicin (active ingredient of chilli peppers) as well as by noxious heat (> 43°C), spider toxins and is modulated by low pH (a common effect of inflammation) (Caterina et al., 1997; Siemens et al., 2006). It is expressed in specific subsets of C and Aδ nociceptors that produce burning pain when they are depolarized during channel activation (Caterina et al., 1997). On the other hand, TRPA1 is activated by environmental irritants and a number of pungent chemicals found in food like isothiocyanates (mustard, horseradish), allicin (garlic) and cinnamaldehyde (cinnamon), excluding capsaicin (Bandell et al., 2004; Bautista et al., 2005; Jordt et al., 2004; Macpherson et al., 2005, 2007; Story et al., 2003a). Furthermore, it is usually coexpressed with TRPV1 in unmyelinated C and slightly myelinated Aδ primary afferents (Nagata et al., 2005; Story et al., 2003a). (Basbaum et al., 2009; Bourinet et al., 2014; Costigan et al., 2009; Patapoutian et al., 2009).

1.3 Pathophysiological Pain

"Pain is a more terrible lord of mankind than even death itself" *(Albert Schweitzer, 1931)*. This statement refers to the all-consuming excruciating sensation of pain, which has lost its protective function. It is considered as major clinical problem and affects around 20 % of the population (Breivik et al., 2006, 2013; Steglitz et al., 2012). Other than acute, nociceptive pain, persistent pain states do not seem to fulfill a useful physiological function (Hehn et al., 2012). Pain and excessive reactions to noxious and innocuous stimuli are evoked by long-lasting alterations in the nociceptive circuitry caused by inflammation, tissue, and nerve injury (Basbaum et al., 2009; Hucho and Levine, 2007).

1.3.1 Inflammatory Pain

Acute inflammation is a protective response characterized by rubor (redness), calor (increased heat), tumor (swelling), dolor (pain), and function laesa (loss of function). Its function is the elimination of the primary cause of injury and the induction of tissue repair. (Ji et al., 2016). Other than acute inflammation, chronic inflammation is often detrimental, causing a number of diseases such as rheumatoid arthritis, periodontitis, atherosclerosis, and even cancer (Ji et al., 2014). Various rodent models of chronic inflammatory pain are used at the level of the skin (e.g. intraplantar injection of CFA or carrageenan), the gut (e.g. dextran-sodium sulfate (DSS)-induced colitis) or the knee joint (CFA monoarthritis model). All models share the characteristic of primary afferent neuron sensitization due to altered ion channel function (among other factors) which can be assessed as allodynia and hyperalgesia, respectively. (Bourinet et al., 2014). Given the tremendous importance of TRP channels in somatosensation, their differential expression is often associated with neuropathic and inflammatory pain (Salat et al., 2013). The essentiality of these channels in sensitization of the afferent pain pathway was confirmed by their regulation via pro inflammatory signaling molecules like chemokines, growth factors, serotonin, bradykinin, prostaglandins and proteases (for review Vay et al., 2012). Moreover, chronic pain syndromes can be caused and preserved in the periphery and/ or the CNS and are not only physiologically but also psychologically debilitating which might negatively affect recovery (Basbaum et al., 2009).

1.3.2 Neuropathic Pain

Neurotoxic chemicals, infection, tumor growth, diabetes or nerve trauma cause lesions to the peripheral nervous system (PNS) that result in peripheral neuropathic pain. A number of pathophysiological alteration within the PNS and CNS are involved in this process (Dworkin et al., 2003; Woolf and Mannion, 1999). Moreover, stroke, multiple sclerosis or spinal cord injury are the most common causes for central neuropathic pain (Ducreux et al., 2006). The neural damage and the primary disease it is caused from are the initiators of the essential neuropathic pain feature that is the manifestation of maladaptive plasticity in the nervous system (Costigan et al., 2009). These changes in the nerve properties often lead to increased spontaneous firing or alterations in their neurotransmitter properties or conduction (Basbaum et al., 2009). Spontaneous pain in the absence of an identifiable stimulus is a major characteristic of neuropathic pain which originates as a consequence of ectopic action potential formation within the nociceptive pathways. The ectopic activity seen in peripheral neuropathic pain arises in primary sensory neurons. Upon peripheral nerve injury, spontaneous activity is formed at various sites, including the site of tissue damage (neuroma), DRG soma (Amir et al., 2005) as well as adjacent unaffected afferents (Wu et al., 2002). The formation of spontaneous pain can be based on ectopic activity in low-threshold large myelinated afferents (Campbell et al., 1988) and from nociceptors (Bostock et al., 2005) caused by altered connectivity in the spinal cord and central sensitization (Woolf et al., 1992). The latter refers to the mechanism by which hyperexcitability within the CNS is established causing amplified processing of nociceptive signals that influences the affective and emotional facets of pain (Woolf, 1983; Woolf and Salter, 2000). Structures involved in the emotional aspects of pain are the anterior cingulate gyrus, amygdala, and prefrontal cortex, respectively (Fu et al., 2008; Pedersen et al., 2007). These might serve as basis for long-term mood and cognitive alterations that are learned and maintained (e.g. addictive and conditioned fear behavior) (Costigan et al., 2009).

Two processes among numerous others that are implicated in central sensitization are alteration in glutamatergic neurotransmission and disinhibition (loss of tonic inhibitory controls) (Basbaum et al., 2009). Nociceptive pain is signaled via glutamate release from central axons of nociceptors causing excitatory postsynaptic currents (EPSCs) in second order neurons within the dorsal horn. This is primarily caused by stimulation of postsynaptic subtypes (kainite and AMPA) of ionotropic glutamate receptors. Action potential generation and transmission of pain signals to higher order neurons will be ultimately caused by the summation of subthreshold EPSCs in the postsynaptic neuron. Under physiological conditions, the NMDA subtype of the glutamate channel is quiescent, whereas injury results in enhanced neurotransmitter release from nociceptors that will trigger silent NMDA receptors. The resulting elevated calcium influx can strengthen the synaptic connection of dorsal horn pain transmission neurons and nociceptors that consequently will amplify responses to noxious

stimuli (Basbaum et al., 2009). Glycinergic or GABAergic inhibitory interneurons are tightly packed within the superficial dorsal horn and provide the basis for the gate control theory of pain that suppose that disinhibition of these inhibitory interneurons would result in enhanced pain (Melzack and Wall, 1965). This loss of interneuron function increases spinal cord output as for NMDA-mediated central sensitization in response to noxious and innoxious stimulation, contributing to mechanical allodynia (Keller et al., 2007; Torsney and Macdermott, 2006). Besides, enhanced intrinsic excitability of second order neurons seems to be the cause for spontaneous pain upon spinal cord trauma (Balasubramanyan et al., 2006; Hains and Waxman, 2007). The solid inhibitory effect of nonselective sodium channels blockers used as local anesthetics indicates the contribution of voltage-gated sodium channels to the formation of ectopic activity (Sheets et al., 2008). Several sodium channels that are sensitive or resistant to tetrodotoxin (TTX) (sodium channel blocker) are expressed by DRG neurons (Fukuoka et al., 2008). (Basbaum et al., 2009; Bourinet et al., 2014; Costigan et al., 2009; Ellis and Bennett, 2013).

1.3.2.1 Neuropathic Pain Models

In order to investigate the maladaptive plasticity evoked by neural injury, a number of rodent preclinical neuropathic pain models have been developed (Barrot, 2012). These models exhibit peripheral nerve injuries commonly affecting the sciatic nerve induced by compression, ligatures or transection (SNI-model) (Bennett, 1988; Decosterd and Woolf, 2000; Kim and Chung, 1992; Seltzer et al., 1990). Moreover, animal models of neuropathic pain are used that display metabolic disorders such as type 1 or 2 diabetes (Courteix, 1993; Latham et al., 2009) or that are induced by the administration of toxic components (e.g. anti HIV therapy and chemotherapy treatments) (Aley et al., 1996; Descoeur et al., 2011; Joseph et al., 2004, 2009; Ling et al., 2007; Ta et al., 2009). The etiology assessed in neuropathic pain models evoked by toxic chemotherapy drugs is notably similar to what is observed in the clinic. Moreover, neuropathic pain conditions as well as inflammatory pain give rise to allodynia and hyperalgesia. Those phenomena are commonly assessed in chronic pain mouse models. The described infiltration of immune cells and the secretion of mediators within the nerve trunk are well characterized in a number of peripheral nerve injury animal models. Additionally, several models of neuropathic pain (including chemotherapy induced neuropathy) reveal inflammatory processes (Nishida et al., 2008; Peters et al., 2007). Moreover, pro inflammatory cytokines are involved in the genesis of diabetic neuropathy (Fornoni et al., 2008; Luis-Rodríguez et al., 2012; Rivero et al., 2009). (Basbaum et al., 2009; Bourinet et al., 2014; Costigan et al., 2009; Ellis and Bennett, 2013).

1.3.2.2 Neuron-Immune Cell Interaction upon Peripheral Injury

Peripheral sensitization is commonly caused by inflammation-associated alterations in the chemical environment of the nerve fiber (Woolf and Ma, 2007). Tissue injury often involves the accumulation of endogenous mediators secreted from nociceptors and activated immune cells that reside within or infiltrate the damaged area. These mediators are known as the "inflammatory soup" and represent a broad range of signaling molecules such as peptides and neurotransmitters (calcitonin gene-related peptide (CGRP), substance P, bradykinin), eicosinoids and cognate lipids (endocannabinoids, thromboxanes, leukotrienes and prostaglandins), in addition to extracellular protons and proteases. Notably, one or more cell-surface receptors that are able to recognize and respond to these pro-algesic or pro-inflammatory factors are expressed by nociceptors. This interplay is responsible for increased nerve fiber excitability that results in enhanced sensitivity to touch or temperature. (Basbaum et al., 2009). More precisely, upon nerve damage, resident mast cells degranulate which results in the release of inflammatory factors (e.g. serotonin, histamine, nerve growth factor (NGF)) that sensitize nociceptors and recruit the first infiltrating immune cells, namely neutrophils (Kim and Moalem-Taylor, 2011; Perkins and Tracey, 2000; Smith et al., 2008; Zuo et al., 2003; **Figure 2**). Neutrophils then again secrete factors capable of sensitizing nociceptors and attract T cells and macrophages to the site of injury (Kumar and Sharma, 2010; Moalem et al., 2004). Recruited macrophages join the resident macrophages and together with Schwann cells promote the Wallerian degeneration of axotomized nerve fibers distal to the damaged nerve (**Figure 2**). Moreover, they release a great number of pro- inflammatory chemokines and cytokines as well as lipid mediators (Nathan, 1987; **Figure 2**). In the majority of cases, macrophages evoke pain by the secretion of pro-inflammatory mediators like TNFα and IL1-β (Zelenka et al., 2005; **Figure 2**), causing increased pain transduction and conduction by ion channel modulation (e.g. TRPV1, TRPA1 and Nav1.7-1.9) (Basbaum et al., 2009; Ji et al., 2014). In addition, related to their functional state, macrophages can have pro-inflammatory M1-like or anti-inflammatory M2-like phenotypes which are differentially involved in the induction or resolution of pain (Ji et al., 2016). T cells can also have different phenotypes also characterized by the secretion of pro- or anti- inflammatory cytokines (type 1 or 2 helper T cells (TH1 and TH2)). TH1 cells release pro-inflammatory cytokines (e.g. TNFα, IL-1β and IL-17) that facilitates neuropathic pain, whereas TH2 cells inhibit it by secretion of anti-inflammatory cytokines (e.g. IL-10, IL-4 and IL-13) (Moalem et al., 2004; Palmer and Weaver, 2009). (Basbaum et al., 2009; Bourinet et al., 2014; Costigan et al., 2009; Ellis and Bennett, 2013).

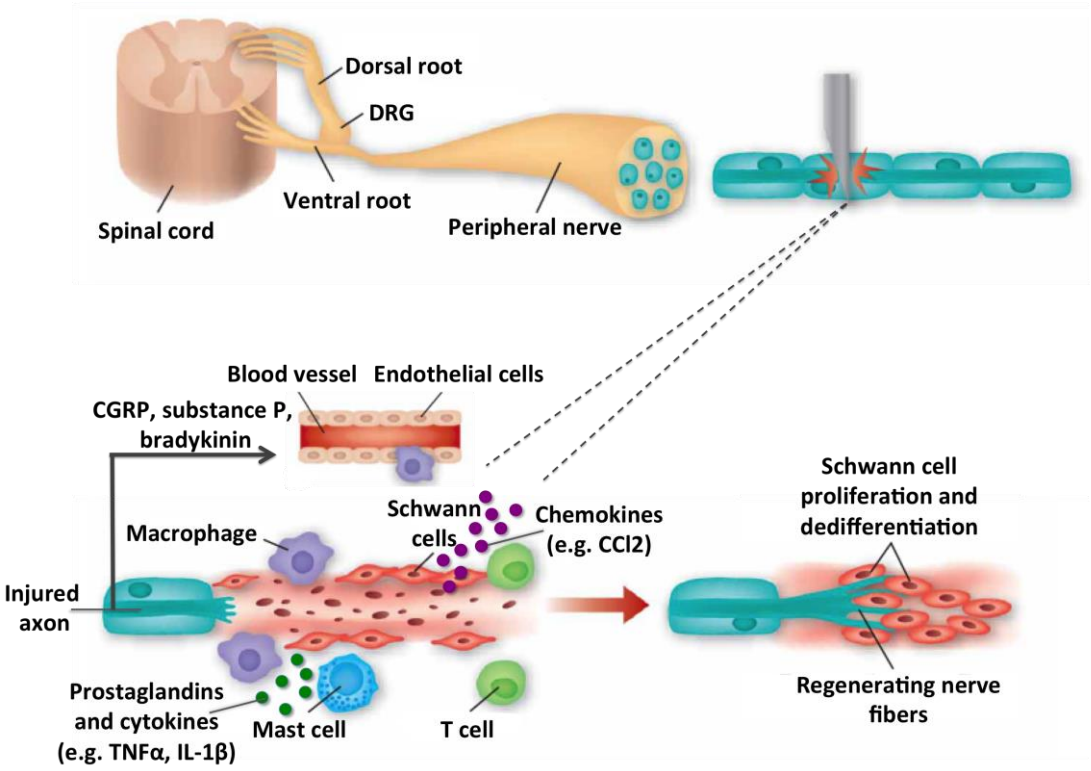

Figure 2: Immune and Glial Cell Reactions at Site of Nerve Injury

Peripheral nerve injury recruits and activates immune cells at the site of the damaged nerve. Mast cells, macrophages and T cells infiltrate the injured nerve and distribute around the distal fiber stumps. Signaling molecules such as CGRP, substance P, and bradykinin are released from the proximal fiber stumps and evoke hyperemia and swelling, supporting further invasion of T cells and monocytes. Chemokines (e.g. CCl2) engage and direct monocytes to the injured area. Mast cells and macrophages set prostaglandins and cytokines (e.g. TNFα and IL-1β) free. TNFα has an autocrine impact on macrophages that is conveyed via the tumor necrosis factor receptor 1 (TNFR1) stimulation and increases cytokine synthesis and release. This prototypic inflammatory mediator also facilitates additional infiltration of macrophages. Schwann cell proliferation and dedifferentiation follows with subsequent formation of bands of Büngner, that are used as guiding tubes for regenerating axonal processes. Adapted from (Scholz and Woolf, 2007).

Moreover, satellite cells, T cells and macrophages drive an immune response in the DRG after peripheral nerve damage, similar to that observed in the injured nerve (**Figure 3**). It was shown that neutrophils invade the ipsilateral DRG upon nerve damage between 7 and 14 days post-surgery (injury dependent) which takes place at lower levels and starts much later than observed peripherally (Morin et al., 2007; Smith et al., 2008). Significant T cell infiltration to the ipsilateral DRG is also induced after peripheral nerve damage (around 7 days post injury) (Hu et al., 2007; Hu and McLachlan, 2002; Smith et al., 2008). This is in line with the upregulation of IL-10, TNFα, IL-1β and

several chemokines (e.g. CCl2) (Jung et al., 2008; Kiguchi et al., 2010; Sun et al., 2006) in the DRG upon injury (Levin et al., 2008; Üçeyler and Sommer, 2008). Those chemokines and cytokines act on their receptors on DRG neurons and evoke ectopic discharges and elevated primary afferent input to the spinal dorsal horn by coupling to TRP and sodium channels (Ren and Dubner, 2010).

Furthermore, peripheral nerve trauma causes the activation of spinal microglia that dominates the early CNS glial response (**Figure 3**), followed by astrocyte activation and proliferation. Microglia (resident mononuclear CNS phagocytes) and macrophages (derived from circulating monocytes) share a number of similarities in regard to their functional and immunological properties (Streit, 2002). (Scholz and Woolf, 2007). Given the resemblance between macrophages and microglia, it is not surprising that the latter form dense clusters around the somata of damaged motor neurons of the spinal ventral horn as macrophages do in DRG around medium to large diameter neurons (peak 7 days post nerve damage) (Hu et al., 2007; Hu and McLachlan, 2002; Smith et al., 2008). Moreover, a massive microglial recruitment and activation (peak 7 days post injury) is found in the dorsal horn adjacent to the central terminals of injured sensory nerve terminals (Beggs and Salter, 2007; Marchand et al., 2005; Tsuda et al., 2005; Watkins and Maier, 2015; **Figure 3**). Their activation is accompanied by upregulation of microglial markers such as IBA1 and CD11b in the spinal cord (Ji et al., 2016).

The signals responsible for microglial recruitment include CSF1, ATP, chemokines (CCl2 and CX3CL1), and proteases that can arise from activated or injured sensory neurons. The enhanced expression of the receptors for ATP, CX3CL1 and CCl2 (P2X7, P2X4, P2Y12, CX3CR1 and CCR2) on spinal microglial takes place in parallel upon nerve damage (Abbadie et al., 2003; Grace et al., 2014; Ji et al., 2013). The receptor activation converges on an intracellular signaling cascade in which the phosphorylation of p38 mitogen activated protein (MAP) kinase is implicated. MAP phosphorylation causes elevated production and release of cytokines (TNFα, IL-1β, IL-18), and brain-derived growth factor (BDNF), in addition to enhanced cyclooxygenase (COX) expression and subsequent prostaglandin E2 synthesis (Coull et al., 2005). The fine-tuning of both inhibitory and excitatory synaptic transmission by these neuromodulators follows, which then increases pain signal transmission to the brain. A number of members of the Toll-like receptors (TLRs) family also play a role in microglia activation upon nerve injury. They are transmembrane signaling proteins expressed by glial and peripheral immune cells (Kim et al., 2007; Tanga et al., 2005).

Besides, Sorge and colleagues suggested that spinal microglia signaling is sex dependent. Reduced neuropathic pain could be achieved by microglial signaling inhibitors like p38 and minocycline inhibitors primarily in male mice, with little to no effect in female mice as pain signaling seems to be mediated by spinal T cells (Sorge et al., 2015). Astrocyte contribution to central sensitization is less defined. These glial cells are unquestionable induced in the spinal cord following nerve or tissue

injury (for review Ren and Dubner, 2010), but other than microglia their activation is usually delayed and lasts much longer (up to several months) (Basbaum et al., 2009). (Basbaum et al., 2009; Bourinet et al., 2014; Costigan et al., 2009; Ellis and Bennett, 2013).

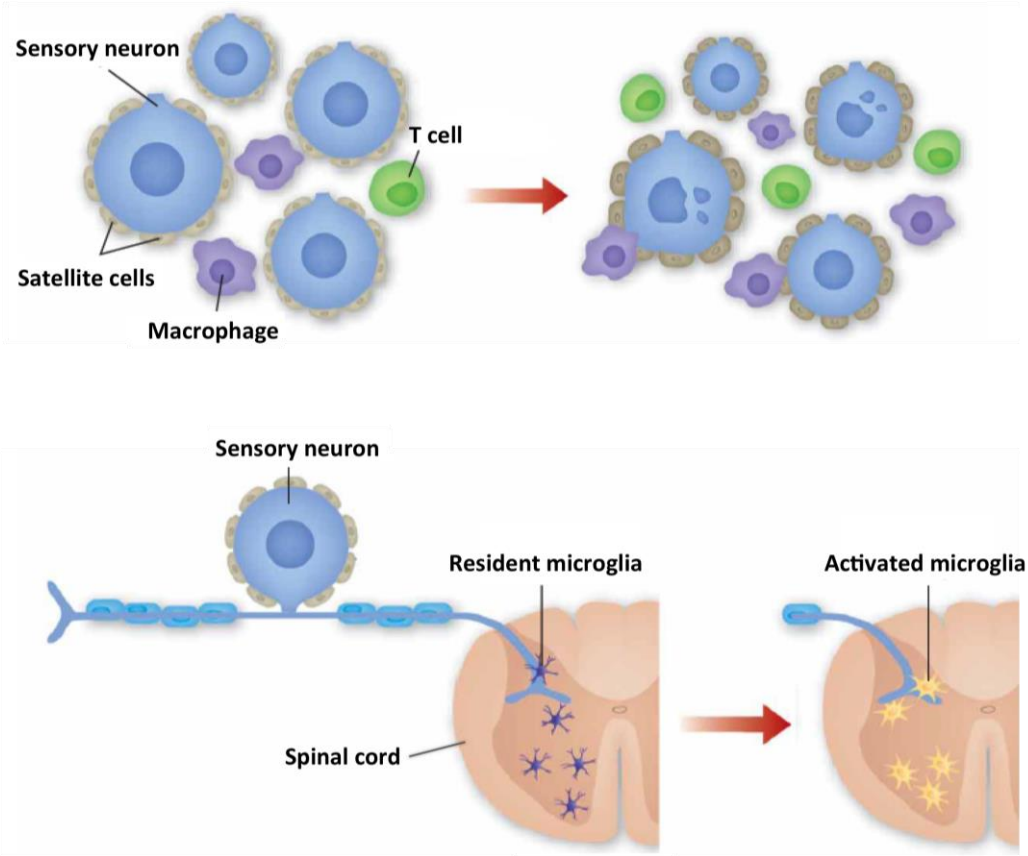

Figure 3: Immune and Glial Cell Reactions in DRG & Spinal Cord upon Nerve Injury

A peripheral nerve lesion results in the recruitment and activation of immune cells in the DRG and spinal cord. Top, some T cells and macrophages are present in the DRG before nerve damage. This number enhances dramatically upon injury. Additionally, macrophages are moving in the sheath that is formed by satellite cells around the soma of primary sensory neurons. Satellite cells can be considered as peripheral counterpart of astroglia, because they trophically support primary sensory neurons and share some astroglial markers (e.g. glial fibrillary protein (GFAP)), respectively. They proliferate upon injury and increase GFAP expression. Bottom, dense bundles of microglia appear after a nerve lesion in the ventral spinal horn around somata of motor neurons. Besides, extensive activation of microglia takes place in the projection areas of the central terminals of impaired primary afferents in the spinal dorsal horn. Adapted from (Scholz and Woolf, 2007).

1.3 Mitochondrial Dysfunction in Chronic Pain

Mitochondria are present in all nucleated eukaryotic cells and in addition to their central role in ATP synthesis, they are responsible for several cellular processes, such as apoptosis, calcium homeostasis and iron-sulfur cluster biogenesis (Duchen, 2000; Stehling and Lill, 2013). These organelles have an outer and an inner membrane that surround the intermembrane space (IMS) and the matrix. The cristae are formed by tubular invaginations of the inner mitochondrial membrane and host the electron transport chain (ETC) complexes. NADH or FADH2 are the electron supplies for the four ETC complexes in the inner mitochondrial membrane. The electrons are used as energy to produce a proton gradient across the membrane that drives ATP generation by the ATP synthase (also known as complex V). The redox systems of these complexes pass the electrons and ultimately, transfer them to molecular oxygen (complex IV). Hence, the ETC uses the energy of the oxyhydrogen reaction indirectly for ATP synthesis. (Dudek et al., 2013). Proteomics analysis suggested that mitochondria contain around 1500 different proteins in mammals and around 1000 different proteins in yeast (Pagliarini et al., 2008; Reinders et al., 2006; Sickmann et al., 2003). The ATP synthase as well as several ETC complexes are composed of subunits of dual genetic origin. Mitochondrial DNA (mtDNA) encodes 7 ETC subunits of complexes III-V in *Saccharomyces cerevisiae*, whereas 13 subunits of complexes I and III-V are mitochondrial encoded in humans. (Mick et al., 2012; Sickmann et al., 2003). However, ETC subunits are mainly nuclear encoded genes that are synthesized as precursor forms on cytosolic ribosomes and subsequently transported into the organelle. This process takes place by the translocase of the outer membrane (TOM) and translocase of the inner membrane (TIM) import machineries (Schmidt et al., 2010; Vögtle et al., 2009). In order to be targeted to mitochondria and be sorted to distinct subcompartments, precursor proteins require specific import signals (signal peptide) within their sequence. The commonly found mitochondrial import signal is an N-terminal extension known as presequence or signal peptide. This signal peptide is an amphipathic α-helical segment with a net positive charge and reveals a length of 15-55 amino acids (Vögtle et al., 2009). These signal peptides are usually removed proteolytically after import by the mitochondrial processing peptidase and other proteases (Mossmann et al., 2012; Taylor et al., 2001).

Moreover, the crucial role of mitochondria in terms of ATP production, ROS formation and calcium buffering, specifically in rodent sensory neurons, was shown by Flatters and colleagues (Flatters, 2015). Given their implication in crucial cellular processes it is not surprising, that mitochondrial dysfunction is involved in diseases such as neurological disorders (e.g. Alzheimer's, Parkinson's, and Huntington's disease) (Abeti and Abramov, 2015; Hroudová and Singh, 2014; Pinto et al., 2012). The role of mitochondria in pain, on the other hand, is less investigated (Flatters, 2015). However, the connection of mitochondrial abnormality to painful peripheral neuropathies caused by chemotherapy, diabetes, and trauma-induced nerve damage in rodents and humans was shown by

several studies (Fidanboylu et al., 2011; Flatters, 2015; Lim et al., 2015; Zhao et al., 2015). Mitochondrial dysfunction appears to arise from several factors such as alterations in the ETC activity (Baloh, 2008; Fernyhough, 2010; Joseph et al., 2009; Osio et al., 2006), a simultaneous enhancement of reactive oxygen species (ROS) causing oxidative stress (Kim et al., 2004; **Figure 4**) or mitochondrial calcium handling (Shishkin et al., 2002). Rouwette and colleagues also demonstrated an association between sensory neuron mitochondrial dysfunction and chronic inflammatory pain. They performed an unbiased proteome profiling of DRG from CFA-injected mice that revealed a myriad of differentially expressed proteins implicated in mitochondrial functioning, including ETC subunits mainly of complex I. Inhibition of the latter *in vivo* by Rotenone, reduced CFA-induced hyperalgesia (Rouwette et al., 2016). Furthermore, inflammatory and neuropathic pain conditions are linked to increased superoxide production in the spinal cord and elevated mitochondrial oxygen consumption in the sciatic nerve, respectively (Lim et al., 2015; Schwartz et al., 2009). In addition, a recent study identified the methyltransferase FAM173B that hyperpolarized mitochondria upon overexpression and thereby promoted mitochondrial and neuronal (cytosolic) ROS generation after peripheral inflammation that caused microglia activation and persistence of inflammatory pain (Willemen et al., 2018; **partly in Figure 4**).

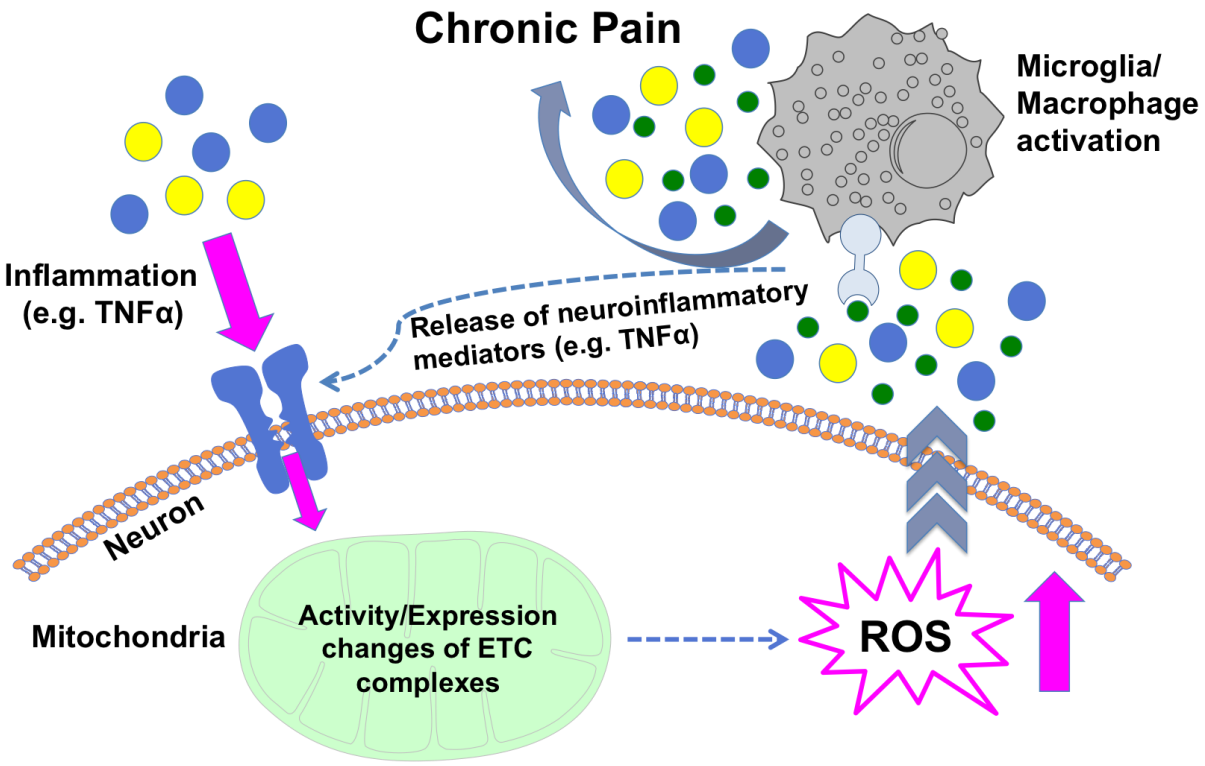

Figure 4: Dysfunctional Mitochondria & Chronic Pain

Proposed model for the connection between dysfunctional mitochondria and persistent inflammatory pain. Inflammation might negatively affect mitochondria, causing malfunctioning organelles by alterations in activity/expression of ETC complexes. These changes can lead to enhanced ROS production resulting in oxidative stress, which stimulates microglia/macrophages and thereby supports persistent inflammatory pain. The illustration was created by modifying images purchased in the PPT Drawing Toolkits-BIOLOGY Bundle from Motifolio, Inc. These Toolkits were kindly provided by the group of translational pain research, PI Prof. Esther Pogatzki-Zahn. Figure generated after (Willemen et al., 2018).

1.4 Inadequate Pain Medication

Side effects limit the currently available treatments for pain. In general, the basis for analgesia is either an increase in inhibition or decrease in excitation of the nervous system. One example are opioids that decrease neurotransmitter release in the presynapse and hyperpolarize neurons in the spinal cord, brainstem and cortex postsynapse (Finnegan et al., 2005). Potassium-channel opening and sodium-channel blocking anticonvulsants diminish excitation of the nervous system. Inhibitors of amine uptake, on the other hand, potentiate inhibitory transmitter actions in the spinal cord and brain (Micó et al., 2006; Wood, 2006). The problem about centrally-acting drugs (e.g. antidepressants, anticonvulsant, opioids, sodium-channel blockers targeting widely expressed channels/ receptors) is a high risk of side effects that can manifest as loss of cognitive function, sedation, somnolence or dizziness (Patapoutian et al., 2009). Opioids can also produce respiratory

depression, addiction, tolerance and hyperalgesia after chronic application (Ji et al., 2014).

Moreover, the most common strategy to treat inflammatory pain includes the inhibition of the accumulation/ synthesis of inflammatory soup components. This is best illustrated by nonsteroidal anti-inflammatory drugs (NSAIDs) (e.g. ibuprofen, Aspirin) that decrease inflammatory pain and hyperalgesia by cyclooxygenase (COX1 and COX2) inhibition, which is involved in prostaglandin synthesis (Basbaum et al., 2009). Unfortunately, selective COX2 inhibitors are limited by cardiovascular defects upon long-term application (Ji et al., 2011). Besides, the high number of inflammatory mediators acting in parallel makes interruption of their effects a fairly inadequate treatment for inflammatory pain (Woolf and Ma, 2007). A number of other strategies targeting specific sensitizers are under development. The main approach includes the blocking of NGF or TNFα action with neutralizing antibodies. Anti-TNFα therapies have been quite effective in the treatment of patients with inflammatory disease (e.g. rheumatoid arthritis) (Atzeni et al., 2005). However, its mode of action is still unclear (Noack and Miossec, 2017), which would be an useful information for the design of optimized therapies and predicting patient responses (Cook et al., 2018). It is also possible that TNFα-targeted approaches cause infection by immunosuppression in the longer term (Ji et al., 2011). Anti-NGF as anti-TNFα antibodies will likely always have a ceiling effect. Given the presence of other sensitizers, they might only reduce but not eliminate pain (Woolf and Ma, 2007).

An alternative approach to develop novel analgesics is to target the DRG that harbor primary sensory neurons expressing receptors and ion channels that are crucially implicated in the beginning of the pain pathway (Basbaum et al., 2009; Patapoutian et al., 2009; Richards and McMahon, 2013). The largest group of nociceptive ion channels is the TRP channel family (Clapham, 2003; Dhaka et al., 2006; Julius and Basbaum, 2001), which is mainly expressed in these neurons. Therefore, specifically targeting them might reduce side effects of pain medication (Patapoutian et al., 2009). However, this approach has also encountered constrictions by on-target side effects. Especially, early TRPV1 antagonists caused pronounced hyperthermia in animal models (Garami et al., 2010; Gavva et al., 2007; Honore et al., 2009; Wong and Gavva, 2008) and in clinical trials (Khairatkar-joshi and Szallasi, 2008). (Bourinet et al., 2014).

1.5 Aim of the Study

An entire understanding of the mechanisms responsible for chronic pain is still missing, even though great progress has been made by identifying ion channels, receptors and signaling proteins that are implicated in nociception and pain (Bennett and Woods, 2014; Patapoutian et al., 2009; Raouf et al., 2010). Hence, the development of therapeutic interventions that target proteins specifically implicated in chronic pain, while leaving an individual's ability to detect noxious stimuli intact, is in urgent need (Bourinet et al., 2014). The basis for this approach would be the identification of these proteins wherein a big step forward was taken by Rouwette and colleagues. They were able to quantify changes in the DRG proteome in two mouse models of chronic pain and could identify alterations in dozens of proteins that have not been identified in the pain context before. The implication in nociceptive signaling and pain of selected candidates was shown by functional validation that elucidated the biological relevance of the proteomics data (Rouwette et al., 2016). A further approach for improvement of pain medication would be a better translation from animal models to patients (Gregory et al., 2013). Chronic pain models are often critized, because they do not fully illustrate pain entities such as spontaneous pain that is clinically relevant (Cobos et al., 2012; Mogil et al., 2010; Urban et al., 2011).

This study was therefore aimed at functionally investigating the uncharacterized mitochondrial protein TM which was identified and shown to be downregulated in the proteomics study of Rouwette and colleagues (Rouwette et al., 2016). Its *in vitro* and extensive *in vivo* characterization by a broad range of behavirol paradigms including tests for spontaneous and stimulus evoked pain will ideally help to get a better picture about the molecular mechanisms of chronic pain.

2. MATERIALS AND METHODS

2.1 Materials

Table 1: Lists of Reagents and Kits

Product	**Company**
$(NH_4)HCO_3$ (Ammonium bicarbonate buffer)	Roth
10X HBSS (Hank's balanced salt solution)	Life Technologies
10X PBS (Phosphate-buffered saline) pH 7.4	Life Technologies
5 x MyTaq Reaction Buffer	Bioline
6-Aminohexanoic acid	Sigma-Aldrich
ADP (Adenosine diphosphate)	Roche
ATP (Adenosine tiphosphate)	Roche
Agarose	Roth
Ampicillin	Roth
Antimycin A	Sigma-Aldrich
AraC (Cytosine arabinoside)	Sigma-Aldrich
Ascorbic acid/ Ascorbate	Sigma-Aldrich
Azur II	Merck
Bis-Tris	Sigma-Aldrich
BPE (Bovine pituitary extract)	Life Technologies
BSA (Bovine serum albumin)	Sigma-Aldrich (Cell culture) Roth (Mitochondria Assays)

$CaCl_2$ (Calcium chloride)	Roth
Capsaicin	Sigma-Aldrich
CFA (Complete Freund's Adjuvant)	Sigma-Aldrich
Collagen 1, rat tail	Life Technologies
Collagenase	Worthington
Complete protease inhibitor	Roche
Complex IV rodent enzyme activity dipstick assay kit	Abcam
Coomassie brilliant blue	Serva
CsCl (Cesium chloride)	Sigma-Aldrich
D-PBS (no calcium, no magnesium)	Life Technologies
DDSA (Dodecenylsuccinic acid anhydride)	Serva
DH5α E. coli competent cells	Life Technologies
DHE (Dihydroethidium)	Invitrogen
DMEM (Dulbecco's modified eagle medium), GlutaMAX	Life Technologies
DMEM (Dulbecco's modified eagle medium)/F-12, GlutaMAX	Life Technologies
DMP Tris(dimethylaminomethyl)phenol	Serva
DMSO (dimethyl sulfoxide)	Sigma-Aldrich
dNTPs (Deoxyribose nucleoside triphosphate)	Bioline (Genotyping), Thermo Scientific (Cloning)
Donkey serum	Dianova

DTT (dithiothreitol)	Callbiochem
EcoMount	Biocare Medical
EGTA (Ethylene glycol tetraacetic acid)	Roth
Emetine	Sigma-Aldrich
Fast digest enzymes: BamHI, Eco105I, EcoRV, KpnI	Thermo Scientific
Fast digest green buffer	Thermo Scientific
FastAP thermosensitive alkaline phosphatase	Thermo Scientific
FBS (Fetal bovine serum)	Life Technologies
FCCP (Carbonyl cyanide 4-(trifluoromethoxy)phenylhydrazone)	Sigma-Aldrich
Forskolin	Sigma-Aldrich
FuGENE HD transfection	Promega
Fura-2 AM	Life Technologies
GeneJuice Transfection Reagent	Merck
Glucose	Roth
Glutaraldehyde	Electron Microscopy Sciences (EMS)
Glycerol	Roth
Glycidyl ether	Serva
Growth factors (NGF, GDNF, BDNF, NT-3, NT-4)	R&D Systems
HEPES (4-(2-hydroxyethyl)-1-piperazineethanesulfonic acid)	Life Technologies (Imaging)

	Roth (Mitochondria Assays)
Horse serum	Life Technologies
HRM Calibration Kit	Biognosys
Human chorionic gonadotropin	Ovogest
Hygromycin B	Life Technologies
Iodoacetamide	Sigma-Aldrich
KCl (Potassium chloride)	Roth
KCN (Potassium cyanide)	Fluka
KH_2PO_4 (Potassium dihydrogen phosphate)	Roth
L-glutamine	Biozym
Laminin	Life Technologies
LB (Lysogeny broth) agar	Roth
Ligase buffer	Life Technologies
Lipofectamin RNAiMAX	Invitrogen
Liquid chromatography (LC) solvent	Sigma-Aldrich
Mannitol	Roth
MEM-EARLES&L-GLUT	Life Technologies
Methylene blue	Merck
$MgCl_2$ (Magnesium chloride)	Roth (PCR, Electrophysiology) Merck (Mitochondria Assays)
$MgSO_4$ (Magnesium sulfate)	Invitrogen
MitoSOX™ (Red mitochondrial superoxide indicator)	Life Technologies

MNA (Methylnadic anhydride)	Serva
Mouse NGF 2.5S	TMH Medizinhandel OHG
Mustard oil (Allyl isothiocyanate, AITC, MO)	Sigma-Aldrich
MyTaq HS DNA polymerase	Bioline
Na_2CO_3 (Disodium carbonate)	Roth
Na_2HPO_4 (Disodium hydrogen phosphate)	Merck
NaCl (Sodium chloride)	Merck
NaH_2PO_4 (Sodium dihydrogen phosphate)	Merck
NucleoSpin gel	Machery-Nagel
NucleoSpin RNA extraction kit	Machery Nagel
OCT (Optimal cutting temperature) compound	Sakura
Oligomycin	Sigma-Aldrich
OPTIMEM medium	Life Technologies
Osmium tetraoxide	Company
Papain	Worthington
PCR Clean-up kit	Machery-Nagel
Penicillin/Streptomycin	Life Technologies
PFA (paraformaldehyde), 16%	Electron Microscopy Sciences

PFA (paraformaldehyde), powder	Serva
PFX Reaction buffer	Life Technologies
Platinum PFX DNA polymerase	Life Technologies
Pluronic F-127 20% solution	Life Technologies
PDL (Poly-D-lysine)	Millipore
PLL (Poly-L-lysine)	Sigma-Aldrich
Power SYBR green PCR master mix	Life Technologies
Pregnant mare serum gonadotropin	Pregmagon
Propylene oxide	Serva
Pure Link HiPure plasmid filter maxiprep kit	Invitrogen
Qiazol lysis reagent	Qiagen
QuantiTect reverse transcription kit (200)	Qiagen
RapiGest	Waters
RNAscope 2.5 HD assay-red	Advanced Cell Diagnostics (ACD)
RNeasy mini kit (50)	Qiagen
Rotenone	Sigma-Aldrich
RPMI (Roswell park memorial institute) medium	Life Technologies
Slowfade gold antifade reagent with/without DAPI	Life Technologies
SOC medium	Invitrogen

Succinate	Sigma-Aldrich
Sucrose	Merck (Embedding) Roth (Mitochondrial Assays)
T4 DNA ligase	Life Technologies
TG PRiME Tris/glycine 8-16 % gradient gels	Serva
Threhalose	Roth
TMPD (N,N,N',N'-Tetramethyl-1,4-phenylendiamine)	Sigma-Aldrich
TMRM (Tetramethylrhodamine, methyl ester)	Invitrogen
Trifluoroacetic acid	Roth
Tris/HCl (Tris hydrochloride)	Roth
Triton X-100	Roth
Tryple express w/ phenol red	Life Technologies
Trypsin/EDTA (10x)	Biozym
Tumor Necrosis Factor alpha (TNF α)	Peprotech
Uranyl acetate	SPI-Chem
Urea	Sigma-Aldrich
Yeast enolase-1 tryptic digest standard	Waters

2.2 Mouse Models

2.2.1 Animal Care and Conditions

All mice examined in this study were group-housed in individually ventilated cages (IVC) and kept in a 12 h light/dark cycle (light from 5:00 a.m. to 5:00 p.m.) with water and food *ad libitum* in the animal facility of the Max Planck Institute of Experimental Medicine (MPI EM) or University Medical Center Münster (UKM) (collaboration with the Group of Translational Pain Research, PI Prof. Esther Pogatzki-Zahn). Experiments were performed during the light phase and according to MPI EM guidelines and with permission of the Niedersächsisches Landesamt für Verbraucherschutz und Lebensmittelsicherheit (LAVES) or Landesamt für Natur, Umwelt und Verbraucherschutz Nordrhein-Westfalen (LANUV). TM wild type (WT) vs. knock out (KO) littermates were assessed in a genotype-blinded-fashion with an age between 8-14 weeks (w). Both genders were analyzed and included in experiments distributed by age and genotypes to respective cohorts.

2.2.2 Generation of Knock Out (KO) Mice

TM KO lines were generated by CRISPR/Cas9 technology (Mali et al., 2013) in collaboration with the DNA core and transgenic facilities of the MPI EM. C57Bl/6JRj females (3-4 w) were superovulated (pregnant mare serum gonadotropin (7.5 U) and human chorionic gonadotropin (5 U)) and mated with C57Bl/6JRj males. Fertilized eggs were collected on the day of plug after the females were sacrificed due to cervical dislocation (adapted from Brooke et al., 2007). Microinjection of CRISPR reagents (hCAS9_sgRNA_HDR.DNA (1 gRNA/loxP site) = 5 + 5_6.2 + 6.2_20 ng/µl) into the pronucleus and the cytoplasm of zygotes at the pronuclear stage followed by usage of the Eppendorf Femtojet and Femtotip II capillaries. The procedure was performed with a constant flow under visual control on an inverted microscope (40x air objective and DIC optics). Subsequently, pseudopregnant NMRI fosters received injected zygotes bilaterally in their oviduct. In this way floxed TM (Exon 1) mice were generated (adapted from Meyer et al., 2010).

Tmem160 floxed allele

-Equal to WT Sequence but loxP sequences inserted

-Primer = **blue** (initial genotyping to confirm correct HDR fragment composition and insertion)

34811 + 34820 upstream Exon 1 loxP1_HDR; **34481 + 34930** Exon 1 loxP2_HDR; **34811 + 35087** HDR fragment

-Primer = light blue (genotyping after *in vivo* CRISPR reagent microinjection)

35690 + 35691 WT (235 bp); 35690 + 35691 floxed allele (269 bp); 34929 + 35691 Exon 1 deletion (202 bp)

-EcoRV and KpnI = **red** (cKO 3251 bp EcoRV to KpnI)

-HDR fragment = underlined (3251 bp)

-PAM sites = **bold**

-guideRNA target site = **green**

-loxP sequences = **orange**

-Exon1, Exon2, Exon3 = **pink**

0001 GTTTTCAGACTGGCATCTTTAATTATGATGAGGGACTGGTAGACTAAGTCCTGCATTCTCTGGCATCCTA

34811

0071 TGTGTGAAGAACATTGAATCTTTTCAGTATGCGTATACCCATTTTCTCTGGTACAATTAGTTTGTGATCA

0142 GCTAGCTGTCCTCCATCATCTCTTAGGACACTGAGACATGGACAGGGTTTTGGCTCAGATCACATCTTCT

0212 GTCTGATCAGAGAGTATGAGGTTTCCTGGGTCTAGGGCAATCAAGGACATGAGGAGCCCAATTTTTAG

0280 GGTCACTCACTGGGCTGTCTCACTGCCCTCTGGGACGGAGTTTAGTCTGTCCTTCTGCCGCCAGAAGGC

0349 CTCTCTCTATATAAATAGTCCCATAGATATCAGCAGTAGCAAAGGCACACTGGCTATCTGTGTCTCTTGT

0419 CTTTTCTCAGCTGTAACGCCTTGGTCAGAGCTGCCACCAGTTCAGCTTTGTGGGTTGATACTCCTGTCCG

0489 GAGTGGCTCTGCACATATGATCTGAGCAGTCATGCAGAGGCCCACCGATCAAGGTCAGGGTCAGGCAG

0557 CAGGGCAGCTGAAAAGTCATCCTGGGGCATTCAAGAAGAGAGGCTGGTAATGAGTCACCCTGGCGTCA

0625 TCTTTAACCAGGAGGCCATTGCTGCACTGGTGTATACACAAGGTGGGGGTCGGCTTCTGGCAATTGGTG

0694 ACAGATTGGCCATTGTCTGATGCCAAGGCCCTGAGTCCCCTGGCTCTAGGGAGGTCACCTGTAGTTAGC

0763 AAAGTAAAGCCTTCTTAGAGGAGGCACAATAGTCCGAACTTTTCAGGGCCCCTAAGAGGTCTTGGTTGT

0832 TTCTTTTGTTTCTGTTGCCACTGAAAGTCACTTATAAACTGATGAGGAGACTTTACCTTCAGGTTTTAGCA

0903 AGGCAGAAAGTTCAACTTTATTATCTACAAACAAGTTGTTGGGTTCCCTTTCACCTTTAGGGCTGCCCTG

0973 GGCTTGGGAGGGGCACCTTTGATCTTTAGCCCCCTCCCTCTTATCTCCTTCTCCTGAGACTATCTGTTTTA

1044 GGCATTTCTTATGTGTCCCGTGGTTTGGCTGTGGCTGCTATCAAGATCTTTGCCAGGTCTTGAGTCTGTT

1114 GCTTCTGTCCCCTCCTCTGCTTCTCCTCTGCAGTCTCTCTTCTGTTAAATACTCTCTCGGCCACTCTCACTAA

1187 GTTTGAGTCCCAGTACCGGTAATAACGTTTTGGAAAGAATCTAAGTAAAGACAGGAATGAATTTCCAGA

1256 AATGACATCTTATTAAAATCTGCATAGAAGAAAAACTGAAGAGGAATACAACAAAATAGTTATGTGTCC

1325 TCTTTAGTGAGGTAACTGGTAGTTGTTTCCGTGAGTTCACCACAGTTTTGCAACTAGTCTAAGCAACTAG

34929

1395 TACAAGTTTTGTTTCCTGGCTGTTGAGAGCATTAACTTTTTTGAAACTACAAGTC**CCA**GCAGATAACTTCG

1466 TATAATGTATGCTATACGAAGTTATATATTCCGCCGCACCCTTCTGCAGGTCGAACTGCCTGCCGTACATT

34820

1537 GATCTCTGGGATTTGTAGTCTGATGATAAAAATAAGGTGGGTCACACACTACCGGCACATATAACTGAA

1606 GTGGAGACACAGCCAGATACACCAATAGGTATTGCGTTCCGGGATAGAGTTGCGGGCAGATCACCAAT

34481

1674 GGTTGTGTCGCTCCTCATGAGTGATGTGACCTCCAGCCTACAGTAGGCCCGTGGGGCGGAGCTGGTGTC

1743 GCGGCCCCATTGCGAGCCATGGGAGGCGGCTGGTGGTGGGCTCGGGTCGCGCGCCTGGCCCGCCTGC

1810 GCTTCCGGGGGTCTCTGCAGCCTCCTCAGCGGCCCCGCAGCGGGGGCGCGCGCGGGTCCTTCGCCCCG

1878 GGCCACGGGCCACGCGCGGGAGCGTCGCCGCCTCCAGTGTCCGAGCTGGATCGCGCGGACGCTTGGCT

1946 CCTCCGCAAGGCACATGAGACAGGTCAGTGGCAGGGGCCGGGGTCGTTCGCGCTACAAGGAGAGGGG

35690

2013 TTTCAATGTGCACGTGGGAGTGGGTTGGCCAGAGTAAGGCAAGCATCTGCTGGGAACAGGGCCTGTGCT

2081 CAGCGGGGGCAGCTTCCTCATGTGAGCGCAGGGAACCGGTGTTGGGGGTTGGAGATTTTGCAGCCTGG

2149 CCGCATAGGACACCATCTTTCGGATAACTTCGTATAATGTATGCTATACGAAGTTATGTCC**TGG**CTAAAG

2219 GGGTACAGCAGGGATTAGTGGGGGTGGGCAGGAGGCTACGGTTAGGAAGAAGTAGTTGGCAGCACC

2285 ACACTGCCTAGGTGAGAGACCGTTCCAGAGGCAGCTGGGAGGGAACAAGTTGCTTGAGACAGGGGTA

2352 TCCGTTAGGATTACAGACAGAGGGGACCACTTGGAATAAAACAAGAGTGTGGCTACCCGCAGAAGATG

2420 GGGAAGTTCCGGATTGGACCAGCGTGTAACCAATGGTAGAGAAGGTGGCTGCTGATTGGAGGGAGAG

2487 GTGATCTAGACTGCAGAGGGAGGAATCTCAAACGAGGCAATGAGTTGAGAGATTGGAGCTGGTCTGGT

2555 GTTGAATGGGGCTAGTAGTGGGAACAGCCTTTTGGCAGCACTCAGGTACTTGAGTGGTGGGGAGGTGT

2623 GGACGCAAGGATGAGGCCATGCTAGGTAGGAGCGGTTACCACACAGGGGAAGGGACAGGCTGGAGA

2689 AGTTTGTCCCAGAGGTCTGAGGGAGAGAGGGAAGACCGCAGGATGCACAAGGGAAGACTTGGGAAGA

2756 CTTTCTATCCTCAAACTTCAATTCGTGCTCTAGATTTTGAACGTCTGGGACAGAAGGGTAAAGGAATGGG

2826 ACTTGCATGGGGCTTCCCGGAAGGGATCCGCATCTAGAATACTTTTGTCTTGTGGCTGAATAGGGTGAG

2895 AGGGGATCTAGGAAGCAGGGCTTGCTGATGCAGAGCTCCATCCCCCAACTCCCCGCAGCTTTTCTCTCCT

2965 GGTTCCGAAATGGACTTCTGTCATCCGGCATTGGGGTCATCTCCTTCATGCAGAGTGACATGGGCCGGG

3034 AAGCTGCCTATGGTGAGTACAGACCATCCCTATGGGAAATGGGCCCCTCCCCCTTTTCCTCCAGTTCTGA

3104 GTCCTCCTACCCTAACAGTTGGAAAAGGAGAGCACTCCCTCCATTTTCTCTTGCCTCACTAGTTACATCTC

3175 CTCTTACACCTCCTTCATCGGCATTGTGAGGAGTCCACCAGACAGTTTCCAAGTAGCCTTGACTTATGTG

3245 GACACCTTTGTTTATACCCCAGACCAGCCCCTTTGGATATTGAATTTCTCCTCCAAGTCTCACATACTTCCT

3317 TTTACAAAGTCTCATGTATTTGAGTCCTTGTCTGCCTTTATTTGTTTGTTTGTTTGTTTATGTATTGCTATAA

3390 CGGGAAGGAAAGCAGCCTACTAGTTAAGTGCTGTGTCACTGAGCTACACATCGCCATCCTTCCACTGGA

3459 ATTTTTTAGCCAAGTGCTCTACCTTTGAGCCACGCCCCCAGTCCCTCACTGGGGGATTCTAGGCAGGGGC

3529 TCGACCACTGAACTACATCACCAGCCTTTTTGTTTTTTTGAGATTTATTTTTATTTTATGTGTATATGTGTA

3601 TATGGAGACCATGTGCATGCCTGGTACCCATGAAGCCAGAAGAGAGCACAAGAACCCCTCGGACTGGA

3669 GGTACAGATGGTTGTGAGCCACCATGTGGGTTCTGGGAACTGAACTCAGGCCATCTGAAAGAGCAACA

3737 AGTACTCTTAACCTTGAAGCCATCTCTCCAGGACTGCCCCCCCCACCCCACCCCTTCCCGTGTTATTTTGA

3808 GGCAGTCGCAGTAGCCCGAGTAAGCCTTCCGTTAGCTAGCACTGCTCCAGCCTCTCACTAGCTGACGTTA

3878 GAAGCCTTGTCCCGCCCTGTGCTCGTACTGACTCATCCTCCCCACCCGTCACCCTGTCAGCCCCTTGGGAT

3950 ACGCTGGACCCTGTAACTATTGACTACTGCTCCTTCTTCCACAGGCTTCTTCCTGCTGGGTGGCCTGTGCG

4020 TGGTGTGGGGCGGAGCCTCCTATGCGGTGGGTCTGGCAGCGCTGCGGGGACCCATGCAACTGTCGCTT

4088 GCTGGTGCTGCCGCTGGTGTGGGGGCAGTGTTGGCTGCCAGTCTGCTCTGGGCTTGTGCAGTAGGTCTC

4157 TACATGGGCCAGTTGGAACTGGACGTGGAACTGGTGCCTGAGGATGATGGGGCAGCCAGTACAGAAG

4224 GCCCAGATGAAGCGGGCAGGCCACCCCCTGAGTAAACAACAGGGCTGTGGGGACTGGCTGGGCCTGA

4291 CGACTGGGACATTAAAACCTGACCCTTCCGCAGTTCAAGACTCTGAGTGATAGCTCCTGTTATCTGGGGA

4361 GGTGGGGAGGGGAGAAGAGGGCAACCTTTGGGGACGAGGCTCAGTGGGTAAAGGCACTTGCTCCTAA

4428 GCCTGGCGACCTGAGTTTGATACTCAGGACCTGCGTGGTAGAAGAAGAGACCTAATTTCCACACCATAC

4497 CACACATGGACACACATACAAGTAAATCAGTTCAAAGGAACAAGGCCAAGCAATCATGAGAGGCAGCA

4565 TCCCCGGGGAGGGAGCCCCTTAGGGCATGGTGTTTAATTCTCAAGAATGACTCCAGGACTTGATCTGTG

4634 TCTCAGGTTTGGCCCTCTGGTGTTACACTGTCTTCAGTCTCCCTTCCGCTGCACCCTAGTACCTGTGGGCC

4705 CCGGATAGGGCAAGCCCAGCGTAGGGTAAAAGGCCTCTGGAAGCGAGGGGCCTGCGCCCAGCCTGTG

4772 CAGATGTGGATACATCAGGCTCAACTCCGCAGGGCCATAGCGGATGGTGCCTGGGGTGCACAGGCCCC

4840 GCACAACGGGTGGCAGGAAGCCTGCATGAAGGAGGGCGGGTGAGGGGTCTCCGGGAGTTGTCAAGCC

4907 CCACGGCAGCACTGGATCAT

2.2.2.1 cTMEM160_cKO r/r x Ella Cre

The constitutive TM KO was generated by crossing the Ella Cre (adenovirus Ella promoter, recombination E0.5 from Jackson Laboratory) driver line (Lakso et al., 1996) with floxed TM mice.

2.2.2.2 cTMEM160_cKO r/r x Dhh Cre

The Schwann cell specific TM KO mice were generated by crossing floxed TM mice with the DHH-Cre driver line (Jackson Laboratory). Desert hedgehog (DHH) is a differentiation marker of Schwann cell precursors (SCPs) resulting in recombination between E11-E13.5 (Jaegle et al., 2003).

2.2.2.3 cTMEM160_cKO r/r x Advillin Cre

The use of Advillin Cre driver mouse lines resulted in TM deletion in sensory neurons of dorsal root ganglia (DRG) and trigeminal ganglia (TG) starting between E14.5 and E16.5 (Zurborg et al., 2011).

2.2.3 Validation of KO Mice

2.2.3.1 Genotyping

The AGCT lab of the MPI EM examined genotypes according to standard PCR methods using DNA isolated from tail biopsies and self-synthesized primers (Table 4: List of Primers).

Table 2: PCR Master Mix Genotyping

Amount (µl)	**Reagent**
9.8	H_2O
4.0	5 x MyTaq Reaction Buffer with 5 mM dNTPs, 15 mM $MgCl_2$
1.0	50 mM $MgCl_2$
0.2	MyTaq_HS DNA Polymerase, 5 units/µl
4.0	Primer set (1 pmol/µl each)
1.0-2.0	DNA
20.0 total	

Final concentration: Mg: 5.5 mM, dNTPs: 1 mM, DNA Pol.: 0.05 U/µl, Primer set: 0.2 pmol/µl-, 200 nM each.

Table 3: PCR Cycle Genotyping

Order	Temperature (°C)	Time (min)
1	96.0	3.0
2	94.0	0.5
3	62.0	1.0
4	72.0	1.0
5	go to 2: 32x	
6	72.0	7.0
7	12.0	∞

2.2.3.2 Real Time Quantitative PCR (qRT-PCR)

RNA of snap-frozen DRG tissue was purified with the NucleoSpin RNA XS Kit as specified by the manufacturer. Obtained RNA was further processed to cDNA with the QuantiTect reverse transcription kit. First of all, genomic DNA (gDNA) contamination was removed by incubation in a thermal cycler (Bio-Rad T100) for 6 minutes at 42°C after addition of gDNA wipe out buffer. Afterwards, cDNA was synthesized by adding a master mix composed of reverse transcriptase (RT), 5x RT buffer and primer mix to the gDNA wipe out product, followed by incubation at 42°C for 30 minutes and at 95°C for 3 minutes. Subsequently, gene expression levels (Table 4: List of Primers) were quantified in a LightCycler 480 (Roche) with the SYBR green system (Power SYBR green PCR master mix). cDNA (ca. 1-100 ng) or H_2O (neg. control) was pipetted in triplicates and the master mix (H_2O, respective primers, SYBR green) was added. qPCR specificity was validated by analyzing the melting curve of the amplified product. The Cp (crossing point-PCR-cycle) values, meaning the cycle number where SYBR green fluorescence is higher than the background, were normalized to the commonly used housekeeping genes (β-Actin and GAPDH). Ultimately, relative expression changes were identified using the "fit point" and "2nd derivative maximum" analysis of the LightCycler 480 (according to Avenali et al., 2014).

Snap-frozen sciatic nerves (SN) were processed equally with the exception of RNA purification. Other than DRG, SN RNA was isolated with the RNeasy mini kit. First, SN were homogenized in Qiazol lysis reagent using the Precellyse24 (Bertin Technologies, 2x shaking for 10 s at 5500 rpm). Afterwards, RNA was extracted according to specifications for "RNA Isolation from fatty tissues" (protocol adapted from manufacturer's instructions by the Department of Neurogenetics, PI Prof. Klaus-Armin Nave, Ph.D).

Table 4: List of Primers

Primers	**Sequence (5'->3')**	**Used for**
TMEM160	FW upstream Exon 1: CCTATGTGTGAAGAACATTGAATCT REV upstream Exon 1: ACTACAAATCCCAGAGATCAATG REV downstream Exon 1: CTTCTTCCTAACCGTAGCCTCCT FW Exon 1: TCACCAATGGTTGTGTCGCTCC REV downstream Exon 2: GGCTCACAACCATCTGTACC	Initial Genotyping for proper HDR fragment composition and insertion
TMEM160	FW upstream Exon 1: ACTAGTACAAGTTTTGTTTCCTGGC FW downstream Exon 1: GGCCAGAGTAAGGCAAGCATC REV downstream Exon 1: CGGTCTCTCACCTAGGCAGT	Genotyping after *in vivo* microinjection of CRISPR reagents
c-Jun	FW: CCTTCTACGACGATGCCCTC REV: GGTTCAAGGTCATGCTCTGTTT	qRT-PCR
CCl2	FW: GCCTGCTGTTCACAGTTGC REV: GATCATCTTGCTGGTGAATGAGT	qRT-PCR
GAPDH	FW: CAATGAATACGGCTACAGCAAC REV: TTACTCCTTGGAGGCCATGT	qRT-PCR
GFAP	FW: ACAGACTTTCTCCAACCTCCAG REV: CCTTCTGACACGGATTTGGT	qRT-PCR
Iba1	FW: GGATTTGCAGGGAGGAAAA REV: TGGGATCATCGAGGAATTG	qRT-PCR

MBP	FW: GCCTGTCCCTCAGCAGATT REV: GCCTCCGTAGCCAAATCC	qRT-PCR
MPZ	FW: ACTTGGCCTTCCCATCTCTC REV: GGGCCACCAGAAGGTAGG	qRT-PCR
mt-Cox1	FW: GAACCCTCTATCTACTATTCGG REV: CAAGTCAGTTTCCAAAGCCT	qRT-PCR
mt-Cytb	FW: ATTCCTTCATGTCGGACGAG REV: GGGATGGCTGATAGGAGGTT	qRT-PCR
mt-ND2	FW: CGCCCCATTCCACTTCTGATTACC REV: TTAAGTCCTCCTCATGCCCCTATG	qRT-PCR
S100b	FW: AACAACGAGCTCTCTCACTTCC REV: CTCCATCACTTTGTCCACCA	qRT-PCR
Tfam	FW: CAGGAGGCAAAGGATGATTC REV: ATGTCTCCGGATCGTTTCAC	qRT-PCR
TMEM160	FW: TCTCCTTCATGCAGAGTGACAT REV: ATCCTCAGGCACCAGTTCCAC	qRT-PCR
TNFα	FW: TGCCTATGTCTCAGCCTCTTC REV: GAGGCCATTTGGGAACTTCT	qRT-PCR
Uqcr10	FW: CGCAGAACTTCCACCTTTGC REV: CCACAGTTTCCCCTCGTTGA	qRT-PCR
β-Actin	FW: GATCAAGATCATTGCTCCTCCTG REV: CAGCTCAGTAACAGTCCGCC	qRT-PCR

2.2.3.3 In situ Hybridization (ISH)

In situ hybridization (ISH) was performed with the RNAscope 2.5 HD Detection Kit (Red) for FFPE (Formalin-Fixed Paraffin-Embedded) sections. The first step was deparaffinization of sections (described in detail in section 2.6.3). Afterwards, 5-8 drops of hydrogen peroxide were added to each section for 10 minutes at room temperature to block endogenous peroxidase activity, followed by washing (2x 3-5 times washing in ddH_2O). Subsequently, slides were boiled for 5 minutes in 1x target retrieval solution in order to improve RNA accessibility for RNA scope probes due to breaking of cross links (which have occurred from tissue fixation). After washing in ddH_2O and 100% EtOH, sections were air dried and circled with the Immedge hydrophobic barrier pen. 5 drops of Protease plus were added and slides were incubated for 30 minutes in a humidified chamber in the HybEZ oven (at 40°C, ACD). This step was performed in order to enhance RNA accessibility. After washing in ddH_2O, 4 drops of RNA scope probe (for the RNA of interest) were added and incubated for 2 hours at 40°C in the HybEZ oven. After slides were washed 2x in 1x wash buffer several amplification steps followed (Amp1: 30 minutes at 40°C; Amp2: 15 minutes at 40°C; Amp3: 30 minutes at 40°C; Amp4: 15 minutes at 40°C; Amp5: 30 minutes at 40°C; Amp6: 15 minutes at room temperature). After each amplification process slides were washed 2x in 1x Wash buffer. Finally, the signal was detected by applying freshly mixed RED-B and RED-A (1:60, 10 minutes incubation at room temperature). When slides were washed in ddH_2O a nuclei counterstaining with Mayer's Hemalaun (1:1 with ddH_2O for 2 minutes) was performed and slides were washed again (tap water and ddH_2O). Before slides were mounted with EcoMount, they had to be dried at 60°C in a dry oven for 15 minutes and dipped into fresh pure xylene. Finally, the sections were air dried for 5 minutes and imaged with the 10x air objective under the Zeiss Axio Observer Z1 inverted microscope (bright field mode), according to manufacturers instructions (ACD).

2.3 Murine Pain Models

2.3.1 Inflammatory Pain Model: CFA

Inflammatory pain was induced by the unilateral injection of CFA (Complete Freund's Adjuvant, 10 µl of 1 mg/ml) into the plantar hind paw. The adjuvant was constituted of heat-inactivated mycobacteria (*Mycobacterium tuberculosis*) and evoked an inflammation with a peak after 24 hours and persisted for around 7 days. PBS was used as vehicle and injected in a uniform manner. The mice were assessed by the performance of behavioral paradigms pre and 1, 2, 3, 5 and 6 days post injection (Minett et al., 2011; Petrus et al., 2007).

2.3.2 Neuropathic Pain Model: SNI

Neuropathic pain was evoked by performing a spared nerve injury (SNI) in one of the hind legs of 8-10 weeks old mice. This form of injury was induced by a 1 mm excision of two sciatic nerve branches. Namely, the common peroneal and tibial nerve, while the sural nerve was left untouched. 10 minutes before the operation mice were injected i.p. (intraperitoneal) with buprenorphine (analgesic agent, opioid; 0.07 mg/kg body weight) followed by a subsequent anesthesia with 1.5-2.5 % isoflurane O_2/Air mix. The procedure usually took 20 minutes and was performed on a heating pad to maintain body temperature. Further pain management was performed 5-6 hours later by i.p. injection of carprofen (5 mg/kg, nonsteroidal anti-inflammatory drug (NSAID)) and 1-3 days post surgery. In order to make the sciatic nerve accessible, the hind leg was shaved, disinfected and a small incision into the skin was performed to expose the biceps femoris. The muscle was cut to expose the sciatic nerve with its branches (common peroneal, tibial and sural nerve). Afterwards, the common peroneal and tibial nerves were ligated with a suture, while the sural nerve was left untouched. After the axotomy the muscle parts were moved back together followed by wound closing with sterile staples. Sham operated mice were used as controls. The surgery was performed in a similar manner without nerve transection. The mice were behaviorally examined before surgery, at post operation day (POD) 7, 14, 21, and 28 and were subsequently sacrificed for organ collection (Decosterd and Woolf, 2000; Richner et al., 2011; Simonetti et al., 2013).

2.4 Phenotyping of Mice

2.4.1 Assessment of Motor Performance

Motor performance of mice was investigated with the TSE RotaRod System Advanced (TSE Systems). It is equipped with a rotating central axis (diameter: 3 cm, width: 6 cm) and 5 lanes for a simultaneous measurement of 5 mice. The animals were adapted to the device for 2 consecutive days. On day 3, a potential motor impairment was investigated by using the accelerated rotation mode (5-52 rpm within 5 minutes). Time spent on the central axis was measured for individual animals until falls were detected by a light-beam causing the timer to stop. Mice had to perform 5 times with a recovery phase of 10 minutes (according to Gess et al., 2011).

2.4.2 Evoked Pain Paradigms

2.4.2.1 Mechanical Hypersensitivity: Plantar Aesthesiometer

In order to investigate mechanical hypersensitivity in mice after the induction of pain, the animals were placed in plastic boxes on a grid. Before testing started, they were acclimated for 2 hours until exploratory behavior ended. Subsequently, the Plantar Aesthesiometer (Ugo Basile) equipped with a filament was placed beneath the mice. The filament was brought in contact with the hind paws until they were retracted. More precisely, the filament is slightly pricked into the paws by an increasing force of 0-10 g within 40 seconds. Withdrawal latency and respective force values were collected 5 times per paw (according to Avenali et al., 2014; Minett et al., 2011).

2.4.2.2 Mechanical Hypersensitivity: Von Frey Filaments

Mice were acclimated for 30 minutes on an elevated grid followed by examination of withdrawal threshold to mechanical stimuli given by calibrated von Frey-filaments (14, 20, 39, 59, 78, 98, 147, 255 mN bending force). Stimuli were given to the plantar surface of each of the hind paws starting with the lowest bending force until a response occurred or cut-off was reached (255 mN). The median from 3 measurements per paw was considered as withdrawal threshold. Force of the next filament was applied (522 mN) if no response was evoked by using the other filaments. This method was performed in collaboration with the Group of translational pain research, PI Esther Pogatzki-Zahn (according to Reichl et al., 2016).

2.4.2.3 Thermal Hypersensitivity: Hargreaves Apparatus

Thermal hypersensitivity of mice was identified with the Hargreaves Apparatus (Ugo Basile) or the IITC Life Science Plantar Test Analgesia Meter (Life Science). Before testing started, mice were acclimated for 2 hours in plexiglas boxes positioned on a glass plate. Infrared heat (set to 20: Hargreaves Apparatus) or in case of IITC the radiant heat (set to 15 % light intensity) beam was positioned beneath the hind paw surfaces. 5 withdrawal latency values were collected per respective hind paw (according to Avenali et al., 2014; Minett et al., 2011).

2.4.2.4 Movement-Evoked Pain Behavior: Catwalk

The Catwalk system (Noldus) was used for automatic gait analysis in order to assess movement-evoked pain behavior. Mice were passing through a corridor upon an illuminated (green LED) glass plate to visualize footprints, while a video camera was detecting them from below. To enhance the contrast, red light was shining down from the lid. Afterwards, the resulting video sequences were analyzed with a specialized software (Catwalk XT, Noldus). Parameters like stand and print area as well as swing speed and duty cycle were analyzed. The test was performed 3 times per mouse (Caballero-Garrido et al., 2017).

2.4.3 Non-Evoked Pain Paradigms

2.4.3.1 Non-Evoked Pain (NEP) Behavior

Spontaneous pain was assessed with a behavioral test called non-evoked pain behavior (NEP). In order to measure foot print intensities, mice were placed in boxes positioned on green illuminated plexiglas covered with red illuminated Plexiglas to increase the contrast. Acclimatization of animals was performed for a duration of 30 minutes until exploratory behavior ended. Afterwards, 20 pictures were taken within a time frame of 10 minutes (every 30 seconds 1 picture). Subsequently, the foot print intensities were analyzed with Image J (foot print intensity macro from the Group of Translational Pain Research, PI Esther Pogatzki-Zahn) by assessing the pixel number. Finally, the ratio between non-operated and operated paw was calculated. The method is a combination of the illuminated footprints (used in the Catwalk system (described in 2.4.2.4)) and observations from the non-evoked pain assessment (using a cumulative pain score, Reichl et al., 2016). The method was established and performed by the Group of Translational Pain Research, PI Esther Pogatzki-Zahn (Linnemann et al., 2018, Poster World Congress on Pain 2018, Boston).

2.4.4 Acute Pain Behavior

Acute pain behavior was explored by injection of the TRPV1 (transient receptor potential vanilloid 1) agonist Capsaicin (0.5 µg/10 µl) or Vehicle (5 % EtOH/D-PBS) into the left hind paw. The time mice spent licking, flicking and lifting of the paw were investigated over a time period of 10 minutes. Afterwards, mechanical sensitivity was assessed with the Plantar Aesthesiometer (Ugo Basile) for 1.5 hours (Caterina et al., 2000).

2.5 Cell Culture

2.5.1 DRG Culture and Nucleofection

Coverslips (12 mm) or MatTek dishes were coated with poly-D-lysine (PDL, 1 mg/ml) for 1.5 hours at 37°C followed by 3x washing in D-PBS and coating with laminin (20 µg/ml) for 0.5 hours at 37°C. Subsequently, 8-12 w old C57Bl/6JRj or TM KO mice and their respective controls were sacrificed by CO_2 according to the animal welfare law. Mice were decapitated and the hairy back skin was removed. Afterwards, the backbone was excised and the covering superficial muscle tissue was cut open. The vertebrae were longitudinally bisected revealing the spinal cord and DRG positioned in the intervertebral foramina. Dorsal and ventral roots were removed and ganglia were collected in 1 ml serum free medium (DMEM/F-12+Glutamax). DRG and medium were transferred to 1 ml Collagenase (12 mg/ml) and digested for 1 hour at 37°C (mixed every 15 minutes). Trituration with P1000 tip and further digestion in Papain (final dilution 1:10) followed for 0.5 hours at 37°C. Afterwards, cells were centrifuged (1000 rpm for 1 minute), 1 ml of serum free medium was added, cells were again triturated and an additional ml of serum free medium was pipetted on top. Bovine serum albumin (BSA, 0.15 g/ml) was slowly given underneath the cells suspension and the column was centrifuged for 10 minutes at 1000 rpm. A cell pellet was formed on the bottom of the falcon covered by the BSA layer, a cell debris layer and on top the medium layer. All layers were removed with a Pasteur pipette in the following order: cell debris layer, medium, BSA. Cells were now re-suspended in the proper amount of medium with serum (DMEM/F-12+Glutamax+horse serum) plus growth factor (100 ng/ml NGF) and were plated on coverslips or dishes. After 20 minutes cells were covered with 1 ml medium with serum and NGF. Cells were used after 24 h for calcium or live imaging experiments (according to Avenali et al., 2014; Narayanan et al., 2016).

Nucleofection was performed with the P3 Primary Cell 4D-Nucleofector X Kit in the 4D-Nucleofector X Unit (Lonza) after the abovementioned centrifugation for 10 minutes at 1000 rpm. Supernatant was removed from cell pellet followed by re-suspension in 36 µl nucleofector solution (P3 primary neurons nucleofector solution including supplement). Subsequently, 0.5 µg plasmid (pCMV6-

TMEM160-Myc-DDK single or in combination with HyPer-mito-YFP or pCDNA3.1-myc-His) were added to cell suspension, transferred to a 16-well cuvette and inserted into the nucleofector (program DC 104). After electroporation the cuvette was immediately removed and 40 µl of RPMI (calcium free) were added followed by a recovery incubation for 10 minutes at 37°C. 60 µl medium (DMEM/F-12+Glutamax) were added and 40 µl of cell suspension was plated on 3 coverslips/dishes. After a 20-minute incubation at 37°C cells were covered with 1 ml medium supplemented with serum and growth factors (DMEM/F-12+Glutamax + 10 % horse serum + 100 ng/ml NGF + 50 ng/ml GDNF + 50 ng/ml NT-3, and 50 ng/ml NT-4). In order to reduce toxicity half of the medium was replaced by fresh medium after 2 hours. After 3dIV (day *in vitro*) cells were used for immunocytochemistry (according to Avenali et al., 2014, Narayanan et al., 2016). HyPer-mito-YFP was kindly provided by the Department of Metabolic and Redox Signaling, PI Prof. Dr. Michael Müller.

2.5.2 Schwann Cell (SC) Culture and Nucleofection

Rat pups (postnatal day 3) were decapitated and sciatic nerves were dissected and placed in a culture dish filled with medium (DMEM+Glutamax+Pen/Strep) on ice. The epineurium was removed and de-sheathed nerves were collected in a fresh culture dish filled with the same medium. Subsequently, nerves were dissociated in 300 µl Trypsin (2.5 mg/ml in PBS) and rat-tail collagenase (approx. 800 U/ml) in a culture dish for 1 hour at 37°C. Afterwards, nerves were triturated by P1000 and P200 tips (each 10x) and digestion was stopped by adding 4 ml medium with serum (DMEM+Glutamax+Pen/Strep + 10 % fetal bovine serum (FBS)). Cell suspension was centrifuged at 1000 rpm for 10 minutes and the supernatant removed. After re-suspension in 1 ml medium with serum the cells were plated on poly-L-lysine (PLL, 100 µg/ml, 1 h at 37°C) coated dishes. After 24 hours 10 µl AraC (cytosine arabinoside) were added to 2 ml cell suspension (final conc. 10^{-5} M) and cultured for 3 days in order to eliminate fibroblasts. AraC containing medium was replaced by fresh expansion medium (DMEM+Glutamax+Pen/Strep + 10 % FBS +70 µg/ml BPE (Bovine pituitary extract) + 4 µM Forskolin). This medium allowed for cell division resulting in confluency after 2-3 days when cells were split 1:3 (adapted from Stevens et al., 1998 by Dr. Susanne Quintes, Department of Neurogenetics, PI Prof. Klaus-Armin Nave, Ph.D).

Nucleofection was performed in the same fashion as abovementioned for the DRG culture with slight modifications: Cells were washed in D-PBS (1x) and detached with 1x trypsin followed by a centrifugation at 1000 rpm for 10 minutes. The supernatant was discarded and cells were re-suspended in 1 ml medium ((DMEM+Glutamax+Pen/Strep + 10 % FBS) and amount was quantified by

using the Neubauer counting chamber. Dilution of cells in respective quantity of medium (200.000 cells/electroporation) followed. Afterwards, SC were centrifuged again (1000 rpm, 10 minutes), supernatant was removed and cells were re-suspended in nucleofector solution. Procedure was performed exactly as for DRG culture with a difference in the program used: CA 138 and usage of SC medium (modified from Avenali et al., 2014, Narayanan et al., 2016).

2.5.3 SC DRG Co-Culture

Pregnant mice were sacrificed by CO_2, followed by the opening of the abdomen. The uterus was excised and transferred to a culture dish on ice filled with basal medium (MEM-EARLES&L-GLUT). Mouse embryos (E13.5) were released and placed (one at a time) into a fresh dish with medium in order to remove extremities (paws were used for genotyping) and organs. Subsequently, the spinal cord was exposed by cutting the rips and removing the surrounding tissue. The spinal cord with its DRG attached was transferred into a new medium-dish where all DRG were plugged off. The medium containing DRG from all embryos was pipetted into a falcon tube and centrifuged (800 rpm, 5 minutes). The medium was removed and replaced by 1.5 ml Trypsin (0.25 %) followed by the digestion for 1 hour at 37°C (water bath). The addition of 4 ml medium with serum stopped the digestion (MEM-EARLES&L-GLUT+Pen/Strep (100 U/ml) + 10 % FBS). Cells were re-suspended with a 5 ml glass pipette and P1000 tip. 10 µl of cell suspension were saved for counting and the remaining solution was centrifuged (800 rpm, 8 minutes). After supernatant removal cells were re-suspended in the proper amount of medium (MEM-EARLES&L-GLUT + Pen/Strep + 10 % FBS + 50 ng/ml NGF; 150000 cells/CS) and distributed to CS (40 µl/CS). CS (18 mm) were coated in advance with collagen and arranged in 12 well plates. The cells were allowed to settle down over night and wells were filled up with 1 ml medium the next morning. After letting them grow for 1 week, basal medium was replaced by myelination medium (MEM-EARLES&L-GLUT + Pen/Strep + 10 % FBS + 50 ng/ml NGF + 50 µg/ml ascorbic acid), which had to be changed every second day. Myelination could be seen 7 days post induction. In order to assess potential differences in myelination CS were stained for MBP (myelin) and Tuj (axons) (after ICC protocol: section 2.7.1, Table 5: Primary Antibodies). Images were taken with the Zeiss Axio Observer Z1 inverted microscope (20x air objective) in a random fashion (12 images/CS; 3 CS/genotype; 2 separate experiments) and MBP segments were counted (protocol provided by Dr. Susanne Quintes, Department of Neurogenetics, PI Prof. Klaus-Armin Nave, Ph.D).

2.5.4 HEK293T Cell Culture and Transfection

Coverslips were coated in the same way with PDL and laminin as aforementioned for DRG culture (section 2.5.1). HEK cells were maintained in medium composed of DMEM+Glutamax + 10 % FBS + 1 % penicillin/streptomycin at 37°C and 5 % CO_2 in T-75 flasks. Medium was aspirated and HEK cells were washed in 10 ml warm D-PBS. After D-PBS removal cells were detached with 1 ml TrypLE Express. 9 ml of warm medium was added and 1 ml of this cell suspension was added to a new flask comprising 9 ml of warm medium. The same dilution was performed in an additional flask and 1 ml of the cells suspension was distributed on coverslips arranged in a well plate. Subsequently, the transfection mixture (100 µl OPTIMEM medium, 3 µl FuGENE and 0.5 µg plasmid (pCMV6-TMEM160-Myc-DDK or pCDNA3.1-myc-His)) was distributed equally on the respective coverslips after an incubation of 20 minutes. Immunocytochemistry (after ICC protocol: section 2.7.1, Table 5: Primary Antibodies) was performed after 3dIV (according to Avenali et al., 2014, Narayanan et al., 2016).

2.6 Histology

2.6.1 Cryo-Embedding

DRG, SN and spinal cords were collected and stored in 4 % PFA (Paraformaldehyde) over night. Subsequently, to protect the tissue from the formation of ice crystals it was placed in 30 % sucrose. Cryo-protection was performed overnight followed by tissue embedding in plastic molds filled with OCT (Optimal cutting temperature) compound. Tissue blocks were stored at -80°C until cut with a microtome cryostat (Leica) (DRG and SN were cut at a width of 10 µm, whereas spinal cords were cut at 20 µm, step serial 5 sections à 6 slides) (as described by Avenali et al., 2014).

2.6.2 Paraffin-Embedding

Tissue of interest was dissected from mice and fixed in 4 % PFA over night. Afterwards, it was placed in 1x PBS and transferred into plastic molds for further processing (1x 50 % EtOH 1 hour, 2x 70 % EtOH 2 hours, 2x 96 % EtOH 1 hour, 2x 100 % EtOH 1 hour, 1x 2-Propanol 1 hour, 2x Xylol 2 hours, 2x Paraffin wax (60°C) 2 hours). Subsequently, the paraffin-infiltrated tissue was transferred to a different plastic mold and adjusted properly for cutting and filled completely with paraffin. When the paraffin blocks were cooled down they were cut with a microtome (Leica) in 5 µM thick tissue sections (step serial, 5 sections à 6 slides) or stored at room temperature. For proper attachment of sections to the slides, they were placed at 37°C over night (according to standard protocols from the Department of Neurogenetics, PI Prof. Klaus-Armin Nave, Ph.D).

2.6.3 Deparaffinization and Rehydration of Paraffin Sections

Slides with tissue sections had to be warmed up in a dry oven (60°C for 10-20 minutes) to melt the paraffin. Afterwards slides were placed in Xylene at RT (2x 10 minutes), followed by 10 minutes incubation in 1:1 Xylene: 2-Propanol (room temperature). Subsequently, sections were rehydrated in diverse EtOH concentrations (100 % EtOH, 90 % EtOH, 70 % EtOH, 50 % EtOH, each 5 minutes at room temperature) and washed in ddH_2O (5 minutes at room temperature). Finally, the slides were first placed in citrate buffer (0.01 M, pH 6.0: 450 ml ddH_2O+9 ml 0.1 M $C_6H_8O_7xH_2O$+ 41 ml 0.1 M $C_6H_5Na_3O_7x2\ H_2O$) for 5 minutes at room temperature and subsequently boiled in the same buffer (10-15 minutes in the microwave), followed by a cool down for 20 minutes leaving the slide in the buffer. After this step, sections were incubated in blocking buffer as described in the IHC section (2.7.2) (according to standard protocols from the Department of Neurogenetics, PI Prof. Klaus-Armin Nave, Ph.D).

2.7 Fluorescence Staining

2.7.1 Immunocytochemistry (ICC)

After 3dIV cells were washed in 1x PBS (3x short, 3x 5 minutes) and subsequently fixed in 4 % PFA for 10 minutes at room temperature. After washing in 1x PBS, (3x shortly, 3x 5 minutes), the cells were covered with blocking solution (5 % donkey serum, 0.4 % TritonX-100 in 1x PBS) for 30 minutes at room temperature. Incubation at 4°C over night with respective primary antibodies (diluted in 1 % donkey serum, 0.1 % TritonX-100 in 1x PBS (Table 5: Primary Antibodies), followed. Upon completion, the cells were washes in 1x PBS (3x short, 3x 5 minutes) and secondary antibody solution was added (Table 6: Secondary Antibodies) for 2 hours at room temperature. Finally, coverslips with cells were washed again in 1x PBS (3x short, 3x 5 minutes) and mounted with Slowfade gold antifade reagent on slides (according to Narayanan et al., 2016).

2.7.2 Immunohistochemistry (IHC)

Frozen tissue sections were thawed for 5-10 minutes and subsequently surrounded by a fat pen and treated for 1 hour with blocking buffer (5 % donkey serum, 0.4 % TritonX-100 in 1x PBS) at room temperature to increase the staining specificity. Afterwards, slides were incubated overnight at 4°C with primary antibody (diluted in antibody solution, 1 % donkey serum, 0.1 % TritonX-100 in 1x PBS) combinations against proteins of interest (Table 5: Primary Antibodies). When the incubation was finished the tissue was washed 3x short in 1x PBS in addition to 3x 5 minutes wash in 1x PBS. 2 hours incubation with secondary antibodies (Table 6: Secondary Antibodies) followed. Upon completion of

incubation time, the tissue was washed again in 1x PBS (3x shortly, 3x 5 minutes) and mounted with Slowfade gold antifade reagent with or without DAPI. All incubation steps were performed in a humid chamber (according to Avenali et al., 2014).

Table 5: Primary Antibodies

Target	**Company**	**Source**	**Dilution**
α 4-HNE	Alpha Diagnostic: HNE11-S	rabbit	1:500
α ATP5B	Self-made (Rehling department)	rabbit	1:500
α c-Myc	Life technologies: 132500	mouse	1:100
α Cox1	Self-made (Rehling department)	rabbit	1:500
α Iba 1	Abcam: ab178846	rabbit	1:400
α MBP	Aves: MBP	chicken	1:500
α NDUFA10	Self-made (Rehling department)	rabbit	1:500
α NDUFV2	Protein tech: 15301-1-AP	rabbit	1:100
α NF200	Sigma Aldrich: N4142	rabbit	1:200
α Peripherin	Abcam: ab39374	chicken	1:100

α Rieske	Self-made (Rehling department)	rabbit	1:500
α SDHA	Self-made (Rehling department)	rabbit	1:500
α β-Tubulin 3 (Tuj1)	Covance: MMS-435P	mouse	1:200

Table 6: Secondary Antibodies

Antibody	**Company**	**Source**	**Dilution**
Alexa Fluor 488 α chicken	Dianova: 703545155	donkey	1:250
Alexa Fluor 488 α mouse	Life technologies: A21202	donkey	1:250
Alexa Fluor 488 α rabbit	Life technologies: A21206	donkey	1:250
Alexa Fluor 546 α mouse	Life technologies: A10036	donkey	1:250
Alexa Fluor 555 α chicken	Life technologies: A21437	goat	1:250
Alexa Fluor 555 α rabbit	Life technologies: A21428	goat	1:250

2.7.3 Image Acquisition: ICC & IHC

After mounted slides were dry, images were taken with a Zeiss Axio Observer Z1 inverted microscope, with 10x, 20x air or 63x oil objective. The exposure time was kept constant for the same staining compared between genotypes or treatment conditions, in addition to secondary antibody controls (according to Avenali et al., 2014).

2.7.4 Image Analysis: IHC

For each condition 7 images were taken and analyzed with Image J. First, brightness and contrast were set to get an optimal signal to noise ratio of the staining. To identify a specific staining a threshold was set by measuring the mean intensity (AU) of 10 unstained cells + 3x standard deviation. A staining was considered positive when its mean intensity was higher than the threshold. The mean staining intensity was quantified followed by the threshold subtraction and multiplication by the area. Finally this value was divided by the sum of all areas to get the mean intensity/pixel/image. These values were taken from all 7 images/condition and last of all the mean was determined. In addition, the percentage of cells positive for the protein of interest in regard to the total number of cells was determined (cell counter tool from Image J) (according to Avenali et al., 2014).

2.8 Live Imaging

2.8.1 Mitosox Imaging

Mitosox is a dye sensitive to mitochondrial reactive oxygen species (ROS), which reveals a red color when oxidized. Coverslips with cultured sensory neurons (primary DRG culture) were washed 3 times in assay buffer (HEPES, HBSS in H_2O) followed by 15 minutes incubation at 37°C in 1 µM Mitosox diluted in DMSO and assay buffer. After incubation, cells were washed 3x in assay buffer and the coverslip was placed in a chamber and covered with buffer for subsequent imaging with a Zeiss Axio Observer Z1 inverted microscope (20 x air objective). 7 pictures were taken in a random fashion and mean intensity of the neuronal soma was analyzed with Image J (Plun-Favreau et al., 2012).

2.8.2 TMRM Imaging

TMRM (tetramethylrodamine, methyl ester) was used as indicator for mitochondrial dysfunction, because of its accumulation capacity in mitochondria with intact membrane potential. Therefore, the signal was strong in healthy cells with active mitochondria, whereas a loss of membrane potential caused a diminished signal. Primary sensory neurons (DRG culture) were incubated in 3 nM TMRM in

assay buffer (HEPES, HBSS in ddH_2O) for 1 hour at room temperature. After incubation, cells were imaged with the Zeiss Axio Observer Z1 inverted microscope (20x air objective). Images were taken every 20 seconds for a time period of 6 minutes (2 minutes baseline (assay buffer + 3 nM TMRM), 2 minutes 1 µM FCCP (mitochondrial oxidative phosphorylation uncoupler; in assay buffer + 3 nM TMRM), 2 minutes wash out (assay buffer). Finally, TMRM mean intensity after membrane potential collapse was normalized to baseline and analyzed in axons from 4 squares/image (12 images/CS; 3 CS/imaging round) (Akude et al., 2011; Nicholls, 2006).

2.9 Ca^{2+}-Imaging

Cell intrinsic calcium concentrations were visualized by Fura 2-AM, which is a specific calcium binding fluorescent dye. Calcium concentration changes were investigated by measuring the excitation ratio of 340/380 nm. 50 µg Fura2-AM were dissolved in 50 µl DMSO and 50 µl Pluronic F-127 and finally diluted 1:200 in warm assay buffer (1x HBSS, 10 mM HEPES in ddH_2O). After media was aspirated from cultured DRG cells they were incubated in Fura2-AM solution for 30 minutes at 37°C. Afterwards, cells were washed again 3x in assay buffer and coverslips were transferred to an imaging chamber and immediately covered with assay buffer. Subsequently, cells were imaged with the MetaFluor Software (Molecular Devices) installed on the Zeiss Axio Observer Z1 inverted microscope (20x air objective). Neuronal excitability was assessed by filling the chamber with assay buffer (2 minutes, baseline), 1 minute 100 nM Capsaicin, 2 minute wash out (assay buffer 2 minutes), 1 minute 1 µM Capsaicin, 2 minutes wash out (assay buffer), 1 minute 60 mM KCl, wash out (assay buffer, 1 minute). Experiments were performed 20 hours after plating and cells from both genotypes were measured on the same day. Data was analyzed by assessing the percentage of neurons, which responded to the respective stimulus. A responder was considered positive when its amplitude peak was bigger than the baseline (5 values before given stimulus) plus 20 %. Furthermore, the mean amplitude of responders (peak amplitude-mean of baseline) was depicted (according to Avenali et al., 2014; Sondermann et al., 2018).

2.9.1 Ca^{2+}-Imaging upon TNFα Stimulation

DRG culture cells were stimulated with TNFα (100 ng/ml in PBS + 0.1 % BSA, known to promote ROS formation (Valko et al., 2007)) or vehicle (PBS + 0.1 % BSA) 16 h after plating. 500 µl medium (DMEM/F-12 + Glutamax + horse serum + NGF) was removed, supplemented with the respective substance and added back on cells. The stimulation was performed over a time period of 6 hours followed by Ca^{2+}-imaging (described above). Ca^{2+}-imaging was performed with the following protocol: 1 minute baseline (assay buffer), 2 minutes 30 µM mustard oil (MO), 2 minutes wash out

(assay buffer), 2 minutes 100 nM Capsaicin, 2 minutes wash out (assay buffer), 1 minute 60 mM KCl, 1 minute wash out (assay buffer) (adapted from Willemen et al., 2018).

3.0 Electrophysiology

Whole-cell voltage-clamp recordings were performed in order to assess the electrophysiological properties (i.e. mechanically activated (MA) currents, membrane potential, amplitude of action potential) of DRG neurons from naive TM KO vs. WT mice. For recording of MA currents the cells were clamped at -70 mV and mechanically stimulated with fire-polished borosilicate glass pipettes (3−5 MΩ resistance). In current-clamp mode, action potentials were recorded using a standard current injection protocol. Whole-cell currents and membrane potentials were recorded with an EPC10 USB amplifier and the PatchMaster software (HEKA Elektronik) and a piezoelectrically driven micromanipulator (Physik Instrumente GmbH&Co.KG) was used for stimulation delivery. 4 µm distance to the cell membrane was the starting position of the probe followed by mechanical stimuli from 0-6 µm in 1 µm increments. During the ramp phase (forward) the probe velocity was 0.8 µm/ms and 150 ms was the time set for stimulus duration (to allow for complete channel adaptation/current inactivation). 15 s were used as inter-stimulus interval and a series resistance lower than 10 MΩ was the requirement for cells to be considered for analysis.

Composition of recording solutions:

Intracellular: 133 mM CsCl, 10 mM HEPES, 5 mM EGTA, 1 mM $MgCl_2$, 1 mM $CaCl_2$, 4 mM MgATP and 0.4 mM NaGTP, pH 7.3, osmolarity = 280 mOsm.

Extracellular: 127 mM NaCl, 3 mM KCl, 1 mM $MgCl_2$, 2.5 mM $CaCl_2$, 10 mM Glucose and 10 mM HEPES, pH 7.3, osmolarity = 285 mOsm. Analysis and illustration was performed with FitMaster (HEKA) and Igor Pro (WaveMetrics). Experiments were performed by Dr. Pratibha Narayanan (according to Avenali et al., 2014, Narayanan et al., 2016).

3.1 Electron Microscopy (EM)

SN and DRG were dissected and post-fixed in 4 % fixing solution (Table 7: Tissue Fixation for Electron Microscopy, containing Karlsson and Schultz (1965), pH 7.4) for at least for 24 hours. Subsequently, tissue of interest was further post-fixed in 2 % osmium tetraoxide, dehydrated and embedded in epoxy resin (21.4 g glycid ether, 14.4 g DDSA, 11.3 g MNA, 0.84 ml DMP) (Table 8). Dehydration, epon infiltration and polymerization were automatically performed with the ASF II (Leica). Semithin (0.5 µm) and ultrathin (50 nm) cross sections of epon embedded SN and DRG were produced with an ultramicrotome (Ultracut S, Leica). Methylene blue/Azure II (1 minute) were used to stain sections for lipid rich tissue. 1 % uranyl acetate and lead citrate contrasted ultrathin sections. Images were taken with the EM912AB electron microscope (Zeiss) with an on-axis 2048 × 2048 charge coupled

device camera (Proscan). Experiments performed by me with the equipment and supervision from the electron microscopy core unit, MPI EM, PI Dr. Wiebke Möbius (according to Fünfschilling et al., 2012).

Table 7: Tissue Fixation for EM

Components	**10 ml fixing solution**
$NaH_2PO_4 \cdot H_2O$	0.018 g
$Na_2HPO_4 \cdot 2H_2O$	0.15 g
NaCl	0.05 g
A. dest.	5 ml
Glutaraldehyd (25 %)	1 ml
Formaldehyd (16 %)	2.5 ml
A. dest.	1.5 ml

Table 8: Epoxy Resin Embedding for EM

Substance	**Time**	**Temperature**
0.1 M Phosphate buffer (PB)	3x 10 min	4°C
2 % Osmium tetraoxide in 0.1 M PB	4 h	4°C
0.1 M Phosphate buffer	3x 10 min	4°C
30 % Ethanol	20 min	4°C
50 % Ethanol	20 min	4°C
70 % Ethanol	20 min	4°C
90 % Ethanol	20 min	4°C
100 % Ethanol	3x 10 min	4°C
2-Propanol	10 min	4°C
Propylene oxide	3x 10 min	RT
2:1 Propylene oxide : Epon	2 h	RT
1:1 Propylene oxide : Epon	2 h	RT
1:2 Propylene oxide : Epon	4 h	RT
Pure Epon	4 h	RT
Transfer to embedding molds	Polymerization: 24 h	60°C

3.2 Molecular Cloning

TM cDNA (Origene) was used as a template for cloning. The sequence was obtained from NCBI: NM_026938.1 (Mus musculus transmembrane protein 160 (Tmem160), mRNA). Primers were designed with BamHI (TTCGTCGACTGGATCCGGTAC) and Eco105I (CGTTACGTATTTAAACCTTATCGTCG TC) restriction sites to insert the PCR product into the pCMV6 vector for *in vitro* studies (pCMV6-TMEM160-Myc-DDK). For generation of TM KO mice a mus musculus BAC clone (AC164880) was used as vector for TM HDR.DNA. In order to visualize PCR products, agarose gel electrophoresis was performed, and bands excised. DNA purification was performed after manufacturer's instructions (NucleoSpin gel and PCR clean-up kit). Subsequently, insert and vector were digested (FastDigest restriction enzymes: BamHI, Eco105I in 1x green buffer, incubation at 37°C, 35 minutes). Dephosphorylation of vector by FastAP thermosensitive alkaline phosphatase followed (at 37°C, 35 minutes, to prevent self-ligation). The reaction was stopped by running the samples on an agarose gel. Bands were excised and product purified in the same way as described above. Mixture with T4 DNA ligase (1 U) in ligase buffer (1x) followed (at 25°C, 2 hours). Afterwards, DH5α E. coli competent cells (50 µl) and ligated DNA product (5 µl) was incubated on ice (30 minutes) followed by heat-shock transformation (at 42°C, 25 seconds in water bath, 2 minutes on ice). Subsequently, cells were incubated (at 37°C, 1 hour, shaking at 250 RPM) after addition of SOC medium (950 µl). Centrifugation of cells (6000 rpm, 1 minute), pellet re-suspension (200 µl SOC medium) and plating on LB agar plates (containing 100 µg/ml ampicillin) was performed. While shaking (250 rpm) plates were incubated overnight (at 37°C). 6 colonies were picked from the LB agar plate and cultured in LB medium (5 ml containing 100 µg/ml ampicillin). Overnight incubation followed (at 37°C, shaking 250 rpm) and finally culture (1 ml) was used for plasmid purification (Pure link HiPure plasmid filter maxiprep kit following manufacturer's instruction). Spectrophotometric analysis was performed to assess amount and purity of eluted DNA as well as verification of sequences by sequencing (according to Avenali et al., 2014). Performed by Sergej Zeiter and Fritz Benseler (DNA Core Facility AGCTLab, MPI EM).

Table 9: PCR Master Mix Cloning

Amount (µl)	Reagent
5.0	10x Reaction Buffer
1.5	10 mM dNTPs (each)
1.0	50 mM $MgSO_4$

3.0	Primer set (1.5 µl each)
1.0	DNA
38.1	H_2O
0.4	Polymerase: Platinum PFX
50.0 total	

Final concentration: 10x Reaction Puffer 1x, Mg 1.0 mM, dNTPs 0.3 mM each, DNA Pol. 1 U, Primer set 0.3 mM each, DNA 150 ng.

Table 10: PCR Cycle Cloning

Order	**Temperature (°C)**	**Time (min)**
1	94.0	3.0
2	94.0	0.25
3	55.0	0.5
4	68.0	1.16
5	68.0	10.0
6	4.0	∞

3.3 Mitochondrial Assays

3.3.1 Enzyme Activity Dipstick (Complex IV)

The enzyme activity dipstick was used according to manufacturer's instructions in order to quantify the activity of the cytochrome c oxidase (COX) enzyme complex (Complex IV of mitochondrial electron transport chain). A COX-specific antibody was immobilized on a dipstick, which enabled immuno-capturing of the enzyme complex. DAB (Di-amino benzidinetetrachloride) served as reporter of COX activity, meaning the greater the DAB signal (precipitated form) the more COX was present. The assay was performed on dissected DRG which were washed in 1x PBS followed by homogenization (pestle) in extraction buffer (provided in the kit, ~3 mg/mouse = 60 µl extraction buffer. Samples were incubated on ice for 20 minutes and centrifuged (18000 g) for 20 minutes at 4°C. Afterwards, the supernatant was transferred to a new tube and protein concentration was measured with a spectrophotometer. 1/10 volume detergent was added, 25 µg were aliquoted in duplicates and filled up with extraction buffer (buffer A) to a volume of 25 µl. A well (96-well microplate) was filled with 25 µl buffer A and 25 µl sample. Subsequently, the dipstick was added (~30 minutes) and washed by adding 30 µl buffer C. After preparation of activity buffer (1:5:94), 300 µl were pipetted into a separate empty well for each dipstick (incubation for 45-60 minutes). Subsequently, dipsticks were washed for 10 minutes in a well filled with deionized water (300 µl). After letting them dry for a few minutes, images were taken followed by analysis with Image J, according to manufacturer's instructions.

3.3.2 Isolation of Mitochondria

Tissue of interest (brain, heart, liver) was cut into pieces and homogenized (30x) in THE buffer (10 mM KCl, 10 mM Hepes-KOH (pH 6.9), 300 mM Trehalose) with BSA (0.1 %). Homogenizates were centrifuged (10 minutes, 4°C, 400 g) and supernatants were collected and re-suspended in THE buffer with BSA. Subsequently, the samples were homogenized again and the suspension was centrifuged (10 minutes, 4°C, 400 g). Supernatants were saved and spun down (5 minutes, 4°C, 800 g). The resulting supernatants were centrifuged again (10 minutes, 4°C, 10000 g) resulting in pellet formation containing mitochondria. Afterwards the pellet was re-suspended in THE buffer without BSA and centrifuged (5 minutes, 4°C, 10000 g). Finally, the resulting pellet was re-suspended in the proper amount of THE buffer (depending on pellet size). Protein concentrations were assessed with the Bradford analysis (BSA was used as standard). The experiments were either performed by Dr. Sven Dennerlein from the Department of Cellular Biochemistry, PI Prof. Dr. Peter Rehling, or by me (adapted from Bareth et al., 2016).

3.3.3 Seahorse Respiration of Isolated Mitochondria

The Seahorse XF Analyzer (Seahorse Bioscience, Billerica, MA) is a device, which provides information about mitochondrial respiration (oxygen consumption rate (OCR)) and glycolysis (extracellular acidification rate (ECAR)). Its basis is a well plate composed of a support plate (equipped with sensor cartridges and ports) and a cell plate filled with mitochondria in assay buffer. Each sensor cartridge is equipped with two fluorophores (embedded in polymer) at the bottom. One is quenched by O_2 and the other is sensitive to protons allowing for kinetic measurements (creating a microchamber by lowering the sensor cartridge 200 µm above mitochondria). The ports of the support plate allow injection of drugs (Oligomycin (4 µM), FCCP (2 µM), Antimycin (2 µM), Rotenone (2 µM), KCN (1 mM)). Baseline restoration was allowed whenever the system detects a drop in O_2 or H^+ by raising the sensor cartridge. In detail the ports of the support plate were loaded and kept at 4°C and equilibrated for 15 minutes before experiment was started at 37°C. Subsequently, 10x mitochondria solution was loaded (18 µl) into the chilled cell plate and spun down (20 minutes at 4°C). Afterwards, the instrument was equilibrated and MAS (Mitochondrial assay solution) buffer pipetted into each well (162 µl) followed by starting of the seahorse program (Table 15). The experiments were performed by Dr. David Pacheu Grau, Department of Cellular Biochemistry, PI Prof. Dr. Peter Rehling (adapted from Duggett et al., 2017; Ferrick et al., 2008).

Table 11: Mitochondrial Assay Solution

Components	**Concentration, pH 7.4**
Sucrose	70 mM
Mannitol	220 mM
HEPES	2 mM
KH_2PO_4	10 mM
$MgCl_2$	5 mM
EGTA	1 mM
BSA	0.2 %

Table 12: Mitochondrial Assay Compounds

Components	**Concentration, pH 7.4**
Succinate	1 M
ADP	80 mM
Ascorbate	0.2 M
TMPD	0.1 M

Oligomycin	10 mM
Antimycin A	10 mM
FCCP	5 mM
Rotenone	1 mM
KCN	1 M

Table 13: MAS Complex II

Components	**Conc. for 1 ml 10 x Solution in MAS**
Succinate	10 mM
ADP	4 mM
Rotenone	1 mM

Table 14: MAS Complex IV

Components	**Conc. for 1 ml 10 x Solution in MAS**
TMPD	0.2 mM
Ascorbate	10 mM
Antimycin A	4 µM

Table 15: Seahorse Program

Command	**Time (min)/Drug injection**
Calibrate	0.0
Equilibrate	---
Mix	1.0
Measure	2.0
Mix	3.0
Inject	Substrate
Mix	1.0
Measure	6.0
Mix	6.0
Inject	Oligomycin
Mix	1.0
Measure	6.0
Mix	3.0
Inject	FCCP

Mix	3.0
Measure	6.0
Mix	1.0
Inject	Antimycin A, Rotenone, KCN
Mix	3.0
Measure	6.0
End	

3.3.4 Blue Native PAGE of Electron Transport Chain Complexes

Post solubilization (described in 3.3.2) mitochondria were placed on ice (15 minutes) followed by centrifugation in order to remove non-soluble material (10 minutes, 4°C, 10000 g). Subsequently, the supernatant was transferred to 10x Blue Native (BN) loading dye (5 % Coomassie brilliant blue G-250, 500 mM 6-aminohexanoic acid, and 100 mM Bis-Tris, pH 7.0). Per lane 65 µl were loaded and separated on polyacrylamide gradient gels (4-13 %, 100 V overnight). Finally, the gel was incubated in SDS running buffer and blotted (300 mA, 2.5 hours). The experiments were performed by Dr. Sven Dennerlein from the Department of Cellular Biochemistry, PI Prof. Dr. Peter Rehling (according to Wittig et al., 2006).

3.3.5 Activity Staining of Electron Transport Chain Complexes

Activity staining of mitochondrial electron transport chain complexes was performed with mitochondria isolated from brain, heart and liver (TM WT vs. KO). After mitochondria solubilization (described in 3.3.2), incubation on ice (15 minutes) and centrifugation (10 minutes, 4°C, 10000 g), the supernatant was transferred to 10x BN loading dye (5 % Coomassie brilliant blue G-250, 500 mM 6-aminohexanoic acid, and 100 mM Bis-Tris, pH 7.0). Gel lanes were loaded with 50 µg (CI, CII, CV) or 100 µg (CIV) mitochondria solution including dye (600 V, 15 mA per gel during the day, until red front was running out plus 1 hour). Subsequently, activity staining was performed at 30°C:

Complex I: gel stripes were incubated for 15 minutes in 30 ml 5 mM Tris / HCl (pH 7.4) and stained in 30 ml 5 mM Tris/HCl (pH 7.4), 20 mg NBT, 300 µl NADH (stock 100x = 10 mg/ml) (for 30 minutes).

Complex II: gel stripes were incubated for 15 minutes in 30 ml 5 mM Tris / HCl (pH 7.4) and stained in 30 ml 5 mM Tris/HCl (pH 7.4), 20 mg NBT, 600 µl Succinate (stock 50x = 1 M), 60 µl PMS (stock 100 mM in DMSO) (for 30 minutes).

Complex IV: gel stripes were incubated for 15 minutes in 30 ml 50 mM KPi (pH 7.2) and stained in 30 ml 50 mM KPi (pH 7.2), 15 mg DAB, 3 ml cytochrome C (-80°C) (for > 12 hours).

Complex V: gel stripes were incubated for 2 hours in 35 mM Tris-Base, 220 mM Glycine (TG-buffer:

1050 µl 1 M Tris-Base (no pH adjusted), 6600 µl 1 M Glycine (no pH adjusted), H_2O to 30 ml (check pH with pH-strips) (pH 8.3) and stained in TG buffer, 600 µl ATP (stock 50x = 0.4 M), 420 µl 1 M $MgSO_4$, 300 µl $Pb(NO_3)_2$ (stock 100x = 20 % w/v) (for a few hours at 30°C). Activities of complexes were assessed spectrophotometrically using a Cary 50 Bio UV/Vis spectrophotometer. The experiments were performed by Dr. Sven Dennerlein from the Department of Cellular Biochemistry, PI Prof. Dr. Peter Rehling (according to Deckers et al., 2014; Wittig et al., 2007).

3.4 Statistics

All statistical analyses were performed with the Graph Pad Prism 8 software (San Diego, CA). The two-tailed unpaired Student's t-test was used for comparisons between two conditions at one time point. One-way ANOVA was applied for more than two groups at one testing time point followed by Sidak's Multiple Comparison test. The Friedman test followed by Dunn's Multiple Comparison test was used for different testing time points within the same group (non parametric data). The two-way ANOVA was utilized for two or more groups and multiple testing time points followed by Sidak's Multiple Comaprison test. When absolute values were depicted (population proportions: responders vs. non-responders Ca^{2+}-imaging) the Fisher's exact test was employed and the one-sample t-test was used for qRT-PCR results (compared to a theoretical value of 1.0). The values are depicted as mean ± SEM, N indicates the number of mice, n represents the sample/ cohort number, the significance is depicted as asterisk or number sign (* < p 0.05, ** < p 0.01, *** < p 0.001, **** < p 0.0001 or # < p 0.05, ## < p 0.01, ### < p 0.001, #### < p 0.0001).

The data depicted in Figure 9 A, was calculated with the median as the data was non parametric. However, in order to standardize the illustration of the data I decided to show the mechanical and thermal testing results in line with the other data from section 3.1.5 as mean ± SEM. The Friedman test followed by Dunn's multiple comparison tests was chosen as proper statistical test for non parametric data (pre vs. post surgery days, only possible within the same genotype). Nevertheless, the Friedman test was not suitable for a comparison of several testing days across genotypes. For this reason, the 2-way ANOVA followed by Sidak's Multiple comparison tests was used to assess the differences between the mouse lines at all testing days. Even though the 2-way ANOVA was not the appropriate test, because it was only suitable for parametric data it appeared robust, because it underscored the Friedman test results showing no significant difference in SNI TM KO mice at pre vs. POD 7 by indicating a significant difference for SNI TM KO vs. SNI WT (POD 7).

3. RESULTS

3.1 Functional Characterization of TM in Regard to Somatosensation and Chronic Pain

3.1.1 Differential TM Expression during Chronic Pain

The unbiased proteomics screen (Rouwette et al., 2016) revealed the hitherto uncharacterized transmembrane protein Tmem160 (TM). It was shown to be downregulated in DRG after induction of inflammatory (CFA model) and neuropathic pain (SNI model) and had not been associated with chronic pain before. In order to examine whether TM mRNA levels were comparable to the differential regulation on protein level, qRT-PCR was performed. However, TM mRNA was upregulated under inflammatory pain conditions in lDRG (lumbar dorsal root ganglia), whereas TM levels were decreased in SN (sciatic nerve) after CFA injection as it was seen by proteomics. These results were not surprising, given the restricted correlation between mRNA and protein changes, as protein variability is the final indicator for gene expression, translation and regulation (Liu et al., 2016; Schwanhäusser et al., 2011; Sharma et al., 2015). This knowledge was the initial motivation to perform the screen for changes on protein level (Rouwette et al., 2016) in order to study the molecular underpinnings of chronic pain more accurately.

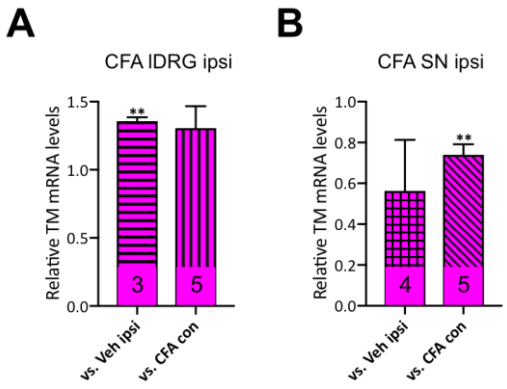

Figure 5: TM Expression Levels during Inflammatory Pain

(A, B) qRT-PCR outcomes displayed relative TM mRNA expression levels in lDRG and SN 1 day post CFA injection. (A) Increased TM expression in lDRG ipsi compared to lDRG Veh ipsi. A similar trend was seen in lDRG ipsi vs. lDRG con. (B) TM mRNA levels were decreased in SN of CFA injected mice. SN CFA ipsi vs. Veh ipsi revealed a trend for reduction and SN CFA ipsi vs. CFA con indicated a significant downregulation. Number of animals in column; data collected from several independent experiments; the one sample t-test; ** $p < 0.01$. Data were represented as mean ± SEM. lDRG, lumbar dorsal root ganglia; SN, sciatic nerve; ipsi, ipsilateral; con, contralateral; CFA, Complete Freund's Adjuvant; Veh, vehicle.

3.1.2 Localization of TM in Mitochondria

TM has a theoretical topology of 3 transmembrane domains (TMD, Figure 6 A) and bioinformatics analyses suggested a mitochondrial localization (Uniprot, https://www.uniprot.org/uniprot/Q9D938). Further investigation of the amino acid sequence revealed a 98.68 percent probability for TM to be exported from the cytosol to mitochondria (signal peptide for import indicated in Figure 6 A, MitoProt II - v1.101, https://ihg.gsf.de/ihg/mitoprot.html, Claros and Vincens, 1996). The unbiased proteomics screen (Rouwette et al., 2016) was performed on membrane enriched lumbar DRG (lDRG) lysates. The obtained membrane proteins were expressed in sensory neurons and additional cell types of DRG (e.g. peripheral glial cells and diverse immune cells). Therefore, I investigated the localization of TM in sensory neurons (DRG culture, Figure 6 C) and Schwann cells (SC, peripheral glial cells, Figure 6 D) by overexpression and immunolabeling (latter experiments performed by Dr. Luca Avenali (former colleague) and Dr. Susanne Quintes, Department of Neurogenetics, PI Prof. Klaus-Armin Nave, Ph.D). Furthermore, TM was overexpressed and labeled in HEK293 cells (Figure 6 B) in order to examine whether it was ubiquitously expressed in mitochondria. The hypothesis could be proofed for all investigated cell types.

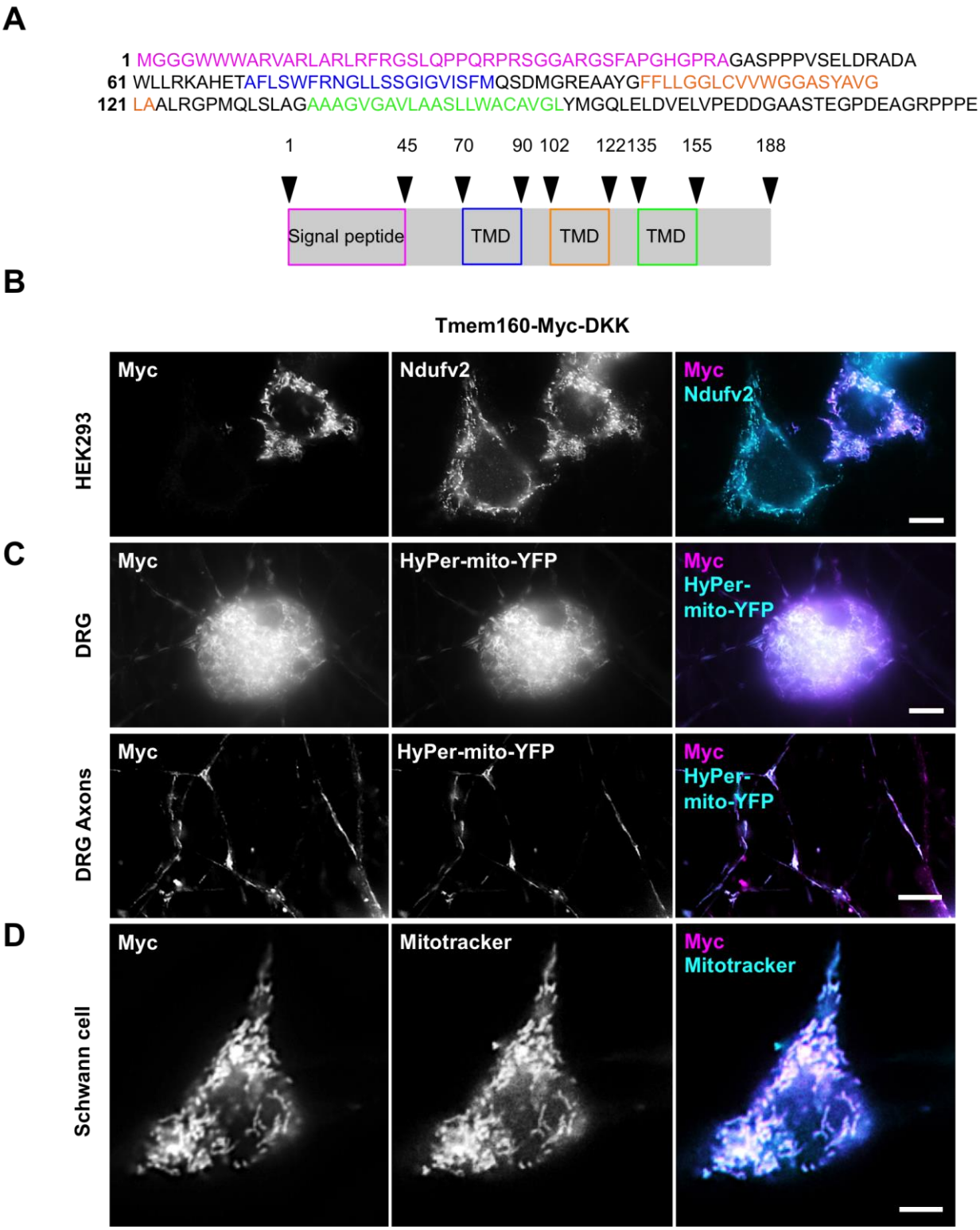

Figure 6: Ubiquitous TM Expression in Mitochondria

(A) TM protein organization with predicted signal peptide (indicated in pink) for import from cytosol into mitochondria and transmembrane domains (TMD 1-3 depicted in blue, orange, green; numbers indicate amino acid residues). (B-D) Representative immunocytochemistry for co-labeling of TM (myc staining) with mitochondrial markers. (B) HEK293 cell culture, (C) DRG culture and (D) SC culture (latter experiments performed by Dr. Luca Avenali (former colleague) and Dr. Susanne Quintes, Department of Neurogenetics, PI Prof. Klaus-Armin Nave, Ph.D) transfected with 0.5 µg TM-myc-plasmid (pCMV6-TMEM160-Myc-DDK) depicted

in magenta. Co-staining with mitochondrial markers shown in cyan (HEK293 cell culture: Ndufv2 (NADH:ubiquinone oxidoreductase core subunit v2, subunit CI), DRG culture: 0.5 µg HyPer-mito-YFP plasmid (kindly provided by Department of Metabolic and Redox Signaling, PI Prof. Dr. Michael Müller), SC culture: Mitotracker) showed TM localization in mitochondria. N = several coverslips from 3 independent HEK293 cell cultures; scale bar, 10 µm. N = several coverslips from 4 independent DRG cultures; scale bar, 10 µm. N = several coverslips from 2 independent SC cultures; scale bar, 5 µm. DRG, dorsal root ganglia; SC, Schwann cells.

3.1.3 Successful Generation of TM KO Mice

In order to assess the relevance of TM *in vivo*, KO mice were generated by deletion of Exon 1 (Figure 7). The CRISPR/Cas9 technology (in collaboration with the DNA core and transgenic facilities of the MPI EM) was used to insert the *loxP* sites for conditional TM removal. TM was shown to be expressed in sensory neurons and SC. Therefore, respective KO lines were bred, composed of a constitutive KO line (cTMEM160_cKO r/r x Ella Cre = referred to as TM KO), a SC specific KO line (cTMEM160_cKO r/r x Dhh Cre = referred to as cKO in SC) and a sensory neuron specific KO line (cTMEM160_cKO r/r x Advillin Cre = referred to as cKO in SeN). Successful TM deletion in the sensory neuron specific KO was validated by genotyping. For the constitutive and SC specific KO, qRT-PCR and *in situ* hybridization (ISH) (RNAscope 2.5 HD Detection Kit) were performed in addition for validation purposes (Figure 7). The ISH results showed an equal TM mRNA expression in DRG subpopulations of WT mice, which was in line with RNA sequencing data from (Usoskin et al., 2015). In addition, I could show TM expression in SC.

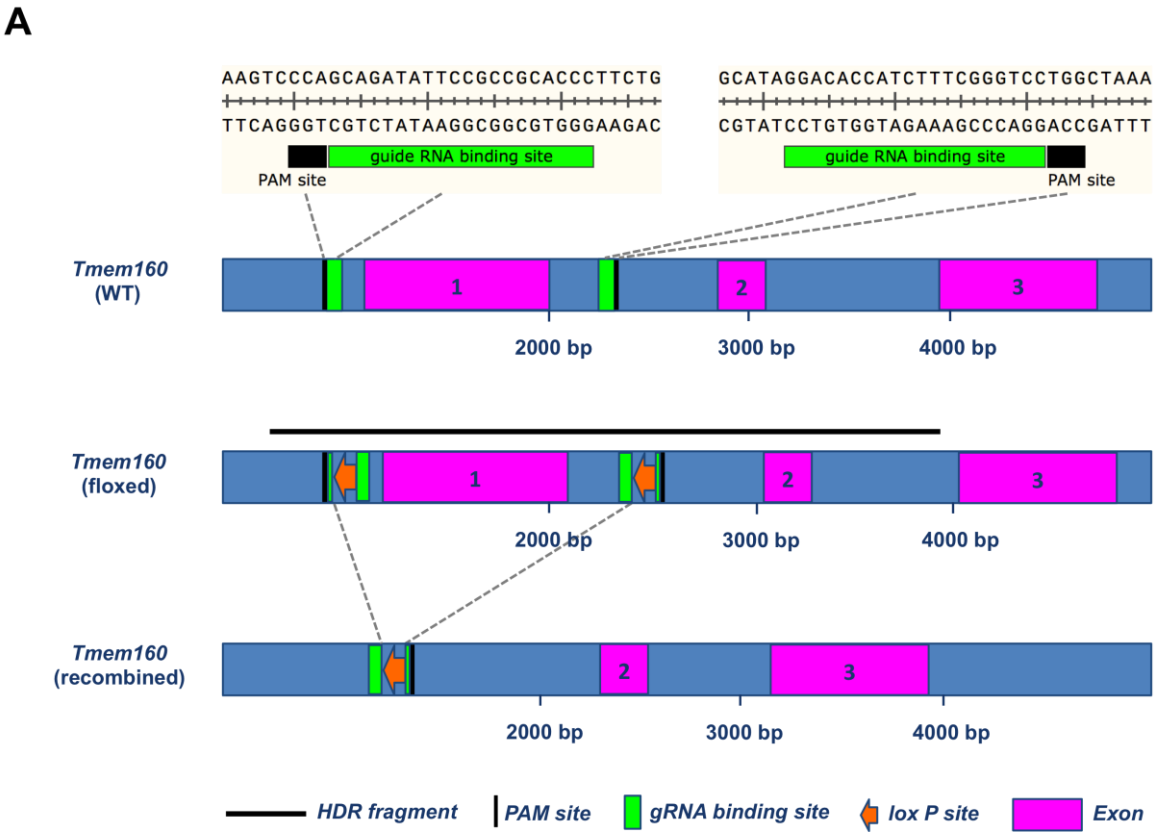
A
AAGTCCCAGCAGATATTCCGCCGCACCCTTCTG
TTCAGGGTCGTCTATAAGGCGGCGTGGGAAGAC
guide RNA binding site
PAM site
GCATAGGACACCATCTTTCGGGTCCTGGCTAAA
CGTATCCTGTGGTAGAAAGCCCAGGACCGATTT
guide RNA binding site
PAM site
Tmem160 (WT)
1
2
3
2000 bp
3000 bp
4000 bp
Tmem160 (floxed)
1
2
3
2000 bp
3000 bp
4000 bp
Tmem160 (recombined)
2
3
2000 bp
3000 bp
4000 bp
HDR fragment
PAM site
gRNA binding site
lox P site
Exon

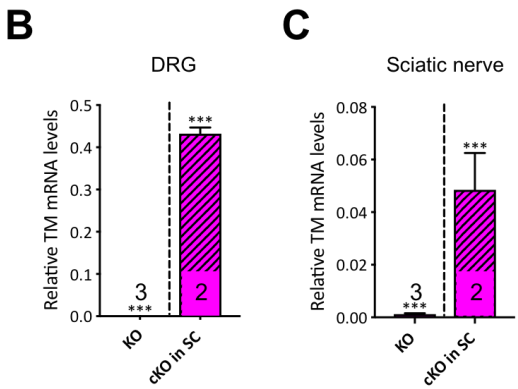
B
DRG
Relative TM mRNA levels
0.5
0.4
0.3
0.2
0.1
0.0
***
***
3
2
KO
cKO in SC
C
Sciatic nerve
Relative TM mRNA levels
0.08
0.06
0.04
0.02
0.00
***
***
3
2
KO
cKO in SC

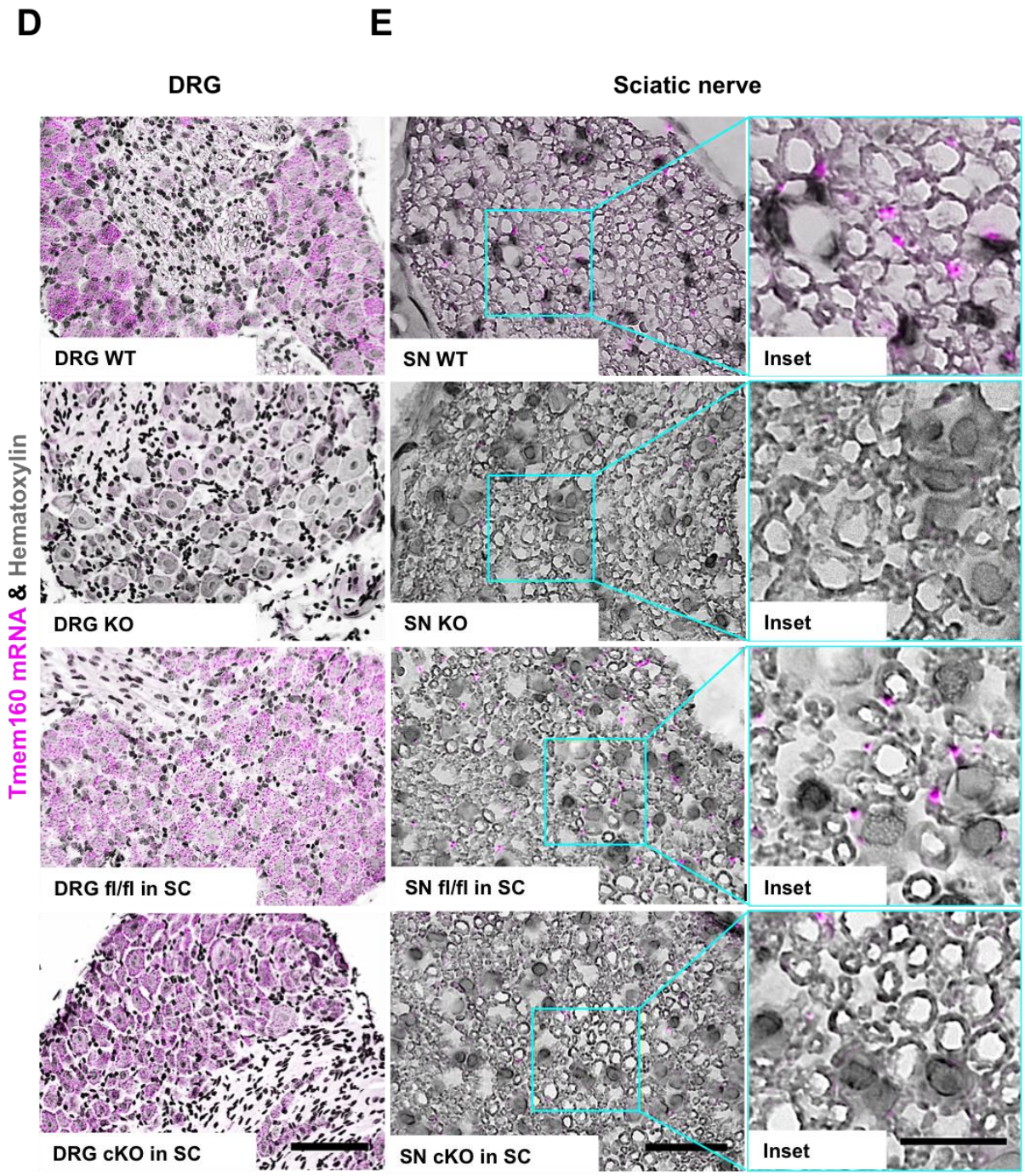

Figure 7: Successful Generation and Validation of TM Deletion in KO Mice

(A) Schematic illustration of TM WT, TM floxed and TM sequence after recombination. The homology-directed repair (HDR) fragment, including PAM sites (black), single guide RNA target nucleotides (green), lox P sites (orange) and Exons (pink) is marked with a black bar. Not drawn to scale. (B, C) qRT-PCR results showed relative TM expression normalized to Actin. (B) 99 % decrease of TM expression in DRG of constitutive KO mice and 70 % TM reduction in SC specific KO's. (C) Reduction of TM levels in SN of constitutive KO's to 99 % and in SC specific KO's to 95 %. (D, E) Representative images of *in situ* hybridization on WT DRG and WT SN cross-sections showed TM expression in all sensory neurons of DRG and in SC of SN. Declined TM mRNA staining in constitutive and SC specific KO's underscores qRT-PCR results. WT: TM wt Ella cre tg, female, 7w; KO: TM r/r

Ella cre tg, female, 7w; fl/fl in SC: TM wt Dhh tg, female, 7w; cKO in SC: TM r/fl Dhh tg, female, 7w; Dhh (Desert hedgehog) cre: SC specific KO (recombination E11-E13.5); Ella cre: constitutive KO: recombination E0.5. 5 µm paraffin slices, 50 % hematoxylin to stain nuclei. qRT-PCR: Number of animals in column; data collected from several independent experiments; *in situ* hybridization: N = 1-2 mice; scale bar, 100 µm (inset, 50 µm); the one sample t-test; *** $p < 0.001$. Data were represented as mean ± SEM. DRG, dorsal root ganglia; SC, Schwann cells; SN, sciatic nerve; HDR, homology-directed repair; PAM site, protospacer adjacent motif; gRNA, guide RNA.

3.1.4 No Myelination Deficit in Consequence of TM Removal

After the successful generation of TM KO mice the general wellbeing (birth rate, size, weight) and motor coordination (latter investigated with the Rotarod device) of the transgenic mice were assessed. A longitudinal investigation (age 8-19 and 32-46 weeks) revealed intact motor abilities (Figure 8 A), which were in line with no major changes in myelin and SC markers in SN examined via qRT-PCR (Figure 8 B). Further analysis of the myelin sheath by electron microscopy (Figure 8 C) and induction of myelination in SC-DRG coculture (Figure 8 D-F) showed no abnormalities and therefore underscored the behavioral results.

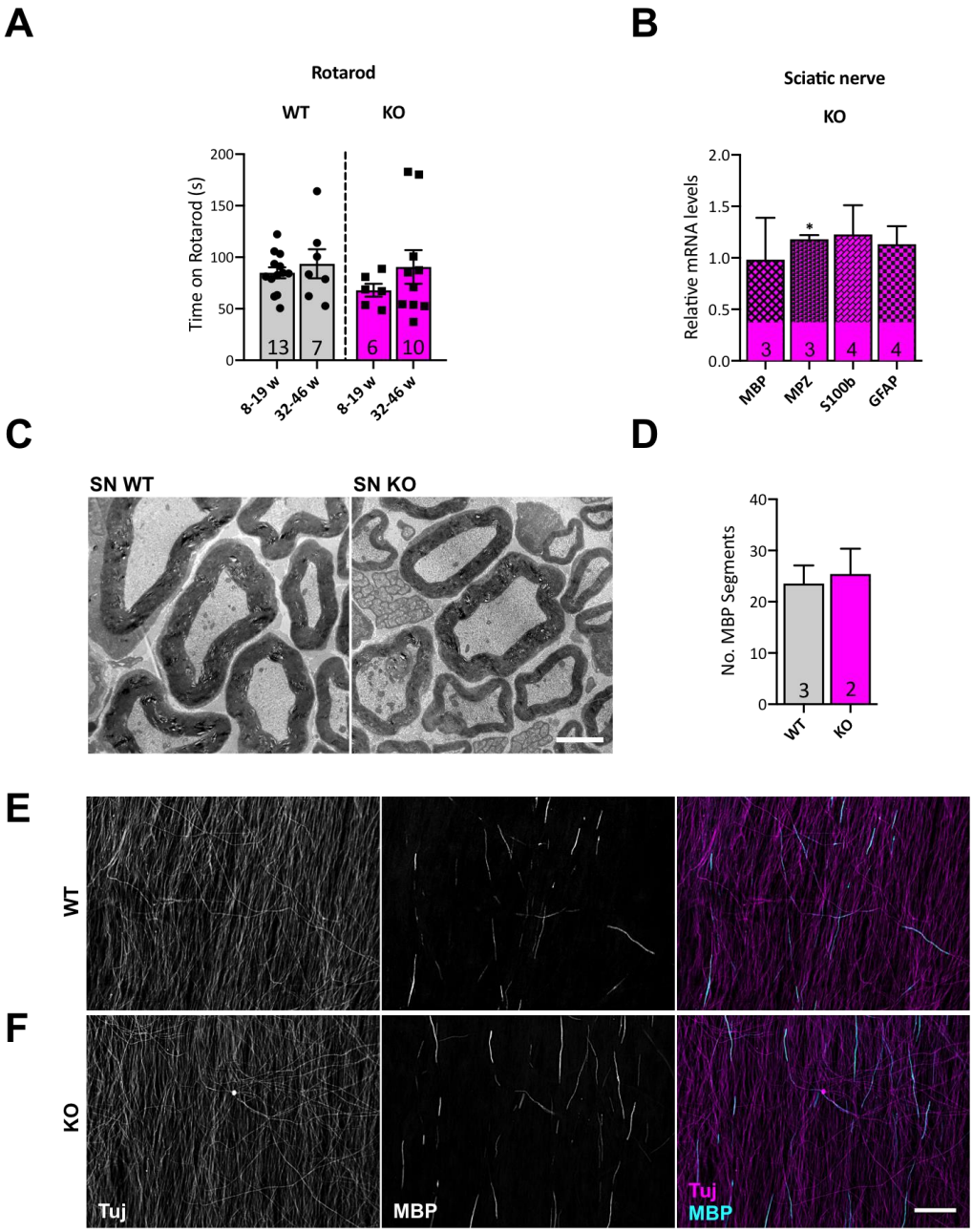

Figure 8: No Hint for Myelination Deficit in TM KO Mice

(A) Longitudinal investigation of TM KO mice (8-46 weeks) revealed no motor impairment. Number of animals in column; n = 4 independent cohorts; 2-way ANOVA followed by Sidak's multiple comparison tests. Data were represented as mean ± SEM. (B) qRT-PCR results showed relative expression of myelin and SC markers normalized to GAPDH. No major changes in mRNA levels of MBP, MPZ, S100b and GFAP in SN of TM KO mice. Number of animals in column; data collected from several independent experiments; the one sample t-test; * $p < 0.05$. Data were represented as mean ± SEM. (C) Representative electron microscope images showing no overt changes in myelin sheath ultrastructure in SN of TM KO compared to WT mice. WT N = 2; KO N = 2; Scale bar, 2.5 µm. (D-F) Similar number of MBP segments in SC-DRG coculture upon induction of myelination compared between genotypes. Number of independent cultures in column, several coverslips/ culture; unpaired student's t-test. Data were represented as mean ± SEM; scale bar, 20 µm. DRG, dorsal root ganglia; SN, sciatic nerve; SC, Schwann cells; MBP, myelin basic protein; MPZ, myelin protein zero; S100b, calcium

binding protein B expressed in SC (promyelination factor); GFAP, glial fibrillary acidic protein (marker for immature SC, negative regulator of SC differentiation); Tuj1, β-Tubulin 3.

3.1.5 TM Deletion results in Pain Modality specific Analgesia

A battery of behavioral paradigms was performed in order to investigate the role of TM in regard to PNS (peripheral nervous system) function and pain pathology. Intact gait properties of TM KO mice were shown with the Catwalk system (experiments performed by Dr. Daniel Segelcke, Group of Translational Pain Research, PI Prof. Esther Pogatzki-Zahn) (Figure 9 H, J, L, N Sham values). Moreover, no difference in basal mechanical and thermal (heat) sensitivity as well as non-evoked pain could be shown in healthy TM KO mice (Figure 9 B, D, F Sham values). Given the comprehensive proteome profiling (Rouwette et al., 2016), which showed a downregulation of TM under inflammatory and neuropathic pain conditions, these pain entities were induced in TM KO and WT littermates. Induction of neuropathic pain conditions (SNI model) and behavioral testing was performed by Dr. Daniel Segelcke (Figure 9). Inflammatory pain was induced by CFA injection in both mouse lines followed by behavioral phenotype investigation (mechanical and thermal testing performed by me, Figure 9 A, B; non-evoked pain and assessment of gait properties carried out by Dr. Daniel Segelcke, Figure 9 C-G). Interestingly, TM KO mice showed a significantly reduced tactile hypersensitivity under early neuropathic pain conditions (post operation day (POD) 7), when inflammation was most prominent (Cobos et al., 2018a). However, hypersensitivity at POD 14, POD 21 and POD 28 was not different compared to WT littermates (Figure 9 A, B). Furthermore, no major changes (no biological relevance for decreased withdrawal latency at POD 21 in SNI TM KO, because no significant difference among genotypes) in the reaction to a heat stimulus could be examined during all assessed testing days (Figure 9 C-D). WT mice did not show thermal hypersensitivity after induction of neuropathic pain. This pain modality is a less constant index for nociceptive responses after SNI than mechanical hypersensitivity (Decosterd and Woolf, 2000; Koltzenburg, 1998). In addition, the investigation of non-evoked pain revealed a similar decrease in the ratio of paw contact area (operated/non-operated paw) compared to pretesting values among genotypes (Figure 9 E, F).

Moreover, movement-evoked pain was assessed with the Catwalk system (Noldus), capable for the investigation of a dozen gait parameters. Pitzer et al. showed 6 specific parameters affected by neuropathic pain (SNI model) (Pitzer et al., 2016b). Based on this study our collaboration partner Dr. Daniel Segelcke decided to investigate the mentioned key features (4 of them depicted in Figure 9 (SNI model) and in Figure 10 (CFA model, mentioned below in detail)). The 4 illustrated parameters were static (print area: surface of the complete print of a paw; stand: duration of ground contact for a single paw) and dynamic parameters (swing speed: velocity (distance/ time) when the paw was not

in contact with the glass plate; duty cycle: duration of paw contact divided by time between consecutive paw contacts). The analysis revealed a similar decrease in the ratio for all investigated static parameters among genotypes after induction of neuropathic pain compared to pretesting values (Figure 9 G-J). However, dynamic parameters were improved in SNI TM KO mice compared to pretesting values (Figure 9 K-N). Nevertheless, a biological relevance was not hypothesized given that no significant difference among genotypes was shown for all tested gait features (Figure 9 G-N). Furthermore, in addition to TM KO mice inflammatory pain was also evoked in TM cKO in SeN (TM KO in sensory neurons) allowing for assessment of cell type specific TM contribution to somatosensory behaviors. Remarkably, both KO lines showed an impairment of mechanical hypersensitivity during inflammatory pain (analgesia) at day 1 and 3 post CFA injection (TM KO, Figure 10 A) and at day 1 post CFA (TM cKO in SeN, Figure 12 A), while thermal hypersensitivity was unaffected in both KO lines (TM KO: Figure 10 B, TM cKO: Figure 12 B). It was unusual to detect mechanical hypersensitivity only at 1 day post CFA but not at 3 days post CFA in WT littermates of TM cKO mice (Figure 12 A). I expected to investigate the effect also at 3 days post CFA as WT littermates of TM KO mice showed mechanical hypersensitivity (Figure 10 B). However, biological variability of mice and the use of different CFA batches could lead to shortened mechanical hypersensitivity in WT littermates in Figure 12 A. It was also noticeable, that the thermal hypersensitivity was present in TM WT and KO mice even after 6 days post CFA (Figure 10 B), whereas this hypersensitivity was only revealed at post CFA day 2 in the WT littermates of TM cKO mice (Figure 12 B). Nevertheless, the slight difference in CFA effectiveness did not negate the fact that TM KO as well as TM cKO showed decreased mechanical hypersensitivity and intact thermal hypersensitivity compared to WT controls (Figure 10 A, B and Figure 12 A, B). As investigated during chronic pain (Figure 9), CFA-treated TM KO mice were additionally investigated for potential alterations in other pain modalities. Non-evoked pain testing showed similar results for TM WT and KO mice (Figure 10 C) as well as in regard to movement-evoked pain (Figure 10 D-G). However, it is important to mention that there was no significant reduction in the ratio of all assessed static and dynamic parameters in WT mice injected with CFA (1-14 days post CFA vs. pretesting values). However, Pitzer et al. could show a decrease in static gait parameters (e.g. print area and paw pressure) in the CFA model. These values were investigated with the dynamic weight bearing (DWB) and the Catwalk system revealing a high degree of comparability (Pitzer et al., 2016a). Other studies underscored the results as they indicated a similar decrease in static parameters with the DWB system upon CFA injection (Cobos et al., 2012; Huntjens et al., 2009). Additionally, Pitzer et al. were able to demonstrate alterations in dynamic gait parameters in the CFA model with the Catwalk system and claimed the detailed gait analysis as important paradigm to assess changes upon inflammation (Pitzer et al., 2016a). However, we were not able to reproduce those findings with our

mouse models. Possible explanations could be different mouse strains (Pitzer et al. used C57BL/6N mice), the pain model (Pitzer et al. injected 10 µl CFA more) or the investigation time point (Pitzer et al., 2016a). Nevertheless, most importantly, no significant difference among genotypes was revealed for all tested days (Figure 10 D-G). Furthermore, the investigated behavioral phenotype of TM KO mice was specific for chronic pain conditions, as physiological pain assessed by the injection of the TRPV1 agonist capsaicin elicited mechanical hypersensitivity and acute pain behavior (time spent licking, flicking and lifting of the paw) equally in TM KO and WT mice (Figure 11).

Collectively, these results suggested a modality-specific TM involvement in inflammatory signaling pathways during early neuropathic and inflammatory pain. It was shown that a sensory neuron specific TM KO was sufficient to evoke the same phenotype during inflammatory pain as investigated in the constitutive TM KO.

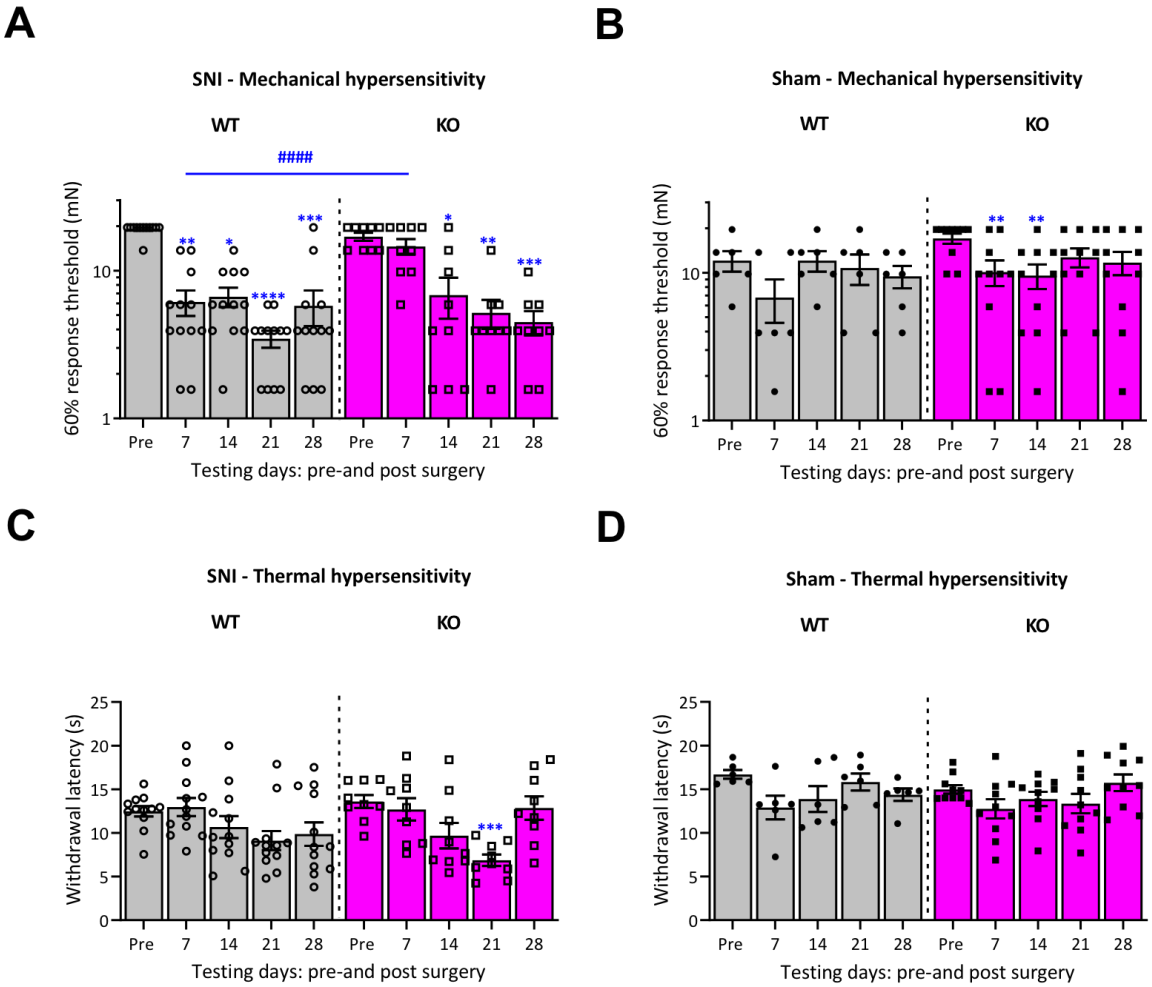

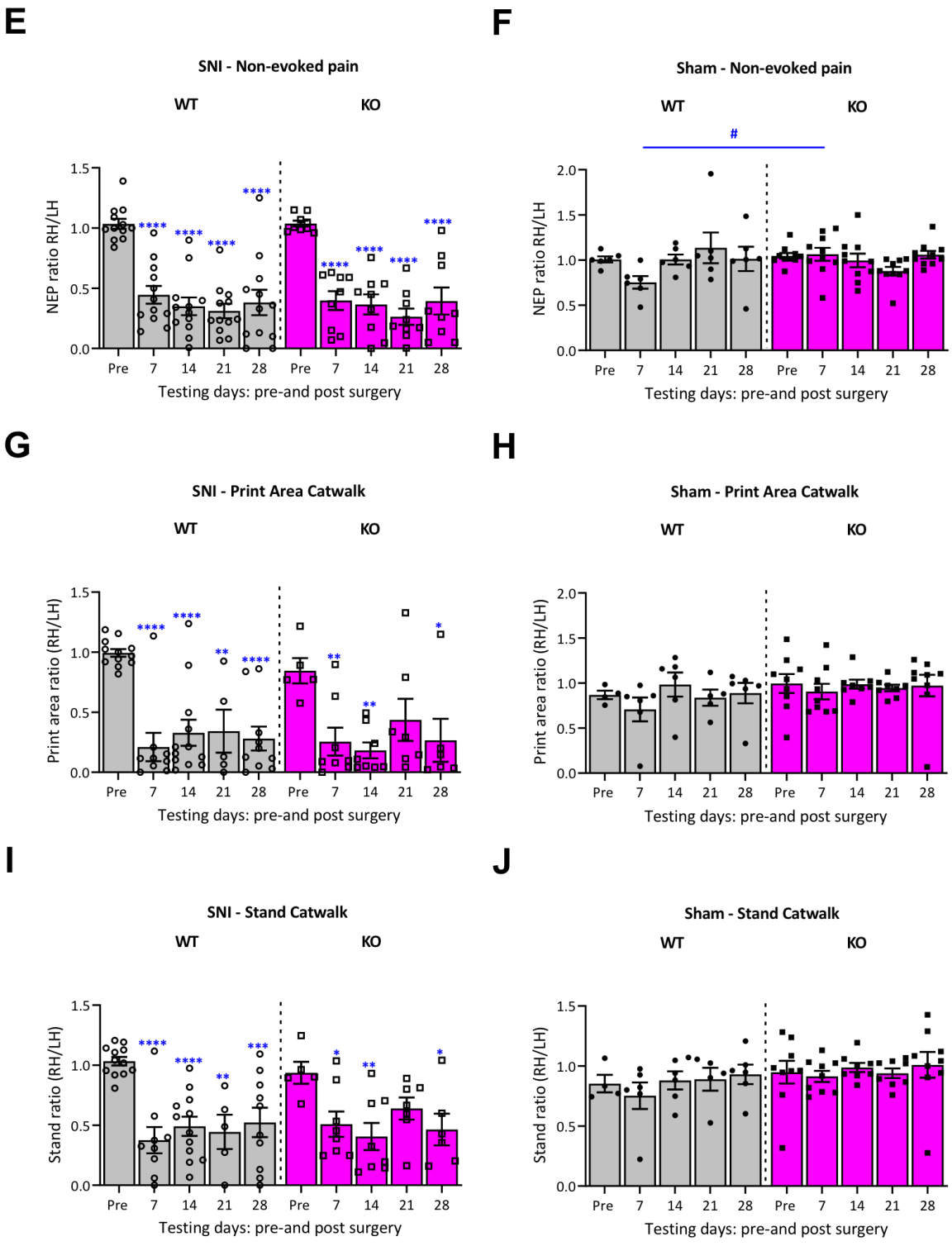
E
SNI - Non-evoked pain
WT
KO
NEP ratio RH/LH
Testing days: pre-and post surgery
F
Sham - Non-evoked pain
WT
KO
#
NEP ratio RH/LH
Testing days: pre-and post surgery
G
SNI - Print Area Catwalk
WT
KO
Print area ratio (RH/LH)
Testing days: pre-and post surgery
H
Sham - Print Area Catwalk
WT
KO
Print area ratio (RH/LH)
Testing days: pre-and post surgery
I
SNI - Stand Catwalk
WT
KO
Stand ratio (RH/LH)
Testing days: pre-and post surgery
J
Sham - Stand Catwalk
WT
KO
Stand ratio (RH/LH)
Testing days: pre-and post surgery
Pre
7
14
21
28

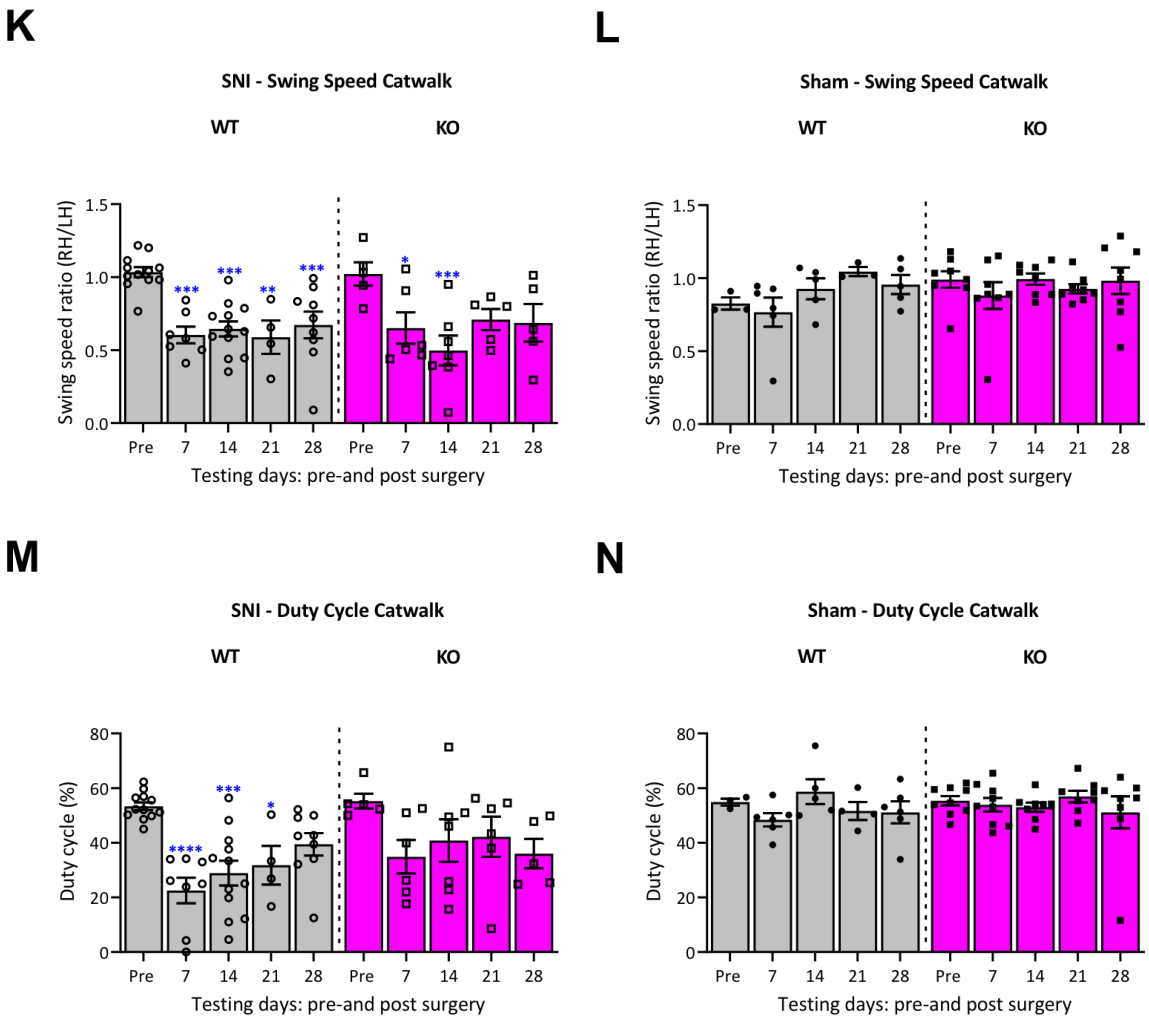

Figure 9: Pain-Modality Specific Phenotype after TM Deletion *in Vivo*

TM KO mice revealed no mechanical hypersensitivity during neuropathic pain (7 days post SNI), whereas thermal sensitivity was unaltered. (A-N) Behavioral paradigms performed with SNI and Sham mice. (A) Mechanical hypersensitivity attenuation in TM KO SNI model at POD 7 compared to pretesting values (when inflammation was most prominent (Cobos et al., 2018)). Significant difference between genotypes at POD 7. (B) Sham mice did not show overt mechanical hypersensitivity. (C, D) No major change in thermal sensitivity in both genotypes after SNI and Sham. (E, F) Unimpaired NEP behavior in TM KO mice. (G-N) Movement-evoked pain assessed by the catwalk paradigm revealed slightly improved gait properties in TM KO mice after SNI surgery compared to pretesting values, but no significant difference between genotypes. (A-N) Experiments performed by Dr. Daniel Segelcke, Group of Translational Pain Research (PI Esther Pogatzki-Zahn). WT SNI N = 12; KO SNI N = 9; n = 3 independent cohorts; WT Sham N = 6; KO Sham N = 10; n = 4 independent cohorts; (A, B) the Friedman test followed by Dunn's multiple comparison tests; * $p < 0.05$ vs. pre, ** $p < 0.01$ vs. pre, *** $p < 0.001$ vs. pre; **** $p < 0.0001$ vs. pre; 2-way ANOVA followed by Sidak's multiple comparison tests; #### $p < 0.0001$ WT vs. KO. Data were represented as mean ± SEM. (C-N) 2-way ANOVA followed by Sidak's multiple comparison tests; * $p < 0.05$ vs. pre, ** $p < 0.01$ vs. pre, *** $p < 0.001$ vs. pre; **** $p < 0.0001$ vs. pre; # $p < 0.05$ WT vs. KO. Data were represented as mean ± SEM. SNI, spared nerve injury; Sham, Sham nerve injury; NEP, non-evoked pain; RH, right hind paw = operated paw.

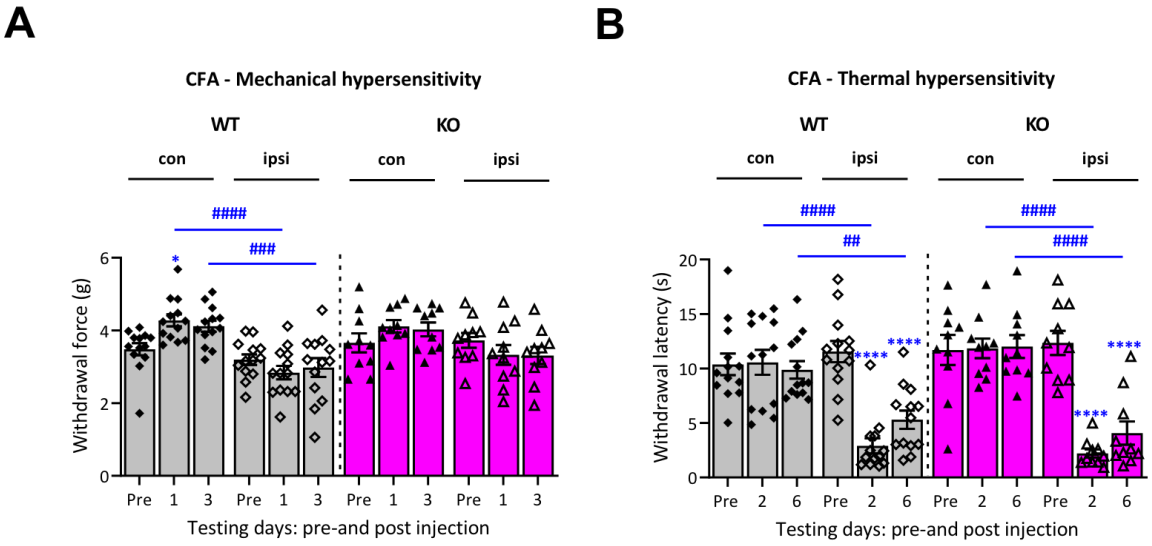
A
CFA - Mechanical hypersensitivity
WT
KO
con
ipsi
con
ipsi
####
###
*
Withdrawal force (g)
0
2
4
6
Pre 1 3 Pre 1 3 Pre 1 3 Pre 1 3
Testing days: pre-and post injection
B
CFA - Thermal hypersensitivity
WT
KO
con
ipsi
con
ipsi
####
##
####
####
****
****
****
****
Withdrawal latency (s)
0
5
10
15
20
Pre 2 6 Pre 2 6 Pre 2 6 Pre 2 6
Testing days: pre-and post injection

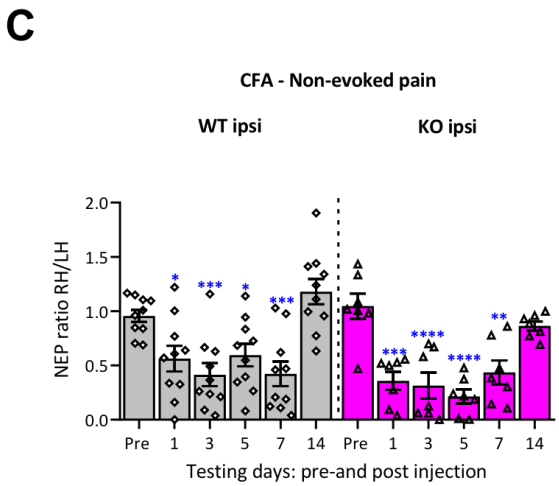
C
CFA - Non-evoked pain
WT ipsi
KO ipsi
*
***
*
***
***
****
****
**
NEP ratio RH/LH
0.0
0.5
1.0
1.5
2.0
Pre 1 3 5 7 14 Pre 1 3 5 7 14
Testing days: pre-and post injection

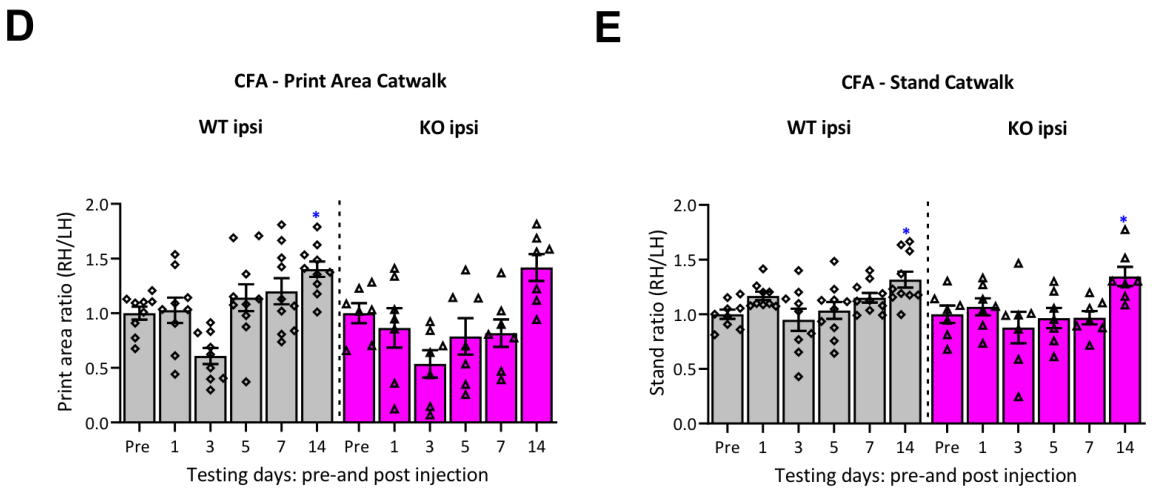
D
CFA - Print Area Catwalk
WT ipsi
KO ipsi
*
Print area ratio (RH/LH)
0.0
0.5
1.0
1.5
2.0
Pre 1 3 5 7 14 Pre 1 3 5 7 14
Testing days: pre-and post injection
E
CFA - Stand Catwalk
WT ipsi
KO ipsi
*
*
Stand ratio (RH/LH)
0.0
0.5
1.0
1.5
2.0
Pre 1 3 5 7 14 Pre 1 3 5 7 14
Testing days: pre-and post injection

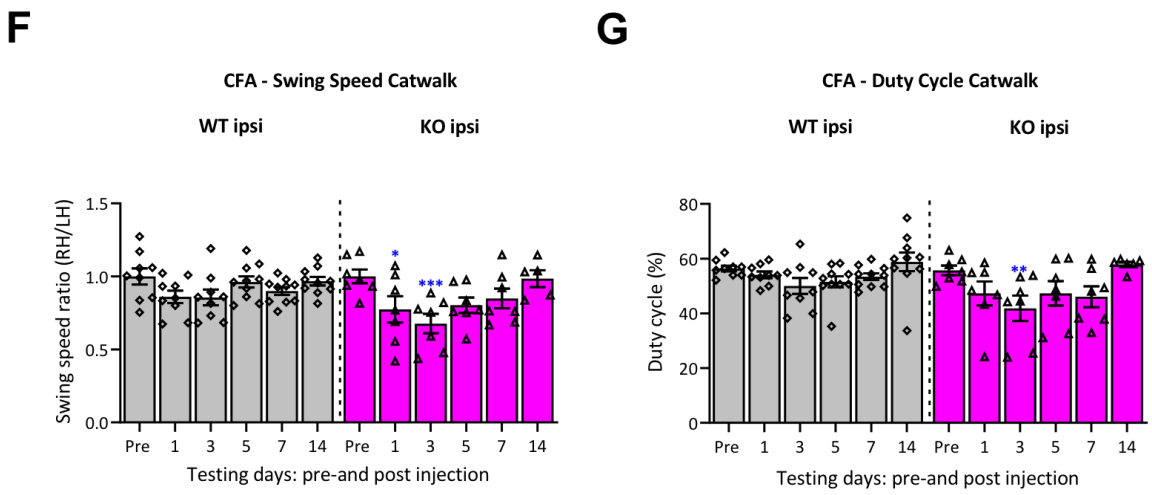

Figure 10: Diminished Mechanical Hypersensitivity upon TM Elimination

(A) Mechanical sensitivity was attenuated in TM KO mice 1 and 3 days (ipsi vs. con) post induction of inflammatory pain (CFA injection), whereas no behavioral alterations were found between genotypes under naive conditions (depicted by pretesting results). (B) WT and KO mice reacted with hypersensitivity to thermal stimulus 2 and 6 days post CFA injection (ipsi vs. con and ipsi vs. pre). No alteration between testing groups in withdrawal latency upon heat application during pretesting (naive condition). (C) Similar results for NEP testing among genotypes after CFA injection. (D-G) Catwalk paradigm revealed no significant changes of movement-evoked pain between WT and KO mice 1-14 days post CFA injection. (A, B) WT N = 13; KO N = 10; n = 3 independent cohorts. (C-G) Experiments performed by Dr. Daniel Segelcke, Group of Translational Pain Research (PI Esther Pogatzki-Zahn). WT N = 10; KO N = 7; n = 1 cohort. (A-G) 2-way ANOVA followed by Sidak's multiple comparison tests; * $p < 0.05$ vs. pre, ** $p < 0.01$ vs. pre, *** $p < 0.001$ vs. pre; **** $p < 0.0001$ vs. pre; ## $p < 0.01$ ipsi vs. con, ### $p < 0.001$ ipsi vs. con, #### $p < 0.0001$ ipsi vs. con. Data were represented as mean ± SEM. CFA, Complete Freund's Adjuvant; ipsi, ipsilateral; con, contralateral.

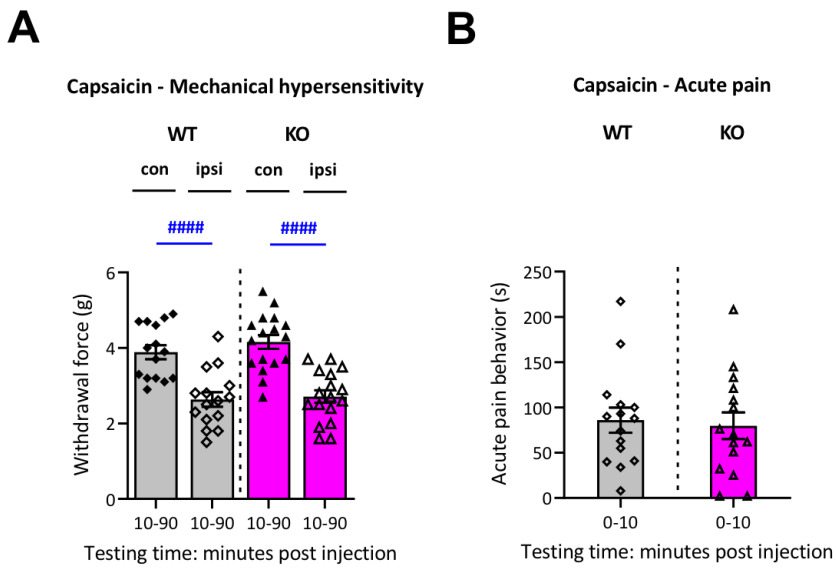

Figure 11: Capsaicin-evoked Acute Pain unchanged among Genotypes

(A) WT and KO mice showed a similar mechanical hypersensitivity upon induction of acute pain (10-90 minutes post injection of the TRPV1 agonist capsaicin). WT N = 15; KO N = 17; n = 2 independent cohorts; 1-way ANOVA followed by Sidak's multiple comparison tests; #### $p < 0.0001$ ipsi vs. con. (B) Comparable results between genotypes in time spent flicking, lifting and shaking of the injected paw (0-10 minutes post injection). WT N = 15; KO N = 17; n = 2 independent cohorts; unpaired student's t-test. Data were represented as mean ± SEM. Ipsi, ipsilateral; con, contralateral.

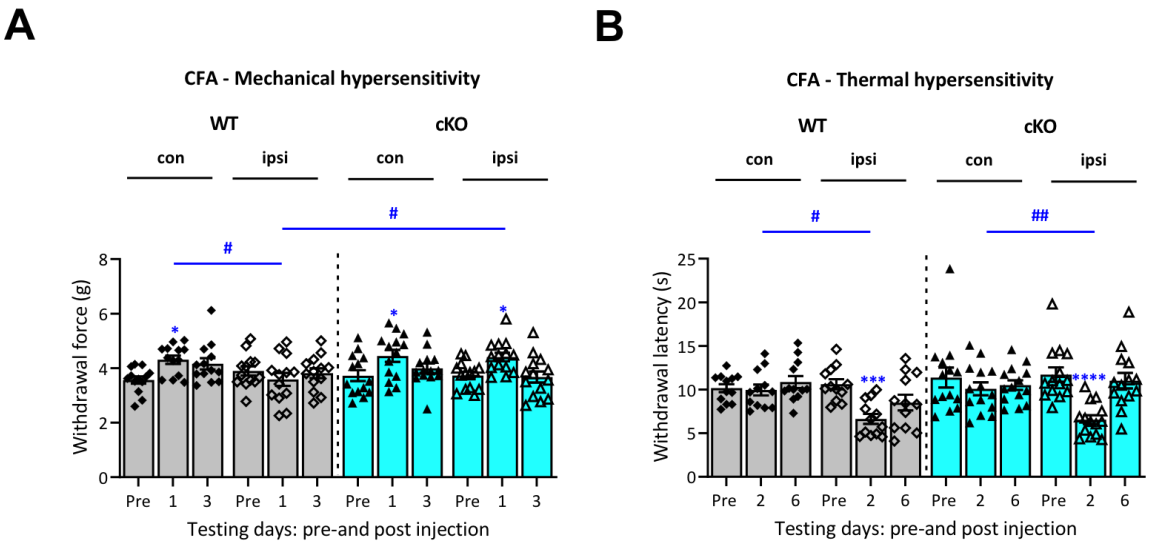

Figure 12: Sensory Neuron-specific TM KO sufficient to evoke impaired CFA-mediated Mechanical Hypersensitivity

(A) Analgesia upon TM deletion *in vivo* in regard to mechanically evoked pain shown as gram needed to elicit paw withdrawal. Compared to WT mice TM cKO's did not show mechanical hypersensitivity at 1 day post CFA injection (ipsi vs. con). The withdrawal force in TM cKO's was significantly increased compared to WT mice (1 day post CFA, ipsi). (B) No apparent alteration in reaction to thermal stimulus in cKO mice. Both mouse lines

showed thermal hypersensitivity 2 days post CFA injection (ipsi vs. con and ipsi vs. pre). WT N = 12-13; cKO N = 14; n = 2 independent cohorts; 2-way ANOVA followed by Sidak's multiple comparison tests; * $p < 0.05$ vs. pre, *** $p < 0.001$ vs. pre; **** $p < 0.0001$ vs. pre; # $p < 0.05$ ipsi vs. con, # $p < 0.05$ WT vs. KO, ## $p < 0.01$ ipsi vs. con. Data were represented as mean ± SEM. Ipsi, ipsilateral; con, contralateral.

3.1.6 Study of Neuronal Expression/ Excitability after TM Elimination

3.1.6.1 Similar PNS Protein Expression in TM KO Mice

To gather more information on the impact of TM in respect to chronic pain and PNS (peripheral nervous system) functions, I studied the abundance and expression pattern of PNS proteins (commonly used markers like peripherin for nociceptors and NF200 for myelinated neurons, according to Avenali et al., 2014) in naive and CFA-injected (1 day post) TM KO and WT mice. More precisely, the percentage and intensity of peripherin and NF200 positive neurons was investigated in naive and CFA-treated (1 day post, ipsilateral vs. contralateral injection side) TM KO and WT mice (lDRG). The investigation of TM KO tissue revealed a similar expression of peripherin and NF200 under naive conditions (Figure 13) as well as after induction of chronic pain (Figure 14). Previous work from Rouwette and colleagues (Rouwette et al., 2016) showed an increased peripherin expression in WT mice after CFA injection (1 d post). However, the difference could be mouse strain dependent as Rouwette et al. analyzed tissue of C57/Bl6 WT mice, whereas I used TM WT littermates in comparison to TM KO mice. The only detectable difference was a decreased NF200 intensity in lDRG WT ipsi and lDRG KO con compared to lDRG WT con (Figure 14). This result could be explained by the unusual high NF200 intensity in lDRG WT con that might be caused by a staining artifact.
All in all, TM deletion did not cause alterations of different neuronal populations (nociceptors vs. large myelinated neurons).

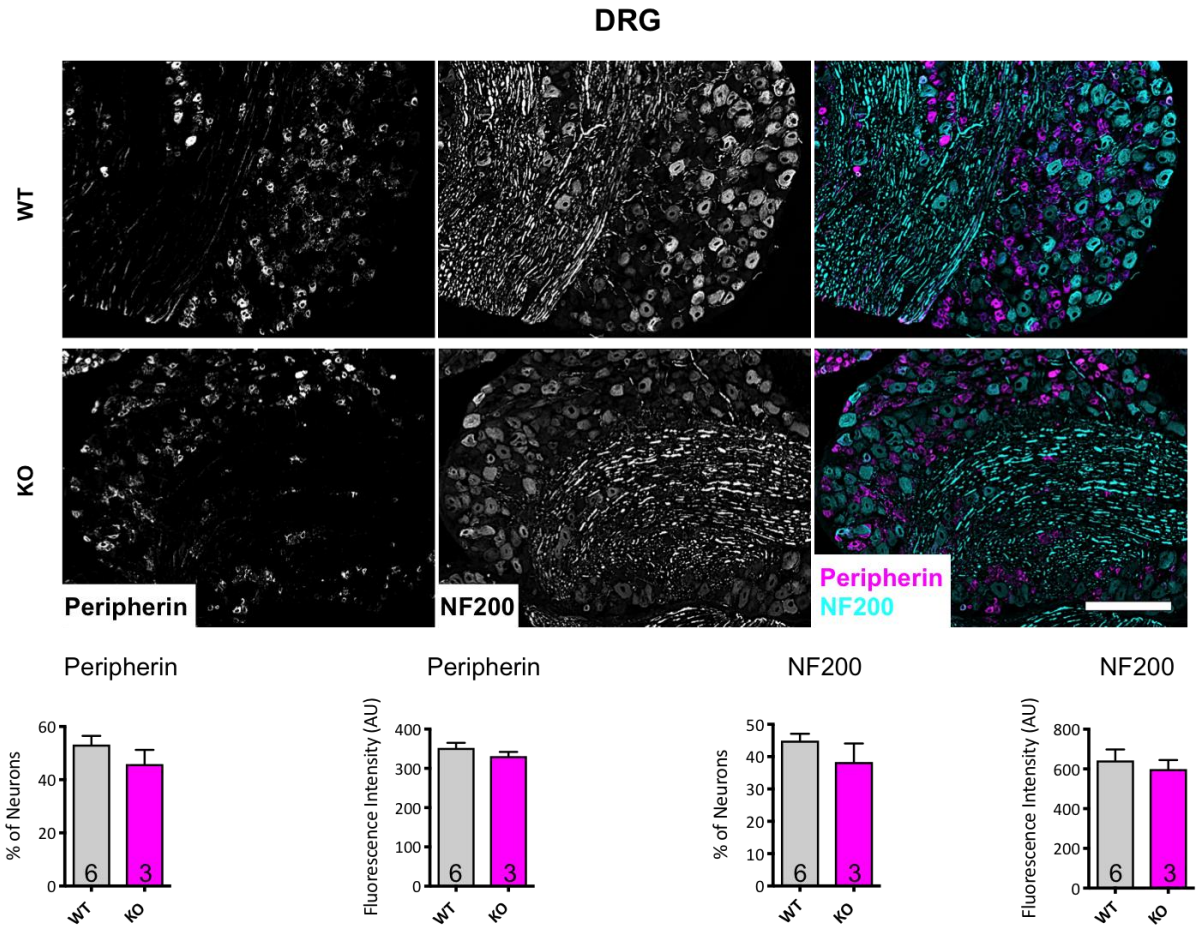

Figure 13: No Difference in Expression of Neuronal Populations in DRG of naive TM KO Mice

Representative immunohistochemistry for peripherin and NF200 expressed in DRG of naive mice and analysis in regard to percentage of neurons positive for respective marker as well as fluorescence intensity. Neither the percentage nor the fluorescence intensity of both marker proteins differed between DRG of WT and TM KO mice. Number of animals in column; WT (3 cryoblocks, in each DRG of 2 mice); KO (2 cryoblocks with DRG of 1 or 2 mice); each); several staining rounds; each block was cut in 10 µm thick tissue sections and 7 DRG sections were analyzed; unpaired student's t-test. Data were represented as mean ± SEM; scale bar, 100 µm. DRG, dorsal root ganglia; Peripherin, marker for nociceptors; NF200, neurofilament 200, marker for large myelinated neurons.

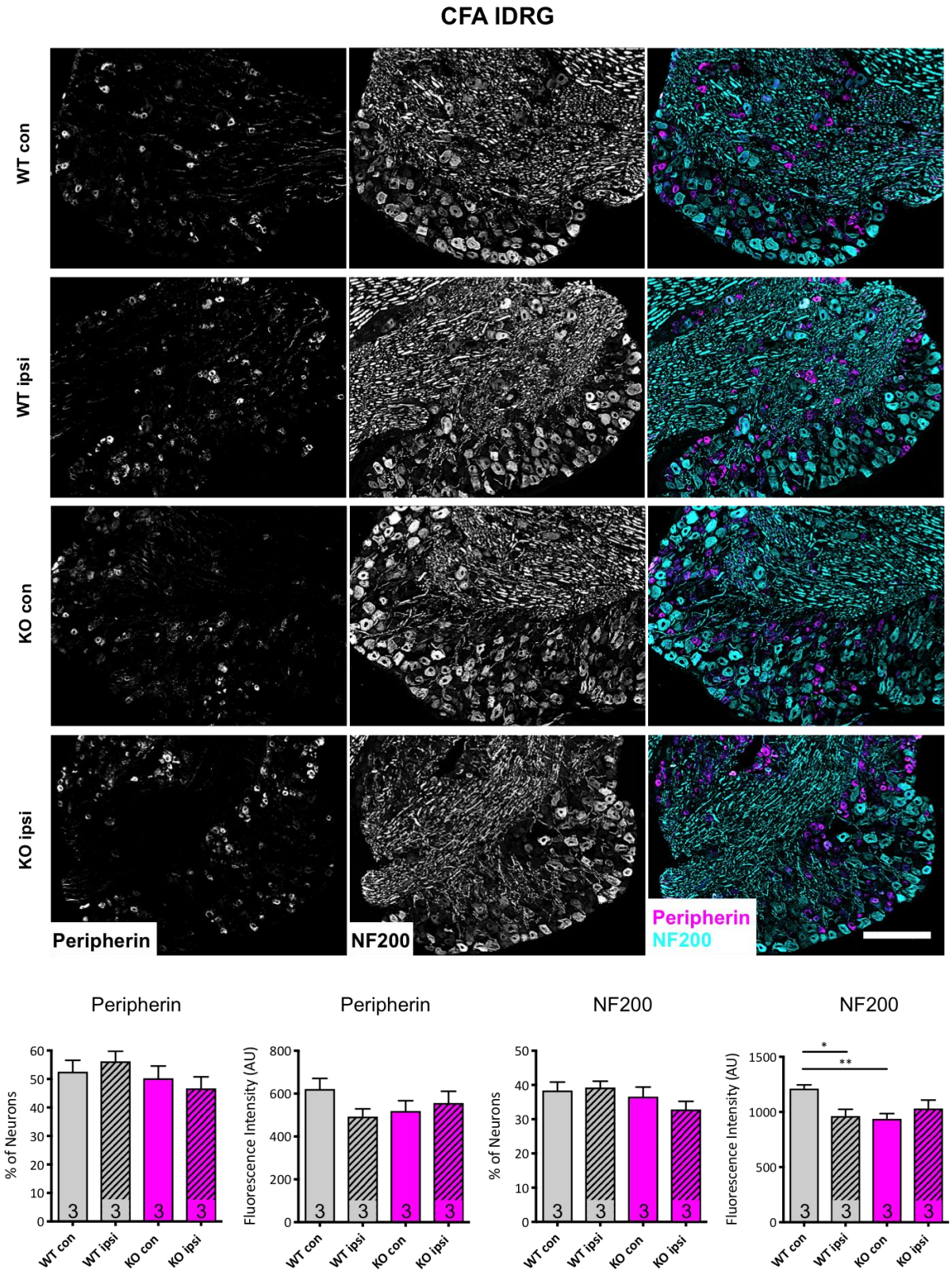

Figure 14: Similar Neuronal Population Expression in DRG of CFA-treated TM KO Mice

Representative immunohistochemistry of both neuronal marker proteins of DRG from mice injected with CFA (sacrificed 1 day post injection). Analysis revealed no overt alteration in percentage of marker expression and fluorescence intensity. Unusual high NF200 intensity in WT DRG con caused significant difference to WT DRG ipsi and KO DRG con. Number of animals in column; several staining rounds; WT (3 cryoblocks, in each DRG of 1

mouse); KO (3 cryoblocks with DRG of 1 mouse); each block was cut in 10 µm thick tissue sections and 7 DRG sections were analyzed; 1-way ANOVA followed by Sidak's multiple comparison tests; * $p < 0.05$, ** $p < 0.01$. Data were represented as mean ± SEM; scale bar, 100 µm. DRG, dorsal root ganglia; Peripherin, marker for nociceptors; NF200, neurofilament 200, marker for large myelinated neurons; ipsi, ipsilateral; con, contralateral; CFA, Complete Freund's Adjuvant.

3.1.6.2 Steady Neuronal Excitability in DRG of TM KO Mice

Based on the *in vivo* data, which showed similar results in TM KO and WT littermates in regard to basal mechanical and thermal sensitivity (3.1.5), I aimed to gain insights into functional properties of my protein of interest. It was known that *in vivo* findings correlate with many features of primary DRG neuron cultures (Avenali et al., 2014; Sondermann et al., 2018). Therefore, the consequences of TM deletion were studied in the DRG culture *in vitro*-system to examine potential differences in sensory neuron physiology. To this end firing properties (e.g. mechanically activated (MA) currents, action potential amplitude) were evaluated among genotypes with electrophysiological experiments (current-clamp mode, performed by Dr. Pratibha Narayanan, former colleague). No overt changes were detected in terms of rapid adapting currents and mean amplitudes of action potentials in sensory neurons from TM KO's compared to WT mice (Figure 15 A, B).

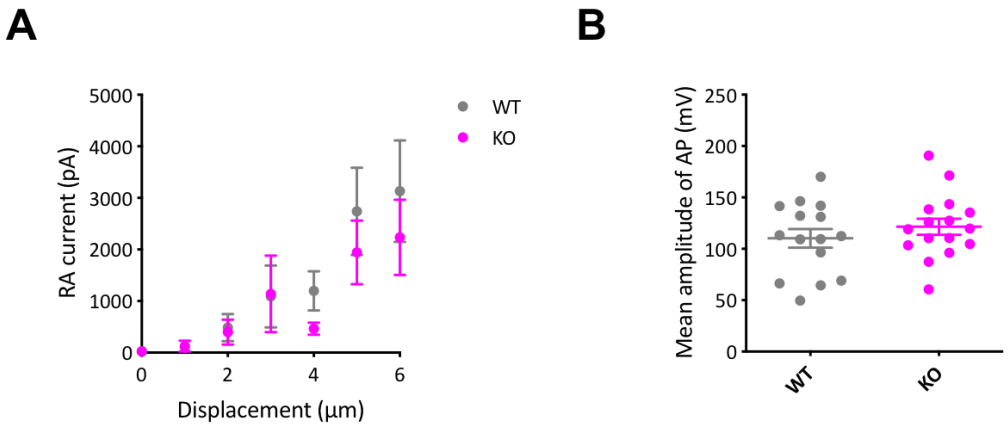

Figure 15: Electrophysiological Investigation revealed no Major Changes in Neuronal Excitability after TM Removal

(A) No difference of rapid adapting currents in sensory neurons of TM KO compared to WT mice. WT N = 4; KO N = 4; WT displacement (µm) 0: 18.44 ± 10.91, n = 25; 1: 103.76 ± 48.78, n = 25; 2: 485 ± 255.70, n = 25; 3: 1088.72 ± 587.21, n = 25; 4: 1198.71 ± 373.51, n = 24; 5: 2737.83 ± 831.78, n = 24; 6: 3130.68 ± 961.38, n = 22. KO displacement (µm) 0: 29.12 ± 28.53, n = 25; 1: 128.48 ± 105.41, n = 25; 2: 397.72 ± 237.35, n = 25; 3: 1140.64 ± 729.45, n = 25; 4: 466.30 ± 116.43, n = 23; 5: 1945.26 ± 606.62, n = 23; 6: 2234.48 ± 713.57, n = 21; 2-way ANOVA followed by Sidak's multiple comparison tests. Data were represented as mean ± SEM. (B) Mean action potential amplitude showed no difference between genotypes. WT N = 4; KO N = 4; WT mean amplitude of AP: 110.255 ± 8.79, n = 15; KO mean amplitude of AP: 121.52 ± 7.57, n = 16; unpaired student's t-test. Data

were represented as mean ± SEM. The experiments were performed by Dr. Pratibha Narayanan, former colleague. RA, rapid adapting; pA, picoampere; AP, action potential.

The calcium-permeable transient receptor potential (TRP) channel family is known to be implicated in nociceptive signaling (Bourinet et al., 2014; Patapoutian et al., 2009). Therefore, I wanted to investigate whether TRPV1 (noxious heat detector ~43°C (Caterina et al., 1997; Julius, 2013; Tominaga et al., 1998)) and TRPA1 (3.1.10.2, involved in mechanical hypersensitivity (Kwan et al., 2006; Petrus et al., 2007)) mediated calcium influx was altered in sensory neurons of TM KO mice. The calcium imaging results (mainly carried out by my Master student Hanna Kristina Fischer, taught and supervised by me) revealed an unchanged neuronal excitability as it was seen by electrophysiological experiments (Figure 15). More precisely, neither calcium signals upon TRPV1 activation assessed as percentage of responders to different stimuli (100 nM Capsaicin (TRPV1 agonist), 1 µM Capsaicin (increased concentration of TRPV1 agonist), 60 mM KCl (neuronal activity)) and the mean peak response amplitude were different between genotypes (Figure 16 A-C).
Together, these *in vitro* findings supported the unmodified somatosensory (thermal and mechanical sensitivity) behaviors in naive TM KO mice.

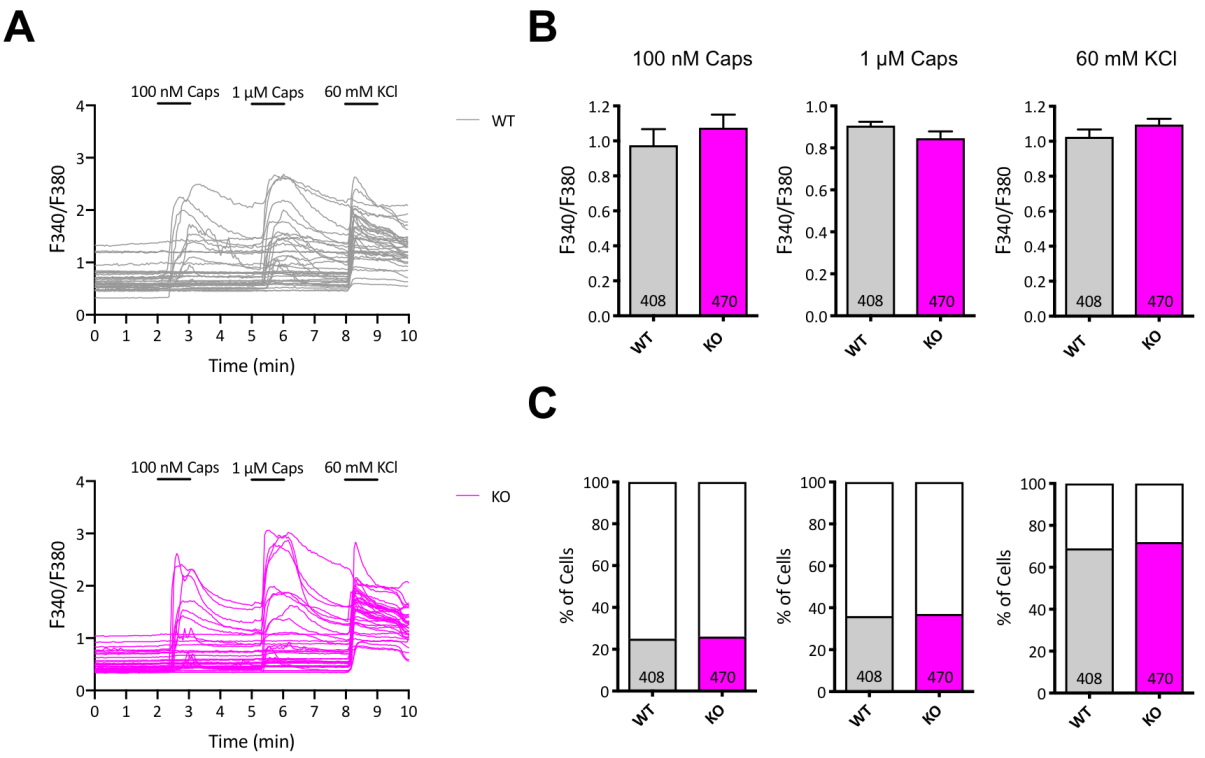

Figure 16: TM Deletion caused no Change in Neuronal Excitability as examined by Ratiometric Calcium Imaging

(A) Representative traces (35 neurons) of calcium increase measured by Ca^{2+}-imaging of dissociated DRG cultures from naive WT and TM KO mice. 3 pulses were applied (100 nM Caps, 1 µM Caps, 60 mM KCl) and amplitudes (peak of fluorescence ratio 340/380 above baseline) were quantified. (B) Mean response amplitudes revealed similar results for WT and TM KO sensory neurons after stimulation with 3 pulses. Cell count in columns; WT N = several coverslips from n = 4 independent cultures; KO N = several coverslips from n = 4 independent cultures; n = 1 imaging round performed by me and n = 3 performed by my Master student Hanna Kristina Fischer, taught and supervised by me; unpaired student's t-test. Data were represented as mean ± SEM. (C) Stacked bar graphs illustrate the fraction of responders (colored) and non-responders (white). Count of total number of neurons in columns; WT N = several coverslips from n = 4 independent cultures; KO N = several coverslips from n = 4 independent cultures; n = 1 imaging round performed by me and n = 3 performed by my Master student Hanna Kristina Fischer, taught and supervised by me; the Fisher exact test. DRG, dorsal root ganglia; Caps, capsaicin; KCl, potassium chloride.

3.1.7 Screen for Molecular Changes upon TM Deletion

3.1.7.1 Pronounced Regulation of Mitochondrial Components and Inflammatory Mediators in TM KO Mice

As mentioned in the introduction it was known that diverse pathological pain conditions are characterized by mitochondrial dysfunction (Baloh et al., 2008; Fernyhough et al., 2010; Joseph et al., 2009; Osio et al., 2006; Rouwette et al., 2016). These could be caused by activity/ expression changes of the electron transport chain (ETC) (Baloh et al., 2008; Fernyhough et al., 2010; Joseph et al., 2009; Osio et al., 2006), increased reactive oxygen species (ROS) leading to oxidative stress (Kim et al., 2004) and microglia activation (Kallenborn-Gerhardt et al., 2013), as well as an unbalanced calcium homeostasis (Shishkin et al., 2002). In order to test whether TM was involved in mitochondrial dysfunction, I started with the investigation of expression levels from ETC components. Furthermore, given that TM seemed to serve as pro-algesic factor during inflammatory pain conditions *in vivo*, I wanted to examine for altered expression of prototypic inflammatory mediators (3.1.5). All KO values shown in Figure 17 were normalized to respective WT values before (WT values set at 1, not shown in Figure; Figure 17 A-F). Ipsi values were normalized to con values of the same genotype (Figure 17 G-H, con values not shown in graph). TM KO and WT mice were assessed for differential gene expression by qRT-PCR under naive and chronic pain conditions. Interestingly, prominent mRNA level changes were mainly detectable in DRG of naive TM KO mice. In detail, 3 subunits of the mitochondrial ETC were differentially expressed (Cox1, cytochrome c oxydase c1 (Complex IV) downregulated; ND2, subunit of NADH dehydrogenase (Complex I) downregulated; Uqcr10, ubiquinol-cytochrome c reductase, complex III subunit X (Complex III) upregulated) in DRG of naive TM KO mice (Figure 17 A). In addition, the mitochondrial transcription factor A (Tfam) was decreased in the same tissue (Figure 17 A). Furthermore, the qRT-PCR results for inflammatory markers revealed a decrease in TNF α (tumor necrosis factor alpha) (Figure 17 B, assessed in TM KO DRG) and CCl2 (chemokine (C-C motif) ligand 2) expression (Figure 17 D, examined in TM KO SN).

Taken together, these findings indicated the involvement of TM in mitochondrial (dys)function and inflammatory signaling.

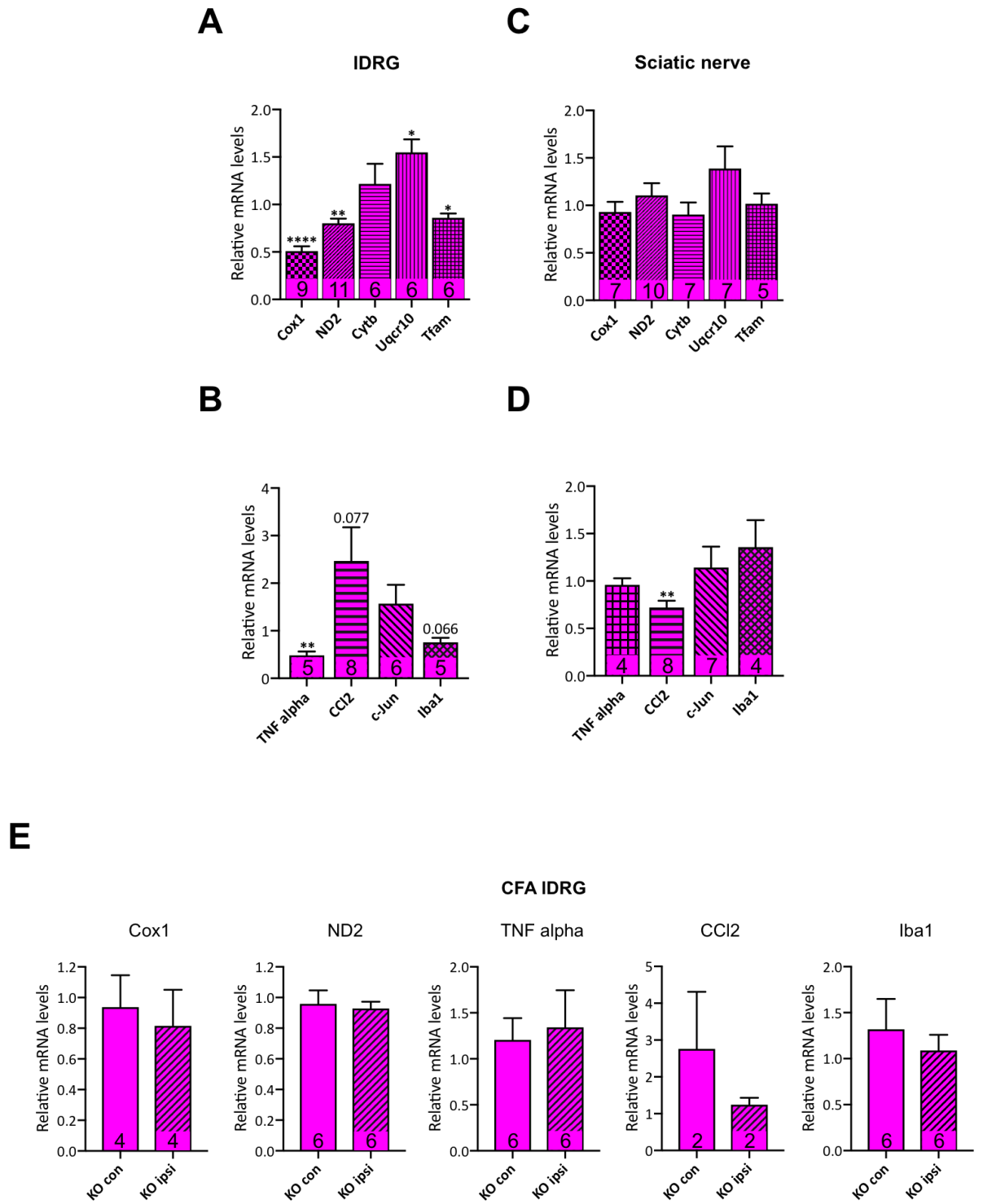
A
IDRG
Relative mRNA levels
2.0
1.5
1.0
0.5
0.0
****
**
*
*
9
11
6
6
6
Cox1
ND2
Cytb
Uqcr10
Tfam
C
Sciatic nerve
Relative mRNA levels
7
10
7
7
5
Cox1
ND2
Cytb
Uqcr10
Tfam
B
Relative mRNA levels
4
3
2
1
0
**
0.077
0.066
5
8
6
5
TNF alpha
CCl2
c-Jun
Iba1
D
Relative mRNA levels
**
4
8
7
4
TNF alpha
CCl2
c-Jun
Iba1
E
CFA IDRG
Cox1
ND2
TNF alpha
CCl2
Iba1
Relative mRNA levels
4
4
6
6
6
6
2
2
6
6
KO con
KO ipsi

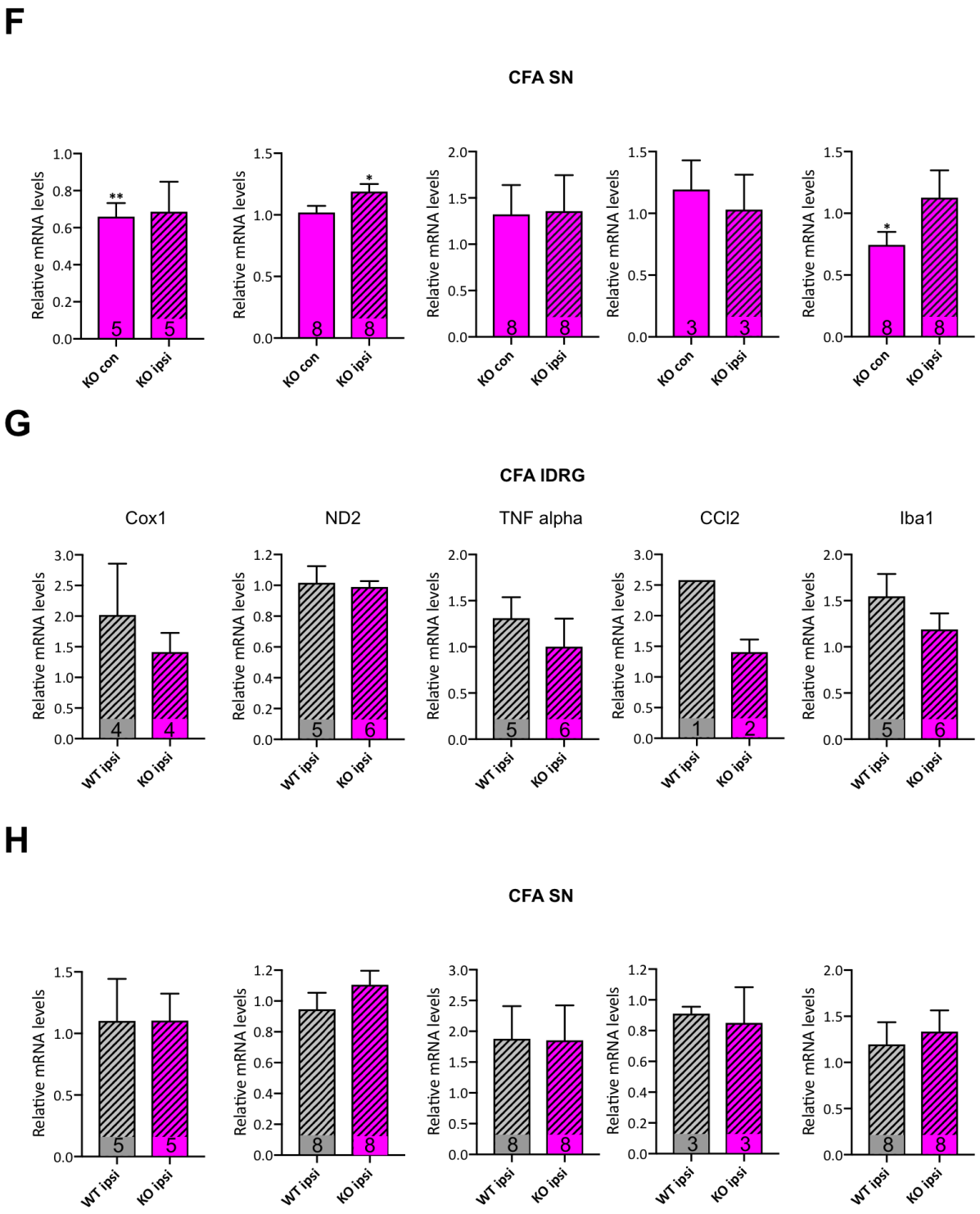

Figure 17: Altered Mitochondrial and Inflammatory Gene Expression in TM KO Mice

(A-H) qRT-PCR results showed relative expression of diverse mitochondrial and inflammatory genes normalized to GAPDH. (A-D) Altered gene expression in lDRG and SN of naive TM KO's referred to WT values (not shown, set to expression level of 1). (A) Relative expression levels in KO lDRG showed Cox1, ND2 and Tfam decrease and an Uqcr10 increase. (B) TNFα levels were down-regulated in lDRG of TM KO's. (C) KO SN revealed no expression changes in regard to tested mitochondrial genes. (D) Relative CCl2 expression was decreased in SN of TM KO mice. (E-F) Investigation of mRNA levels in lDRG and SN of WT and KO mice 1 day post CFA injection (KO values compared to WT values which were not shown, set to relative expression level of 1). (E) No

significant difference in lDRG gene expression post CFA. (F) Cox1 and Iba1 levels were decreased in SN CFA KO con compared to SN CFA WT con and ND2 expression was increased in SN CFA KO ipsi compared to CFA WT ipsi. (G-H) Relative expression level changes of lDRG and SN from CFA WT ipsi vs. CFA KO ipsi (CFA WT ipsi values compared to CFA WT con and CFA KO ipsi values related to CFA KO con before; con values not shown, relative expression set as 1). (G) No significant changes in lDRG CFA KO ipsi mRNA of investigated candidates. (H) SN revealed no overt alterations in CFA KO ipsi gene expression. Number of animals in column; data collected from several independent experiments; (A-F) one sample t-test, * $p < 0.05$, ** $p < 0.01$, **** $p < 0.0001$; (G-H) unpaired student's t-test. Data were represented as mean ± SEM. Cox1, cytochrome c oxydase c1 (Complex IV); ND2, subunit of NADH dehydrogenase (Complex I); Cytb, cytochrome b; Uqcr10, ubiquinol-cytochrome c reductase, complex III subunit X; Tfam, mitochondrial transcription factor A; TNFα, tumor necrosis factor alpha; CCl2, chemokine (C-C motif) ligand 2; c-Jun, Jun proto-oncogene AP-1 transcription factor subunit; Iba1, ionized calcium-binding adapter molecule 1. lDRG, lumbar dorsal root ganglia; SN, sciatic nerve; ipsi, ipsilateral; con, contralateral; CFA, Complete Freund's Adjuvant.

3.1.8 Investigation of Mitochondrial Function Upon TM Deletion

Motivated by the altered ETC component expression (3.1.7), I wanted to explore the hypothesis of TM involvement in mitochondrial dysfunction in more detail. To this end, our collaboration partners and me performed a number of experiments in order to investigate mitochondrial protein abundance, ETC component activities, oxygen consumption rate and mitochondrial membrane potential. All of the evaluated parameters were similar among tissue isolated from TM KO and WT mice.

3.1.8.1 No Overt Abundance Changes of Mitochondrial Proteins

Mitochondria were isolated from brain, heart and liver of both mouse lines (adapted from Bareth et al., 2016), because previous studies revealed that DRG of 10 mice would be needed in order to extract a sufficient amount of mitochondria. Blue native PAGE (BN-PAGE) was performed for segregation of the mitochondrial ETC multiprotein complexes followed by western blotting. Protein abundance was tested subsequently by applying antibodies directed against subunits of ETC complexes I-V. No overt changes were detected among ETC subunit proteins among the investigated tissue between genotypes. The experiments were performed by Dr. Sven Dennerlein, Department of Cellular Biochemistry, PI Prof. Dr. Peter Rehling.

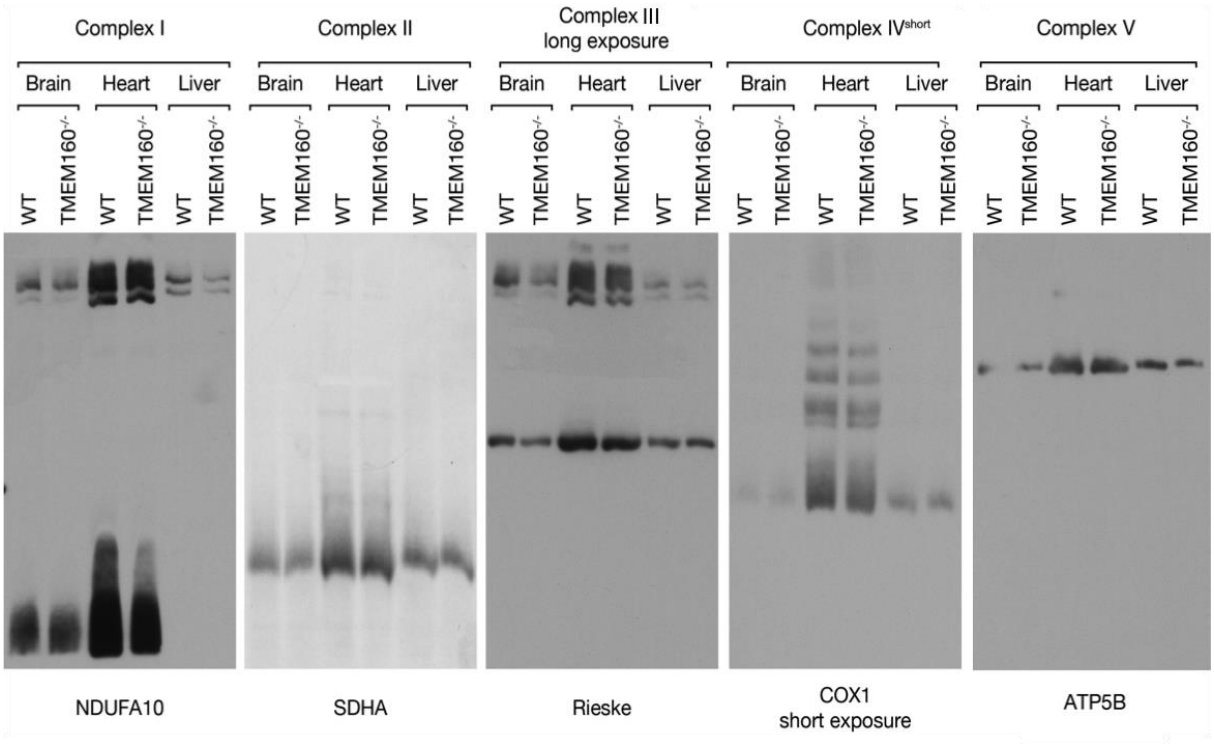

Figure 18: No Major Protein Abundance Change in ETC Subunits of TM KO Brain, Heart and Liver

Representative image of western blot results of BN-PAGE showed minor variations (in mitochondria of TM KO brain slightly reduced) in mitochondrial protein expression across genotypes. Isolated mitochondria from brain, heart and liver of TM WT and KO mice were used for the experiment. N = 4 mice; 4 independent experiments. The experiments were performed by Dr. Sven Dennerlein, Department of Cellular Biochemistry, PI Prof. Dr. Peter Rehling. NDUFA10, NADH:ubiquinone oxidoreductase subunit a10 (Complex I); SDHA, succinate dehydrogenase complex flavoprotein subunit A (Complex II); Rieske, ubiquinol-cytochrome c reductase, rieske iron-sulfur polypeptide 1 (UQCRFS1, Complex III); COX1, cytochrome c oxidase c1 (Coomplex IV), ATP5B, ATP synthase f1 subunit beta (Complex V).

3.1.8.2 Similar Activity Levels of Electron Transport Chain (ETC) Components in TM KO Mice

BN-PAGE allowed for assessment of ETC complexes in their enzymatically active form. Therefore, we were able to investigate potential alterations in activity of complex I, II, IV and V by incubation with substrates specific for the respective ETC complex. Spectrophotometric analysis revealed no major changes of the mitochondria isolated from brain, heart and liver of TM KO and WT mice (Figure 19). The experiments were performed by Dr. Sven Dennerlein, Department of Cellular Biochemistry, PI Prof. Dr. Peter Rehling (according to Wittig et al., 2007; Deckers et al., 2014). In order to verify the mentioned unmodified CIV activity in the investigated 3 tissue types of TM KO mice, I investigated the enzyme activity by an alternative approach. To that end the CIV enzyme activity dipstick assay was performed on DRG dissected from both genotypes. It was composed of a specific antibody attached to a dipstick in combination with DAB as reporter of CIV activity (according to

manufacturer's instruction). The mean pixel intensity of the precipitated DAB signal revealed comparable results between genotypes (Figure 20).

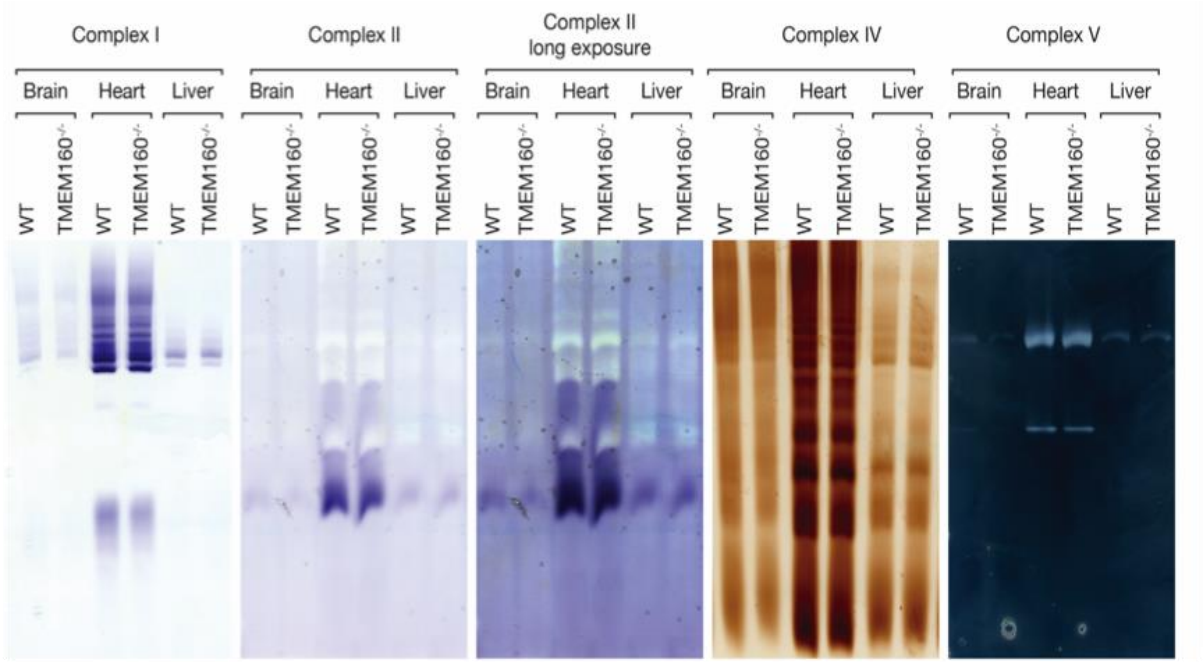

Figure 19: ETC Activity Staining revealed no definite Difference among Genotypes

Representative image showed the activity of ETC complexes I, II, IV and V. Mitochondria isolated from brain, heart, liver were fed with substrates for the mentioned complexes and activity levels were assessed spectrophotometrically. No overt changes could be detected compared between the genotypes. N = 2 mice; 2 independent experiments. The experiments were performed by Dr. Sven Dennerlein, Department of Cellular Biochemistry, PI Prof. Dr. Peter Rehling.

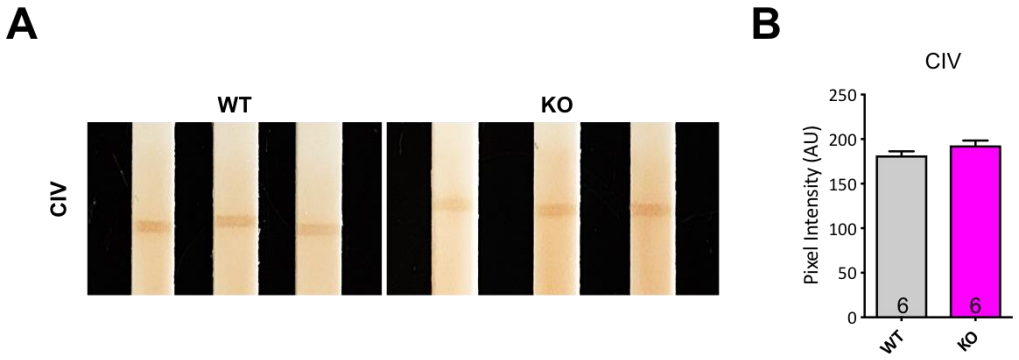

Figure 20: Similar Complex IV Activity in TM KO Mice

(A, B) Enzyme activity dipsticks for cytochrome c oxidase (COX, Complex IV) revealed no difference in DRG lysates of TM KO and WT mice. (A) Representative image of dipsticks from both genotypes. (B) The activity quantification (depicted as Pixel intensity) showed similar results. Number of animals in column; 3 independent experiments with DRG of 2 mice pooled from the same genotype; 3 technical replicates/ genotype/ experiment; unpaired student's t-test. Data were represented as mean ± SEM. DRG, dorsal root ganglia.

3.1.8.3 Consistent Oxygen Consumption Rate Among Genotypes

A commonly used approach to test for mitochondrial dysfunction is the determination of mitochondrial respiration by measuring the oxygen consumption rate (OCR) (Ferrick et al., 2008; Duggett et al., 2017). Pharmacological agents (Oligomycin: inhibits complex V, FCCP: ionophore which uncouples ATP synthesis from ETC function, Rotenone: inhibits complex I, Antimycin A: inhibits complex III (Duggett et al., 2017), KCN: inhibits complex IV (Puntel et al., 2013)) were utilized to modulate mitochondrial function to assess the bioenergetics profile. First, basal respiration was investigated by addition of substrates for complex II (Succinate) and complex IV (Ascorbate), followed by assessment of ATP-linked respiration and proton leak (Oligomycin), maximal respiratory capacity (FCCP) and reserve capacity (Antimycin A, Rotenone, KCN, respiratory ability to overcome stress) (Ferrick et al., 2008, Duggett et al., 2017). All investigated aspects of OCR were similar between genotypes (Figure 21). The experiments were performed by Dr. David Pacheu Grau, Department of Cellular Biochemistry, PI Prof. Dr. Peter Rehling.

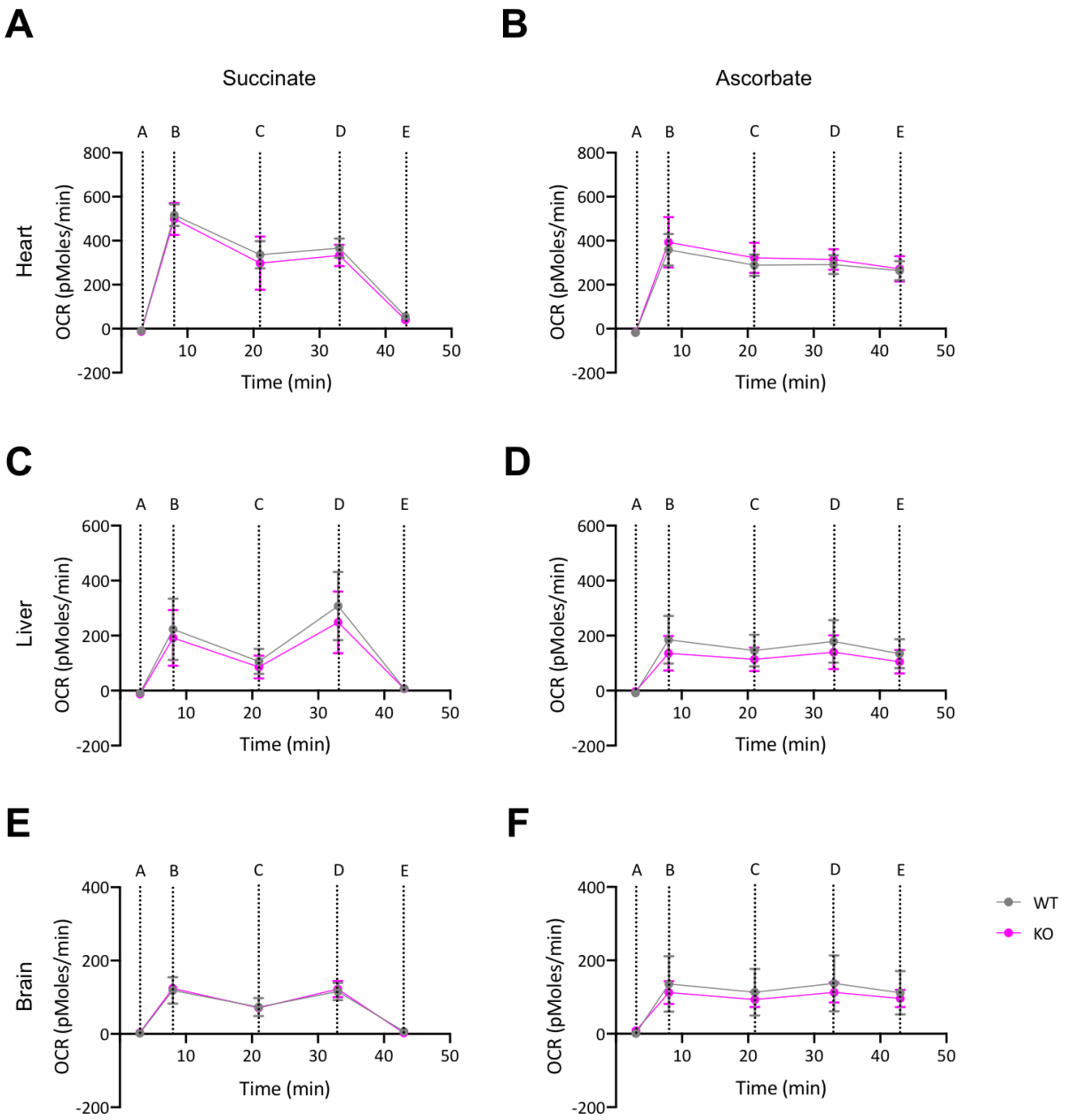

Figure 21: Seahorse Experiments revealed unaltered Oxygen Consumption Rate in TM KO

(A-F) OCR of isolated mitochondria from heart, brain and liver of TM KO and WT mice. (A, C, E) Similar OCR of mitochondria from heart, brain, and liver mitochondria after addition of Succinate (substrate for complex II) among genotypes. (B, D, F) Steady OCR from mitochondria of heart, brain, and liver from both genotypes after Ascorbate (substrate for complex IV) addition. Within each graph: A, calibration; B, substrate (basal respiration); C, Oligomycin (ATP-linked respiration + proton leak); D, FCCP (maximal respiratory capacity); E, Antimycin A + Rotenone + KCN (spare reserve capacity). N = 2-3 mice; 3 independent experiments; 2-way ANOVA followed by Sidak's multiple comparison tests. Data were represented as mean ± SEM. The experiments were performed by Dr. David Pacheu Grau, Department of Cellular Biochemistry, PI Prof. Dr. Peter Rehling. OCR, oxygen consumption rate.

3.1.8.4 Similar Mitochondrial Membrane Potentials in DRG Culture of TM KO's

Alterations in mitochondrial membrane potential are generally associated with mitochondrial dysfunction, e.g. after chemical inhibition of ETC (Cannino et al., 2012). Therefore, I further tested for potential mitochondrial dysfunction after TM deletion by using the cell permeable dye TMRM (tetramethylrodamine, methyl ester) in DRG cultures (TM KO vs. WT). TMRM accumulated in mitochondria with intact membrane potential (major driving force for calcium uptake and proper ETC activity (Nicholls and Budd, 2000)) resulting in a strong signal. When the mitochondrial oxidative phosphorylation uncoupler FCCP was used to induce a membrane potential collapse the signal lost its strength as expected (Akude et al., 2011, Nicholls 2006). Using this approach, I studied potential changes in the mitochondrial membrane potential, which could not be validated among genotypes (Figure 22).

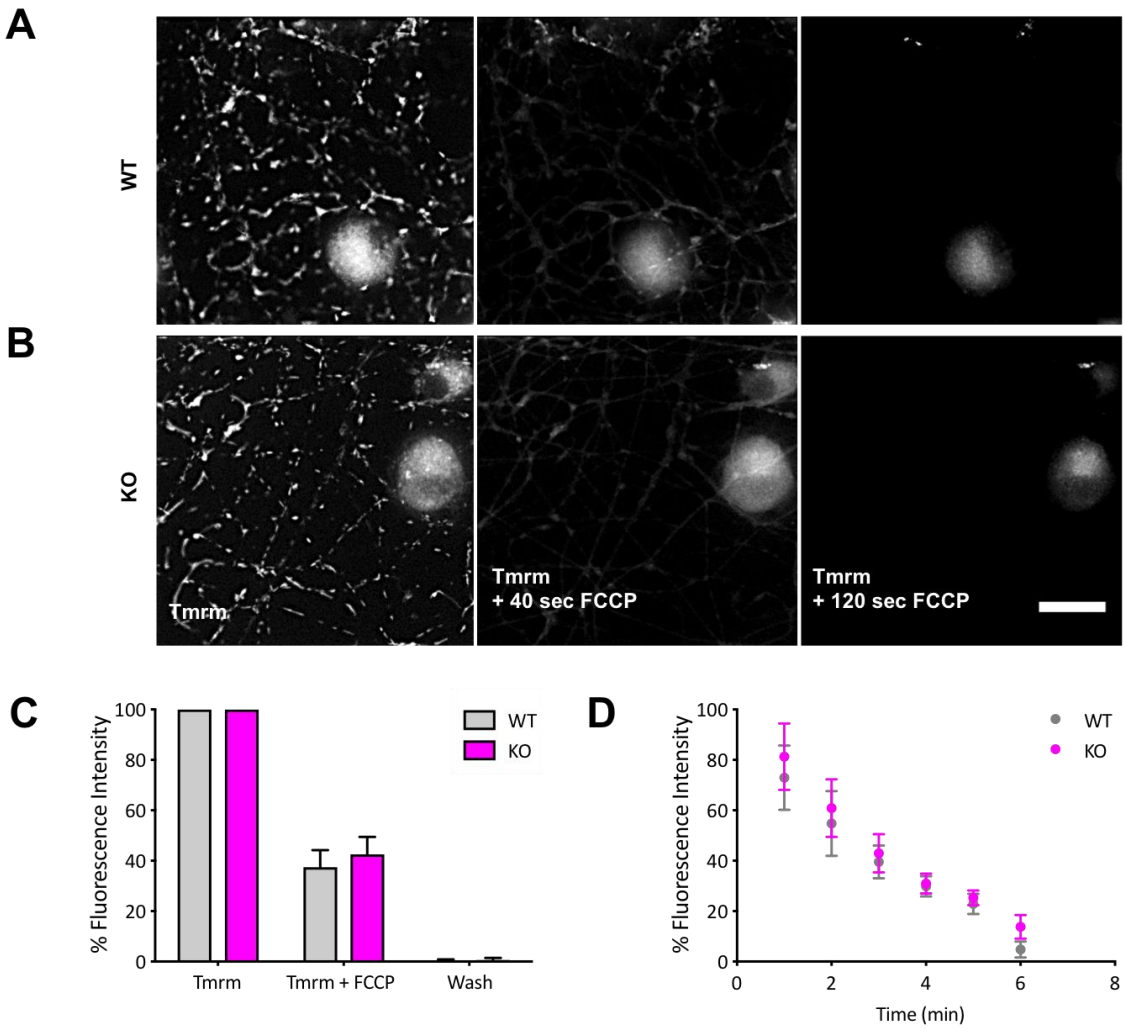

Figure 22: TM KO DRG exhibited a normal Mitochondrial Membrane Potential

(A-D) Course of TMRM imaging comprised of TMRM baseline, membrane potential collapse with FCCP and wash out with assay buffer. (A) Representative images for the TMRM signal, and two time points after FCCP

addition in DRG culture of both genotypes. (C) Pooled percentage of TMRM fluorescence intensity for the respective stimuli (each given for 2 minutes). (D) Imaging broken down into minutes revealing the time course of TMRM signal mitigation (min 1-2: TMRM; min 2-4 TMRM + FCCP; min 4-6 wash out with assay buffer). WT N = several coverslips from n = 3 independent cultures; KO N = several coverslips from n = 3 independent cultures; scale bar, 20 µm; 2-way ANOVA followed by Sidak's multiple comparison tests. Data were represented as mean ± SEM. DRG, dorsal root ganglia.

3.1.9 Oxidative Stress Response Compared Between Genotypes

Malfunctioning mitochondria (e.g. due to altered ETC expression (Baloh et al., 2008; Fernyhough et al., 2010; Joseph et al., 2009; Osio et al., 2006)) have been shown to cause oxidative stress by increased ROS production (Kim et al., 2004). Given the investigated change in expression levels of ETC components (Figure 17 A), but not on protein level (Figure 18), I was interested in studying a potential difference in the oxidative stress response among genotypes. Therefore, mitochondrial ROS was assessed under naive conditions, as well as protein adduct formation due to oxidative stress under inflammatory pain conditions. These experiments revealed a slight increase in mitochondrial ROS in DRG cultures of TM KO mice. However, modified lipid peroxidation upon inflammatory pain could not be shown in DRG of both mouse lines upon CFA injection.

3.1.9.1 Increased Mitochondrial ROS in DRG Culture of TM KO's

I investigated mitochondrial ROS by live-imaging of sensory neurons with Mitosox (mitochondrial ROS sensitive dye, which revealed a red color when oxidized) and measured its mean intensity in the soma. Furthermore, the percentage of Mitosox positive neurons was examined among genotypes. A minor increase in the mean Mitosox intensity was determined in somata of sensory neurons from naive TM KO mice. This result could indicate a slight augmentation in ROS production, which could be caused due to the shown differential expression of ETC components on mRNA level (Figure 17 A) (Hall et al., 2014; Willemen et al., 2018). However, no alteration of ETC subunits could be examined on protein level (Figure 18). As mentioned in the first results section (3.1.1), differential mRNA and protein levels were not surprising given the well-known limited correlation (Liu et al., 2016; Schwanhäusser et al., 2011; Sharma et al., 2015). Therefore, it can only be speculated that the differential mRNA levels were involved in the increased Mitosox intensity in TM KO sensory neurons.

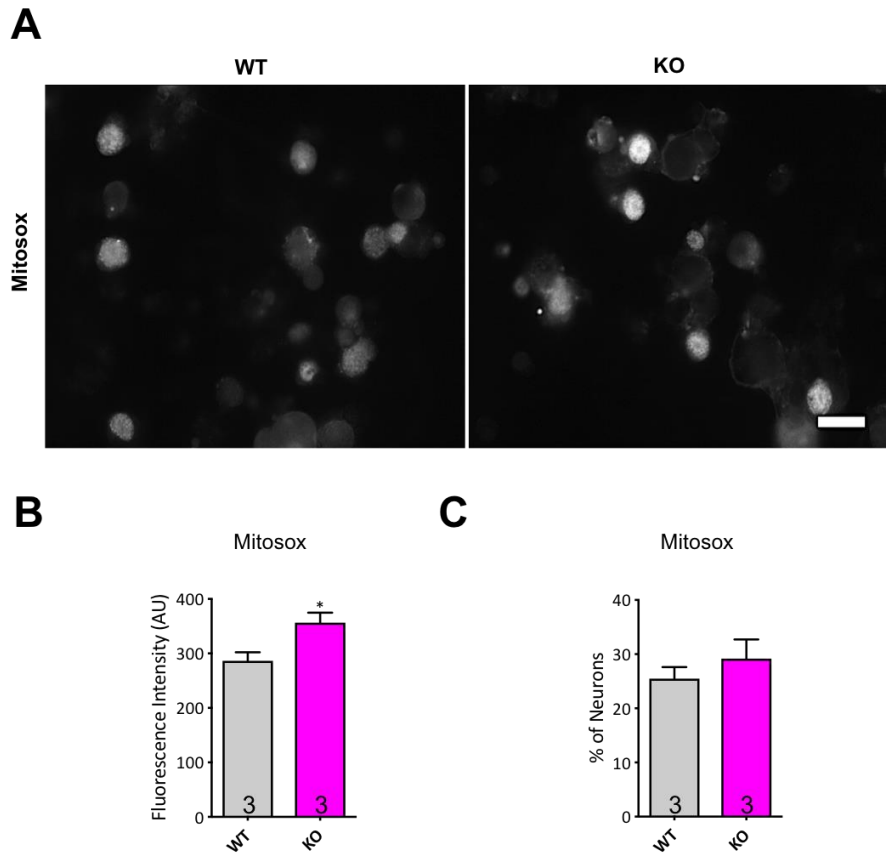

Figure 23: Slightly increased Mitosox Signal in DRG of TM KO Mice

(A) Representative image of DRG culture from both genotypes stained for Mitosox. (B) Fluorescence analysis revealed a slight increase of Mitosox in DRG of TM KO's. (C) No alteration in percentage of neurons positive for the mitochondrial ROS marker. Number of cultures in column; several coverslips/ culture; scale bar, 50 µm; unpaired student's t-test; * $p < 0.05$. Data were represented as mean ± SEM. DRG, dorsal root ganglia.

3.1.9.2 Unmodified Lipid Peroxidation after TM Deletion

Given the fact that the behavioral phenotype (3.1.5) was specific for inflammatory pain conditions, I investigated DRG from both genotypes after CFA injection. Therefore, immunohistochemistry was performed on cryo-embedded lDRG from TM KO and WT mice post CFA injection (24 h post CFA, ipsi and con lDRG). I examined oxidative stress among genotypes with a 4-HNE (4-hydroxy-2-nonenal)-protein adduct antibody (Akude et al., 2010; Obrosova et al., 2007) and could not detect any differences in terms of 4-HNE fluorescence intensity (Figure 24).

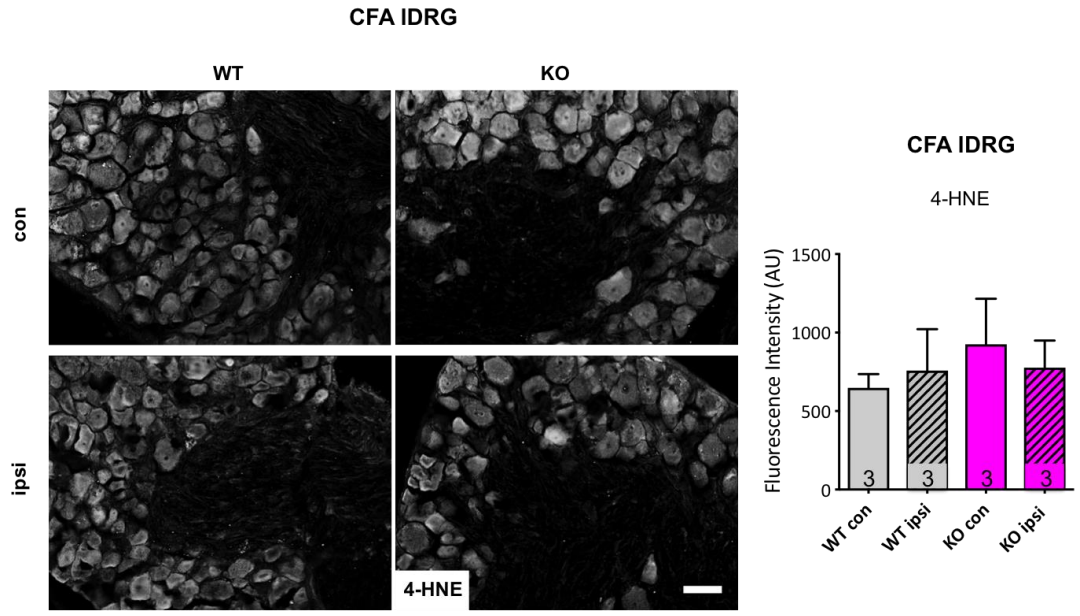

Figure 24: Unchanged 4-HNE Intensity in TM-deficient CFA-treated Mice

Fluorescence intensity of 4-HNE- protein adducts assessed in lDRG of mice (CFA injected paw: ipsi vs. non injected paw: con of both genotypes) revealed no difference. Number of animals in column; scale bar, 50 µm; 1-way ANOVA followed by Sidak's multiple comparison tests. Data were represented as mean of 7 analyzed images/ mouse ± SEM. lDRG, lumbar dorsal root ganglia; ipsi, ipsilateral; con, contralateral; CFA, Complete Freund's Adjuvant.

3.1.10 Altered Inflammatory Signaling Pathways in TM KO mice

Painful conditions are correlated with numerous inflammatory signaling pathways. During inflammatory pain the "inflammatory soup" (inflammatory mediators) could lead to dysfunctional plasticity of the pain axis resulting in chronification (Woolf, 2007). Based on that knowledge and on our promising qRT-PCR results (3.1.7, Figure 17 B), which showed a significant decrease in TNFα levels in DRG of TM KO mice, I wanted to perform further assays in order to investigate inflammatory signaling. Ca^{2+}-imaging results revealed a lower amount of TRPA1 expressing neurons in Veh treated cultures. Upon TNFα incubation the amount of TRPA1 responders could be compensated back to WT Veh levels. These results underscored the lower TNFα mRNA levels in DRG of TM KO mice as the inflammatory cytokine causes surface delivery of TRPA1 (Meng et al., 2016).

3.1.10.1 Equal CFA induced Macrophage Activation in TM KO DRG

Microglia/ macrophages are activated by ROS (Kallenborn-Gerhardt et al., 2012), which results in the production and release of inflammatory mediators contributing to chronic pain (Clark and Malcangio, 2014; Graeber and Christie, 2012; Milligan and Watkins, 2009; Old et al., 2015; Ren and Dubner, 2010). Therefore, the amount of macrophages was evaluated by measuring the Iba1 (ionized calcium-binding adapter molecule 1) positive area in lDRG (isolated 24 h post CFA injection) normalized to the total tissue area. However, the experiment was not successful as the Iba1 area was not increased in the positive control (Iba1 should have been increased in lDRG ipsi of WT mice compared to lDRG con, Willemen et al., 2018). The trend for an increased Iba1 in lDRG ipsi of WT mice resulted from 1 of the 3 analyzed animals (7 analyzed images of several lDRG sections/ mouse, Figure 25). Therefore, the question if impaired macrophage activation was involved in the behavioral phenotype characterized by mitigated mechanical hypersensitivity during inflammatory pain, (1 and 3 days post CFA injection, 3.1.5) remained open. The experiment will be performed in regard to microglia activation in the spinal cord of TM KO and WT mice 24h post CFA injection.

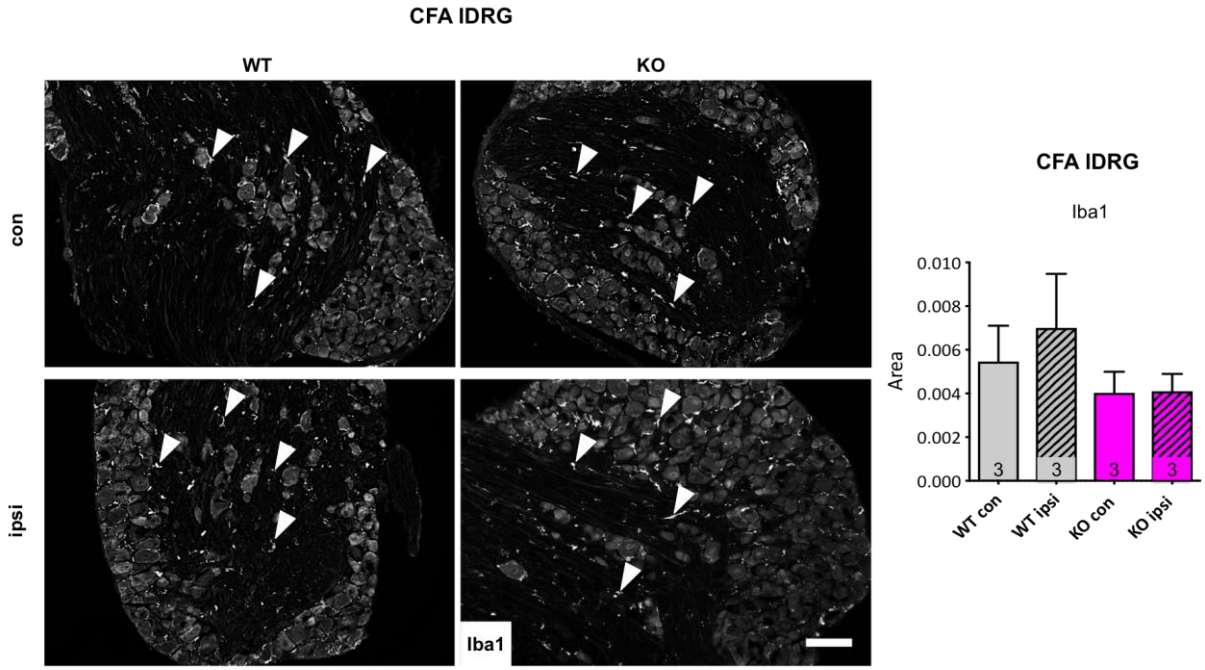

Figure 25: Macrophage Staining in DRG of TM KO and WT Mice under Inflammatory Pain Conditions

No difference in Iba1 area among lDRG con and ipsi of both genotypes after induction of inflammatory pain (24 h post). Experiment was not successful, because positive control (Iba1 area should be increased in lDRG WT ipsi compared to lDRG WT con) failed. Number of animals in column; scale bar, 100 µm; 1-way ANOVA followed by Sidak's multiple comparison tests. Data were represented as mean of 7 analyzed images of several DRG sections/ mouse ± SEM. Area of Iba1 signal (indicated by arrow heads) normalized to total lDRG area. Iba1, ionized calcium-binding adapter molecule 1; lDRG, lumbar dorsal root ganglia; ipsi, ipsilateral; con,

contralateral; CFA, Complete Freund's Adjuvant.

3.1.10.2 Differential TRPA1 dependent Calcium Signaling in TM KO's

Based on the decreased TNFα expression investigated in DRG of TM KO mice (mRNA level Figure 17 B), I aimed to examine inflammatory signaling upon incubation with TNFα. DRG cultures from both genotypes were stimulated with TNFα or vehicle for 6 h followed by Ca^{2+}-imaging in order to imitate inflammatory conditions (Willemen et al., 2018). It was shown that the prototypic inflammatory mediator evokes an increased Ca^{2+} influx via TRPV1 and TRPA1 due to an elevated surface delivery of those channel proteins (Meng et al., 2016). Based on that data, I was interested in studying calcium levels in cultured DRG from TM KO and WT mice by stimulation with mustard oil (30 µM MO, TRPA1 agonist), capsaicin (100 nM Caps, TRPV1 agonist) and potassium chloride (60 mM KCl, neuronal activity). Interestingly, fewer TRPA1 expressing neurons were activated in DRG of TM KO's (vehicle treated) compared to WT controls (vehicle treated). This lower amount of MO responders in TM KO DRG could be compensated by TNFα resulting in the same percentage of responders in WT (vehicle treated) and KO (TNFα treated). This effect was based on the significant increase of MO responding cells in TM KO after TNFα stimulation compared to vehicle stimulation. Furthermore, the capsaicin amplitude was increased in TM KO DRG after cytokine application. The lower percentage of MO responders in TM KO's in vehicle treated cultures, which could be compensated with TNFα application (Figure 26) might explain the attenuated mechanical hypersensitivity assessed under inflammatory pain conditions in TM KO's (3.1.5). Given TRPA1 involvement in inflammatory pain signaling (Dai et al., 2007; Meng et al., 2016; Schmidt et al., 2009; Wang et al., 2008) and mechanical hypersensitivity (Kwan et al., 2006; Petrus et al., 2007), it could be possible that the behavioral phenotype was based on the lower amount of TNFα expression, which leads to reduced TRPA1 surface delivery (Meng et al., 2016). The experiments were performed by my Master student Hanna Kristina Fischer, taught and supervised by me.

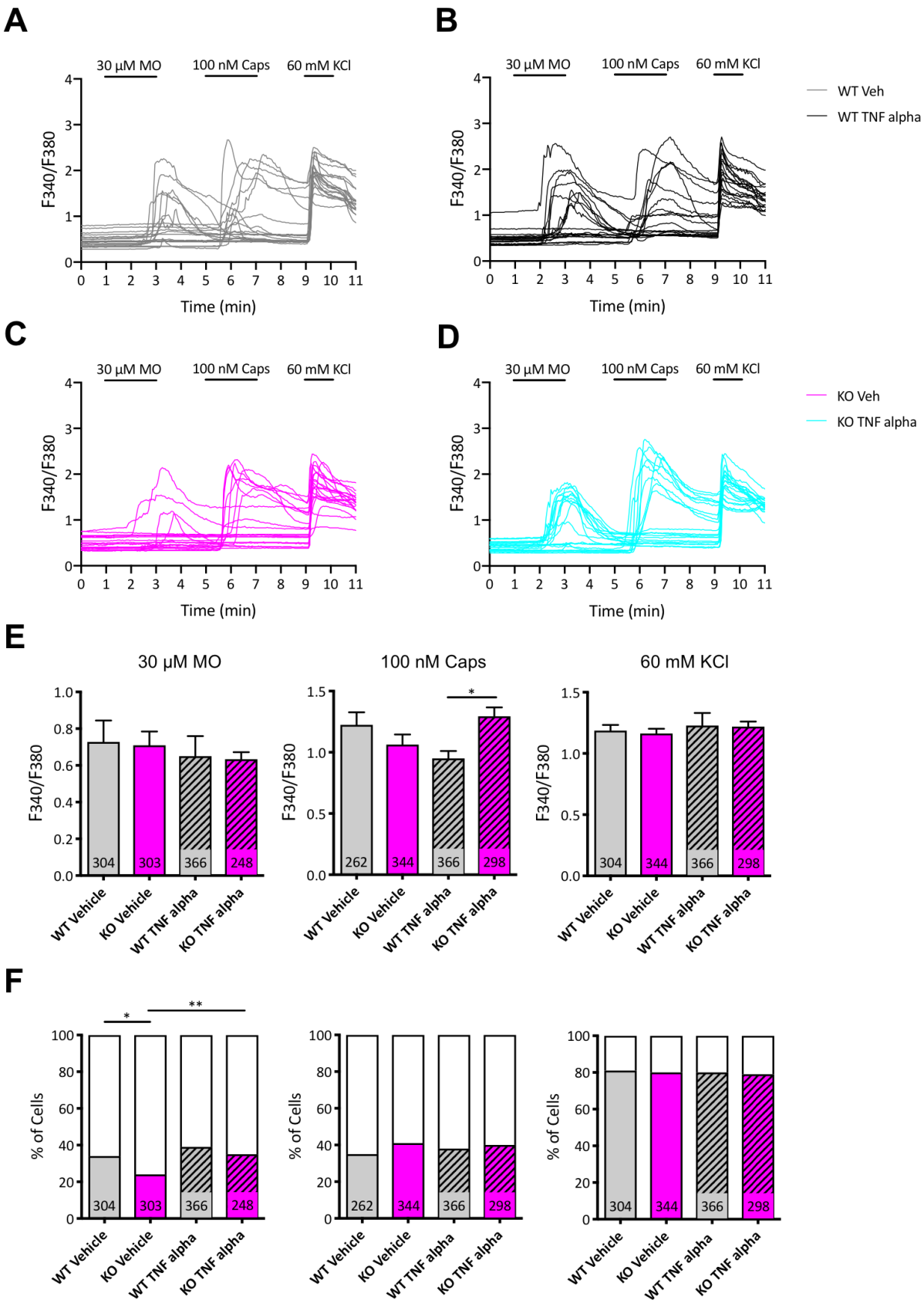

Figure 26: TNFα Stimulation compensated lower Amount of TRPA1 Responders in TM KO Neurons

(A-D) Representative traces (20 neurons) of response amplitudes (peak of fluorescence 340/380 above baseline) of (A) WT Veh, (B) WT TNFα, (C) KO Veh and (D) KO TNFα studied by ratiometric calcium imaging of

sensory neurons of WT and TM KO mice. 3 stimuli were given (30 µM MO, 100 nM Caps, 60 mM KCl) and resulting amplitudes were measured. (E) Lower WT TNFα mean amplitude compared to KO TNFα after 100 nM Caps stimulus, whereas no alterations were seen for other stimuli. Cell count in columns; WT N = several coverslips from n = 3 independent cultures; KO N = several coverslips from n = 3 independent cultures; 1-way ANOVA followed by Sidak's multiple comparison tests; * $p < 0.05$. Data were represented as mean ± SEM. (F) Decreased proportion of MO responders in KO Veh compared to WT Veh. Incubation with the cytokine TNFα resulted in the adjustment of the previously lower amount of KO responders to a level with is similar to WT Veh during the MO pulse. This increase of responses specific for TRPA1 expressing neurons after TNFα stimulation in DRG of TM KO mice was significantly higher compared to KO Veh. No alterations for Caps or KCl responders. Colored area of stacked bar graphs showed proportion of responders (colored) and non-responders (white). Count of total number of neurons in columns; WT N = several coverslips from n = 3 independent cultures; KO N = several coverslips from n = 3 independent cultures; the Fisher exact test; * $p < 0.05$, ** $p < 0.01$.The experiments were conducted by my Master student Hanna Kristina Fischer, taught and supervised by me. DRG, dorsal root ganglia; MO, mustard oil; Caps, capsaicin; KCl, potassium chloride; Veh, Vehicle; TNFα, tumor necrosis factor alpha.

4. DISCUSSION

4.1 Characterization of TM as Novel Pain Modality-specific Mitochondrial Protein

The specific mechanisms underlying persistent pain states remain to be fully understood. Here, I present a completely novel and important role for the hitherto uncharacterized mitochondrial transmembrane protein TM in inflammatory pain. The comprehensive proteome profiling study from Rouwette and colleagues revealed a downregulation of TM upon inflammatory and neuropathic pain conditions (Rouwette et al., 2016). Based on this finding, I investigated its functional role in somatosensation and pain *in vivo*. I showed that TM KO mice exhibit an impairment of mechanical hypersensitivity during inflammatory pain and early neuropathic pain (POD 7, when inflammation is most prominent (Cobos et al., 2018)). Strikingly, other investigated pain modalities (e.g. thermal hypersensitivity, non-evoked and movement-evoked pain) were unaltered upon TM deletion. While further work is needed to fully comprehend the mechanistic basis for the observed chronic pain phenotype in TM KO mice, there is strong evidence for altered inflammatory signaling pathways after TM ablation. Calcium imaging revealed a decreased activation of TRPA1 expressing neurons in DRG cultures of TM KO mice, which could be compensated by incubation with TNFα. These findings were in line with lower mRNA levels of the prototypic inflammatory mediator TNFα in DRG of naive TM KO mice. Furthermore, the chemokine CCl2, also known to be implicated in inflammatory pain signaling, was downregulated in sciatic nerves of TM KO's. Additionally, TM depletion caused an alteration in the expression of several subunits of the mitochondrial electron transport chain as well as decreased levels of the mitochondrial transcription factor Tfam (mRNA level). However, alterations on protein level and further assays to test for mitochondrial dysfunction could not be detected. Moreover, major changes were not detected among genotypes regarding oxidative stress responses in naive TM KO mice and after induction of inflammatory pain. Altered neuronal excitability (naive TM KO mice) and expression (naive and CFA-treated TM KO mice) could not be identified as potential mechanism for the behavioral phenotype. All together, these findings suggest a role for TM in inflammatory pain signaling.

4.1.1 No overt Mitochondrial Dysfunction upon TM Deletion

Pain medication has a great potential for improvement, because the existing analgesics are inadequate as they are targeting molecules with important physiological functions resulting in strong side effects. However, the basis for the suboptimal treatment is the incomplete knowledge about the molecular mechanisms underlying chronic pain (Patapoutian et al., 2009). A major step forward was taken by performing unbiased quantitative proteome profiling (mass spectrometry) with DRG of mice exhibiting 2 pain entities, which revealed the differential regulation of known pain players as well as novel mediators (Rouwette et al., 2016). These results included the modulation of dozens of mitochondrial proteins. TM was identified among them and functionally investigated as it was scarcely characterized, had a differential regulation upon pain and revealed a high expression in DRG. I was able to proof its ubiquitous expression in mitochondria (Figure 6), which was particularly interesting given the evolving notion that diverse pathological pain conditions are accompanied by mitochondrial dysfunction (Baloh et al., 2008; Fernyhough et al., 2010; Joseph et al., 2009; Osio et al., 2006; Rouwette et al., 2016). Impaired mitochondrial function can arise from oxidative stress induced by increased ROS production (Kim et al., 2004), which leads to microglia activation (Kallenborn-Gerhardt et al., 2012). Moreover, electron transport chain (ETC) activity changes (Baloh et al., 2008; Fernyhough et al., 2010; Joseph et al., 2009; Osio et al., 2006) and an unbalanced calcium homeostasis (Shishkin et al., 2002) are implicated in altered mitochondrial function. Therefore, I examined TM KO mice regarding potential changes in mitochondrial function and could identify the downregulation of the mitochondrial transcription factor A (Tfam) on mRNA level (Figure 17 A) in DRG of naive TM KO mice. Tfam is a nuclear encoded mitochondrial protein, which is crucial for mitochondrial DNA (mtDNA) transcription and replication (Ekstrand et al., 2004; Larsson et al., 1998). Reports have shown that mice with a tissue specific Tfam KO reveal a serious mtDNA deficiency and mitochondrial respiratory chain depletion (Larsson et al., 1998; Silva et al., 2000; Sörensen et al., 2001; Wang et al., 1999; Wredenberg et al., 2002). Moreover, Viader et al. claim that a mitochondrial dysfunction caused by a Schwann cell (SC) specific Tfam deletion in mice is sufficient to cause demyelination and axonal degeneration. Furthermore, mitochondria isolated from sciatic nerves of these Tfam KO's revealed a decrease of Cox (Complex IV) activity by half and decreased mitochondrial respiration. These deficiencies might be caused by Complex I, III, IV defects as these incorporate mtDNA-encoded subunits (Viader et al., 2011). The decreased Tfam mRNA levels identified in DRG of naive TM KO mice in my study could therefore also explain the downregulation of Cox1 (cytochrome c oxydase c1 (Complex IV)) and ND2 (subunit of NADH dehydrogenase (Complex I)) given their mitochondrial encoding. However, the mitochondrial encoded subunit of Complex III (Cytb, cytochrome b) was not differentially expressed and the nuclear encoded Uqcr10 (ubiquinol-cytochrome c reductase, complex III subunit X (Complex III)) was upregulated in DRG of TM KO mice

(Figure 17 A). Since the composition of Complex III is based on mitochondrial and nuclear encoded proteins, I expected a decrease in Cytb mRNA levels as well upon Tfam reduction. However, this could be explained by the relatively mild decrease in Tfam expression which does not necessarily have to affect all subunits of the ETC in a similar manner. Additonally, I continued with the investigation of ETC components expression after the induction of inflammatory pain (1 d post CFA), showing no major changes in TM KO DRG and sciatic nerve. Furthermore, the altered ETC subunit expression under naive conditions seems to be compensated under inflammatory pain conditions, because no major differences among genotypes were identified (Figure 17). This finding indicates a different mechanistic basis for the attenuated mechanical hypersensitivity upon CFA injection in TM KO mice (3.1.5). Nevertheless, motivated by the differential expression under naive conditions, I intented to investigate further aspects of mitochondrial function. These included the study of mitochondrial protein expression (ETC subunits, Figure 18), activity levels of ETC components (Figure 19, 20), oxygen consumption rate (Figure 21) and mitochondrial membrane potentials (Figure 22). Collectively, all of the mitochondrial function parameters were similar among genotypes. However, it is important to mention that the assays were either performed with DRG lysates/ cultures (Figure 20, 22) or with mitochondria isolated from brain, heart, liver of naive mice from both genotypes (Figure 18, 19, 21). Mitochondria from DRG were not used, as previous studies showed that DRG of 10 mice would be needed to extract enough of these organells. As the TM KO was constitutive, all tissues were affected making the use of brain, heart and liver informative after all.

Furthermore, I examined whether TM deficiency in DRG affected the oxidative stress response. Based on the analgesic phenotype of TM KO mice and the implication of oxidative stress in distinct chronic pain pathologies, (Akude et al., 2011; Baloh et al., 2008; Flatters et al., 2015), I expected decreased ROS levels upon TM deletion. An additional guiding principle for this assumption was the nexus between oxidative stress and differential expression of ETC components leading to increased ROS production (Kim et al., 2004). I demonstrated the regulation of ETC subunits in DRG of TM KO mice on mRNA (Figure 17 A), but not on protein level (Figure 18). However, experiments assessing the amount of mitochondrial ROS (Mitosox used as indicator) revealed an opposite outcome. A slight increase in ROS levels was shown in DRG isolated from TM deficient mice (Figure 23). Given the moderate increase I do not assign a biological relevance to this outcome, which is also supported by intact mitochondrial function examined in naive TM KO mice. These findings correlate with unaffected basal somatosenstation (3.1.5, pretesting values). Nonetheless, to investigate whether mitochondrial dysfunction is the basis for the observed chronic pain phenotye in TM KO mice (3.1.5), the mentioned assays need to be performed with DRG/ mitochondria isolated from mice exhibiting chronic pain.

4.1.2 The Need for an extended Pain Paradigm Portfolio

Rouwette et al. were able to identify dozens of novel chronic pain mediators by proteomics and functionally validated the biological significance of some candidate proteins in nociception and pain (Rouwette et al., 2016). This study is a crucial stepping stone for the determination of the molecular pain signature. However, a further hurdle for the identifcation of proper analgesics is the translation from animal studies to the clinic (Gregory et al., 2013). Criticizm is often addressed to pain models as they do not fully reflect clinically relevant pain entities like spontaneous pain (Cobos et al., 2012; Mogil et al., 2010; Urban et al., 2011). In fact, non-evoked pain at rest considered as spontaneous pain, is the pain entity often reported by chronic pain patients (Gottschalk and Ochroch, 2008; Maguire et al., 2006; Wildgaard et al., 2009). Thus, the first step for an improved translation into clinics might be the expansion of commonly used reflexive behavioral paradigms by non reflexive pain measurements (test for spontaneous pain) (Gregory et al., 2013). This is further emphasized by a study showing that measures of spontaneous pain correlated with altered dynamic gait parameters (movement-evoked pain) in the initial phase of neuropathic pain in the SNI model. Pitzer and colleagues also demonstrated that static gait parameters upon induction of neuropathic pain (SNI model) were timely congruent with stimulus-evoked pain behavior (mechanical and thermal hypersensitivity). These findings indicated the gait analysis as valuable tool to examine movement-evoke pain in the SNI model (Pitzer et al., 2016). Based on the mentioned critizism and the findings from Pitzer et al. our collaboration partner Dr. Daniel Segelcke (Group of Translational Pain Research, PI Prof. Esther Pogatzki-Zahn) implemented non reflexive parameters (non-evoked pain and movement-evoked pain) in the functional investigation of TM *in vivo*. The broad behavioral investigation of TM KO mice revealed a modality-specific phenotype under inflammatory pain conditions (CFA injection, 3.1.5). More precisely, TM KO mice showed attenuated mechanical hypersensitivity at day 1 and 3 post CFA injection as well as in the initial phase of neuropathic pain (POD 7), where inflammation is most prominent (Cobos et al., 2018). These results indicate that TM is a pro-algesic factor specifically involved in the stimulus-evoked mechanical pain hypersensitivity. Further behavioral investigation of mice harboring a sensory neuron specific TM KO showed a similar phenotype suggesting a sensory neuron specific TM contribution. Non reflexive parameters like non-evoked pain and movement-evoked pain are not altered among genotypes after chronic pain induction. Therefore, TM is proposed to be implicated in mechanical stimulus evoked- but not spontaneous pain. This could be explained by different mechanisms underlying evoked and spontaneous pain (Hung et al., 2016; Mogil et al., 2010). This specific involvement of TM in chronic pain underscored the importance for the performance of a wide range of behavioral paradigms to pinpoint the mechanistic basis for potential pain mediators. Our results are in line with findings from Pitzer et al. (Pitzer et al., 2016). However, it is important to mention that altered gait parameters

during chronic pain are controversially debated. Mogil et al. claim that gait changes do not correlate with pain (Mogil et al., 2010), whereas others suggest that a correlation exists (Coulthard et al., 2002; Möller et al., 2012; Parvathy and Masocha, 2013; Piesla et al., 2009). The basis for differential findings could be diverse mouse strains, the investigated pain model as well as the time point of investigation and the test chosen for the examination (Pitzer et al., 2016). It was argued that inflammatory pain per se causes altered gait in inflammatory pain models (Piesla et al., 2009), while the gait impairment during neuropathic pain is assigned to motor system malfunction (Piesla et al., 2009). On the other hand, it was shown that motor impairment was not the basis for gait alteration during neuropathic pain (Deumens et al., 2007; Vrinten and Hamers, 2003). Moreover, chronic pain is a complex and multidimensional disease involving affective and emotional elements as well as the general well-being (Melzack and Casey, 1968; Twillman, 2007). Given that, a promising approach would be to extend the battery of behavioral tests even further in future studies examining these components to get a more thourough picture of pain (Pitzer et al., 2016).

4.1.3 Decreased Neuronal Subpopulation Excitability after TM Elimination

Calcium-permeable TRP (transient receptor potential) channels like TRPV1 and TRPA1 are highly expressed in nociceptors. They are mainly implicated in the transduction of noxious stimuli and modulation of nociceptive processing (Bourinet et al., 2014; Patapoutian et al., 2009). Their activation is involved in physiological and pathophysiological pain signaling based on their regulation and sensitization (Caterina et al., 1997, 2000; Obata et al., 2005; Sousa-Valente et al., 2014; Story et al., 2003). Furthermore, Piezo2 ion channels play crucial roles in vertebrate light touch (Coste et al., 2010, 2012; Ranade et al., 2014). Given the important roles of the mentioned ion channels, I wanted to examine whether their neuronal activity was altered in TM depleted mice. Therefore, electrophysiology was performed in addition to ratiometric calcium imaging. More precisely, Ca^{2+}-imaging was carried out by application of specific chemical stimuli to activate the TRP channels (capsaicin: TRPV1 agonist (Caterina et al., 1997); mustard oil: TRPA1 agonist (Bautista et al., 2006; Jordt et al., 2004)). The experiments indicated decreased mustard oil-evoked calcium responses upon TM elimination (Figure 26 A, KO Vehicle), whereas the capsaicin dependent calcium influx was unaltered (Figure 16 and Figure 26, KO Veh). Besides, Piezo2-mediated mechanotransduction (Coste et al., 2010, 2012; Ranade et al., 2014) was not affected in naive TM KO mice (Figure 15). These *in vitro* findings were in line with the unaltered basal sensitivity of TM KO mice to thermal (TRPV1 involvement, Caterina et al., 1997; Julius, 2013) and mechanical (Piezo2 mediated, Coste et al., 2010, 2012; Ranade et al., 2014) paw stimulation (pretesting values) as well as nocifensive behavior upon intraplantar capsaicin (TRPV1 mediated acute pain, Caterina et al., 2000) injection (3.1.5). Whether mustard oil induced acute pain behavior (Bautista et al., 2006; Kwan et al., 2006) correlates to the

reduced levels of TRPA1 mediated calcium influx (Figure 26 A, KO Veh) needs to be determined in future experiments.

All together, the results suggest that TM elimination does not affect basal somatosensation and capsaicin induced physiological pain but rather advocate for the described implication in chronic pain.

4.1.4 Modulatory Role for TM in Inflammatory Pain Signaling

It was noticeable that TM depletion alleviated only mechanical hypersensitivity during inflammatory pain and the initial stage of neuropathic pain (POD 7), while thermal sensation was unaffected (3.1.5). This modality-specific TM involvement might be based on a functional connection to the immune system. This hypothesis is supported by decreased mRNA levels of the prototypic inflammatory mediators TNFα (tumor necrosis factor alpha, Figure 17 B) and CCl2 (chemokine (C-C motif) ligand 2, Figure 17 D) in DRG or sciatic nerves of naive TM KO mice. However, the downregulation of these inflammatory markers could not be shown after CFA injection (Figure 17 G, H), which could be explained by a high sample variability that might underrepresent an effect. Furthermore, Cobos et al. showed the linkage of immune cells and neurons to mechanical hypersensitivity (tactile allodynia) and mainly neurons to thermal hypersensitivity (cold allodynia) upon neuropathic pain (SNI model). They demontrated that cold allodynia develops relatively fast having its peak at POD 4-5, whereas tactile allodynia reveals a slower progression with maximal hypersensitivity at POD 7-8 (Cobos et al., 2018). This finding is in line with other studies showing a slower course of mechanical hypersensitivity compared to cold allodynia (Decosterd and Woolf, 2000; Pertin et al., 2007; Wijnvoord et al., 2010). Interestingly, POD 7 defined by maximal tactile allodynia post SNI, was the exact time point where TM KO mice revealed an impairment in this pain modality (3.1.5). Motivated by the different starting points of mechanical and cold allodynia Cobos et al. performed transcriptomics (ipsilateral DRG post SNI, daily until POD 10) in order to correlate the relative timing of gene expression with the evoked pain behavior (Cobos et al., 2018). Intriguingly, the onset of cold allodynia nicely corresponded to early neuronal gene regulation as well as mechanical allodynia which correlated to the differential expression of immune cell related genes (Cobos et al., 2018). The immune cell genes seemed to be enriched in macrophages and T cells known to be abundant in DRG after nerve damage (Hu and McLachlan, 2002; Moalem and Tracey, 2006). Moreover, Trpv1-deficient mice (to a great part insensitive to temperature as TRPV1 is an early developmental marker of all cold- and hot neuronal detectors, (Mishra et al., 2011)) revealed impaired cold hypersensitivity after SNI, while tactile allodynia was present. On the other hand, macrophage or T cell-depleted mice, showed alleviated mechanical hypersensitivity and unimpaired

cold allodynia post SNI. These findings suggest a distinct cellular and molecular mechanism necessary for the induction of cold and tactile allodynia upon nerve injury (Cobos et al., 2018). The basis for cold allodynia might be paracrine signaling from injured DRG neurons which alter the sensitivity of neighboring intact thermo-nociceptors to cold or abnormal processing in the central nervous system (CNS). The ectopical activity of injured C-nociceptors (Kirillova et al., 2011) could support central sensitization leading to painful perception of low-threshold thermoreceptor inputs into the dorsal horn (Latremoliere and Woolf, 2009). Contrarily, tactile allodynia seems to be evoked by low-threshold mechanoreceptors (LTMRs) (Campbell and Meyer, 2006; Xu et al., 2015) of which a broad range expresses Piezo2 relevant for touch sensation (Ranade et al., 2014), and activated immune cells (Cobos et al., 2018). These cells might trigger the phenotypic switch of A-fibers after nerve injury which thereby gain the capacity to initiate central sensitization. Another possibility could be the sensitization of intact high-threshold A-fiber nociceptors by immune cells upon PNS damage. The basis for mechanical allodynia could be either of these mechanisms or a combination of both (Cobos et al., 2018). This study from Cobos and colleagues highly supported my hypothesis for the specific contribution of TM in immune signaling. I showed that TNFα and CCl2 mRNA was downregulated in naive TM KO mice (Figure 17). These inflammatory mediators are known to be secreated from immune cells like macrophages upon nerve injury (accompanied by inflammation) contributing to hypersensitivity (Andrade et al., 2014; Schuh et al., 2014; Zhu et al., 2014). However, as mentioned above a reduction of these signaling molecules could not be demonstrated upon inflammatory pain as samples revealed a high variability. The reduction under naive conditions might indicate a slightly suppressed immune system that manifests as behavioral outcome only when challenged by the induction of inflammatory pain. Furthermore, interferon-gamma (IFN-g) secreted by Th1 T cells can lead to macrophage attraction to inflamed tissue and cause pain (Liou et al., 2011). On the other hand, type 2 inflammatory cytokines (e.g. TGF-b, IL-10, IL-4) can alleviate neuropathic pain-like behavior (Chen et al., 2015; Dengler et al., 2014; Kiguchi et al., 2015). Yet, the role of T cells in neuropathic pain conditions has been investigated in several studies with controversial outcomes. Some did not correlate T cell action to the pain- phenotype (Sorge et al., 2015), while others where able to show the connection (Cao and Deleo, 2008; Cobos et al., 2018; Costigan et al., 2009a; Kobayashi et al., 2015; Leger et al., 2011; Zhang et al., 2014). This divergency might originate from the balance between the mentioned pro-and anti-inflammatory subdivisions in distinct experimental settings (Austin et al., 2012; Kiguchi et al., 2015). Moreover, all studies were performed with male rodents except for Sorge and colleagues, who investigated both sexes. Sorge et al. showed that mechanical hypersensitivity during inflammatory and neuropathic pain was microglia-mediated in male and based on adaptive immune cells (probably T cells) in female mice (Sorge et al., 2015). This finding could be approved by another study suggesting that T cells mediate pain hypersensitivity in

female mice (Mapplebeck et al., 2016). Interestingly, my study revealed that the sensory neuron specific (cKO in SeN) TM KO mice showed a similar attenuation of mechanical hypersensitivity upon CFA injection as constitutive KO mice (3.1.5.). Even though half of the investigated cKO in SeN mice were females, mainly TM KO males were tested. This similar outcome among sexes might indicate alterations in immune signaling in both KO lines which cannot specifically be associated to macrophages or T cells. As Cobos et al. proposed that it could be an interaction of both immune cells leading to alterations within the DRG that cause tactile allodynia. However, the underlying mechanism needs to be further investigated (Cobos et al., 2018). Given the involvement of macrophages in mechanical hypersensitivity, I investigated the amount of these cells within the DRG of male TM KO and WT mice upon induction of inflammatory pain (1 d post CFA). Unfortunately, the experiment was not successful as WT DRG isolated from the CFA-injected body part did not reveal an increased amount of macrophages compared to the contralateral side. Therefore, it is not possible to conclude whether the unaltered level of macrophages in TM KO DRG (ipsi vs. con) was reliable. Furthermore, it will be important to assess potential alterations of T cells in DRG as well as microglia levels within the spinal cord in order to advance towards the understanding of the mechanism which underlies impaired mechanical hypersensitivity during inflammatory and early neuropathic pain. Cobos et al. stated that macrophages and T cells most probably act on sensory fibers which do not belong to the TRPV1 lineage (Cobos et al., 2018). However, uninjured TRPA1 expressing high-threshold A-fiber nociceptors might be sensitized by these immune cells. Several studies claim TRPA1 involvement in the development and preservation of hypersensitivity in diverse animal pain models. A definite mitigation of mechanical hypersensitivity was shown in inflammatory pain models due to TRPA1 antagonists or TRPA1 deficiency. Inflammation was either induced by TNFα, CFA or monoiodoacetate injection (Fernandes et al., 2011; Laing and Dhaka, 2016; McGaraughty et al., 2010). Moreover, decreased cold and mechanical hypersensitivity was also reported upon neuropathic pain due to pharmacological inhibition or genetic TRPA1 ablation (Nassini et al., 2014). In addition, TRPA1 channels are targeted by inflammatory molecules and act as molecular oxidative stress sensors. One example is ROS, which levels severely increase upon tissue damage/ inflammation and can cause the induction of lipid peroxidation (Bautista et al., 2013). Thereby, diverse lipid peroxidation products (e.g. 4-oxononenal (4-ONE) and 4-hydroxynonenal (4-HNE)) were generated that can activate TRPA1 channels (Taylor-Clark et al., 2008; Trevisani et al., 2007). Given the implication of oxidative stress in inflammatory pain and the involvement of TRPA1, I wanted to investigate whether 4-HNE levels were altered in DRG from CFA injected TM KO and WT mice. However, I could not detect any differences among genotypes (Figure 24). These results were in line with Ca^{2+}-imaging results upon TNFα stimulation which revealed unaltered TRPA1- and TRPV1-mediated calcium responses (Figure 26). On the other hand, responses to mustard oil (MO)

application were reduced in Veh-treated TM KO mice which were compensated to WT Veh levels after stimulation with TNFα. These results underscored the reduced TNFα mRNA levels investigated in naive TM KO mice (Figure 17 B). Previous studies revealed that the basis for enhanced TRPV1-and TRPA1-mediated Ca^{2+} influx might be the increased surface delivery of these channels triggered by the prototypic inflammatory mediator TNFα (Meng et al., 2016). Intriguingly, all mentioned alterations in TM KO mice were investigated under naive conditions. These findings indicate a protective mechanism in regard to inflammatory pain susceptibility in TM deficient mice. In sum, there is evidence that this altered inflammatory signaling has its basis in decreased TNFα levels investigated in DRG of naive TM KO mice.

4.1.5 Conclusion and Outlook

Motivated by the significantly decreased TNFα mRNA levels in DRG of naive TM KO mice (Figure 17 B), I wanted to obtain a vast overview of inflammatory mediators in the KO mice of interest. To this end, cytokine proteome profiling for 40 cytokines (CXCL13, C5a, G-CSF, GM-CSF, CCL1, CCL11, sICAM-1, IFN-γ, IL-1α, IL-1β, IL-1ra, IL-2, IL-3, IL-4, IL-5, IL-6, IL-7, IL-10, IL-13, IL-12p70, IL-16, IL-17, IL-23, IL-27, IP- 10, CXCL11, KC, M-CSF, CCL2, CCL12, CXCL9, CCL3, CCL4, CXCL2, CCL5, CXCL12, CCL17, TIMP-1, TNF-α and TREM-1) in DRG lysates from both mouse lines has been performed by my Master student Hanna Kristina Fischer, supervised and taught by me. The cytokine array allows for detection of all mentioned cytokines by incubation of protein lysates with antibody-coated membranes (according to Keskinov et al., 2016). The comparison of resulting cytokine spot intensities revealed a first trend (data not shown) for an overall reduction in DRG lysates of TM KO mice compared to WT mice. This potential dampened cytokine expression upon TM ablation needs to be verified by experimental repetitions. The trend for reduced cytokine levels is in line with the mentioned modifications in naive TM KO mice. However, the experiments will be additionally carried out upon induction of inflammatory and neuropathic (DRG isolation at POD 7) pain in order to investigate potential changes of inflammatory signaling during chronic pain. Among these cytokines were TNFα as well as GM-CSF (Granulocyte-macrophage colony-stimulating factor) and CCl17 (Chemokine (C-C motif) ligand 17) proposed to be implicated in the inflammatory and algesic action of TNFα (Cook et al., 2018). Based on these findings and the trend for a reduction of TNFα, GM-CSF and CCl17 on protein level in DRG lysates of TM KO mice, we will further proceed in this direction in order to identify the molecular mechanisms of the attenuated pain phenotype upon TM ablation. If the trend can be verified with DRG from additional TM KO mice, calcium imaging could be performed with sensory neurons of both genotypes being stimulated with GM-CSF and CCl17. qRT-PCR will also be performed to investigate a potential alteration of these cytokines on mRNA level. Furthermore, it is known that TNFα triggers ROS formation (Valko et al., 2007) and our qRT-PCR data showed a significant downregulation of the

prototypic inflammatory mediator in DRG of naive TM KO mice (Figure 17 B). Given that, I postulate lower ROS levels in DRG of TM KO mice after TNFα stimulation. So far the mitochondrial ROS indicator revealed a slightly increased intensity in DRG cultures of naive TM KO mice (Figure 23) and lipid peroxidation was unaltered upon CFA injection in DRG among both genotypes (Figure 24). However, in order to valdiate the hypothesis, the assessment of oxidative stress by the ROS-sensitive DHE (dihydroethidium)-dye is in progress. Cultured sensory neurons were stimulated for 6 h with TNFα (Hall et al., 2014; Hervera et al., 2018; Willemen et al., 2018) followed by DHE imaging and analysis (performed by my Master student Hanna Kristina Fischer, taught and supervised by me). In future experiments inflammatory pain will be induced by intraplantar injection of TNFα (Fernandes et al., 2011) in order to investigate whether decreased endogenous levels result in decreased pain behavior in TM KO mice. Moreover, TM KO and WT mice will additionally be injected in one of the hind paws with mustard oil (MO) in order to examine whether the acute pain behavior (Bautista et al., 2006; Kwan et al., 2006) is connected to the lower amount of TRPA1 mediated calcium responses in DRG of TM KO mice (Figure 26). The outcome can be valuable, given the implication of TRPA1 in mechanical hypersensitivity upon inflammatory pain (Fernandes et al., 2011; Laing and Dhaka, 2015; McGaraughty et al., 2010). In addition, TM will be re-expressed in TM KO mice by standard nucleofection *in vitro* and by virus-mediated gene transfer *in vivo*. Virus-mediated gene transfer was already successfully performed in our lab by sciatic nerve injections leading to transduction of sensory neurons of DRG in mice (Sondermann et al., 2018). Upon re-expression *in vivo*, behavioral paradigms will be performed in order to test whether the observed attenuated mechanical hypersensitivity upon inflammatory pain can be “rescued”. If the “rescue-experiment” was successful, it would underscore the essential role of TM downregulation *per se* to attenuate inflammatory mechanical hypersensitivity. These results would additionally support the hypothesis that the downregulation of TM serves as modality specific analgesic mechanism.

I could show that the decreased TRPA1 dependent calcium influx in DRG of TM KO mice was equalized to WT levels upon stimulation with TNFα (Figure 26). This stimulation mimicked inflammatory conditions. However, the behavioral phenotype in TM KO mice was identified upon CFA injection (1 day post). Therefore, calcium imaging will also be carried out with DRG isolated from mice 1 day post CFA injection (with the same stimuli as given upon TNFα/ Veh stimulation (Figure 26)). Neuronal acitivity (30 mM KCl) as well as TRPV1- (100 nM Caps) and TRPA1-mediated (30 µM MO) nociceptive signaling will be compared among genotypes. These DRG cultures prepared from CFA injected mice will also be subjected to electrophysiological experiments. In this way Piezo2-mediated mechanotransduction in DRG cultures during inflammatory pain might give more insights about the mechanism underlying the phenotype investigated in TM KO mice. Piezo2 is crucially implicated in light touch and a role in tactile hypersensitivity during inflammatory and neuropathic

pain was shown. It was reported that inflammatory mediators can have a modulatory effect on Piezo2 (Dubin et al., 2012; Prato et al., 2017). Given those findings it might be possible that Piezo2 alterations contribute to the investigated behavioral phenotype of TM KO mice. However, Piezo2 KO mice showed basal touch sensitivity in addition to tactile hypersensitivity upon capsaicin-induced inflammation. These findings are not in line with the behavior demonstrated by TM KO mice. Therefore, an exclusive role for Piezo2 is not supposed. All mentioned experiments will also be performed with DRG isolated from SNI-mice at POD 7, which is the time point at which reduced mechanical hypersensitivity was detected in TM KO mice (3.1.5).

Collectively, we were able to characterize TM as a modality-specific contributor of inflammatory pain signaling. Its downregulation in DRG of mice exhibiting inflammatory and neuropathic pain (proteome profiling, Rouwette et al., 2016) could be identified as part of an analgesic system. A detailed behavioral analysis of chronic pain conditons by reflexive and non-reflexive paradigms accompanied by a wide variety of *in vitro* techniques enabled this approach. For future studies it would be promising to implicate a broadened pain paradigm portfolio standardized within the pain field in order to achieve an improved understanding of chronic pain mechanisms. Our findings underscored the importance for the identification of distinct mechanistic etiologies for thermal and mechanical hypersensitivity. In terms of tactile allodynia immune cells or mechanoreceptors negative for TPRV1 should be targeted. Therefore, the medication of patients suffering from either type of allodynia should be adjusted in order to ashieve a good treatment outcome (Cobos et al., 2018).

5. BIBLIOGRAPHY

Abbadie, C., Lindia, J. A., Cumiskey, A. M., Peterson, L. B., Mudgett, J. S., Bayne, E. K., et al. (2003). Impaired neuropathic pain responses in mice lacking the chemokine receptor CCR2. 100, 7947–7952.

Abeti, R., and Abramov, A. Y. (2015). Mitochondrial Ca 2 + in neurodegenerative disorders. 99, 377–381.

Akude, E. L. I., Zherebitskaya, E., and Chowdhury, S. K. R. O. Y. (2010). 4-Hydroxy-2-nonenal Impairs Mitochondrial Physiology and Induces Aberrant Axonal Outgrowth in Adult Sensory Neurons that Mimics Features of Diabetic Neuropathy. 17, 28–38. doi:10.1007/s12640-009-9074-5.4-Hydroxy-2-nonenal.

Akude, E., Zherebitskaya, E., Chowdhury, S. K. R., Smith, D. R., Dobrowsky, R. T., and Fernyhough, P. (2011). Diminished Superoxide Generation Is Associated With Respiratory Chain Dysfunction and Changes in the Mitochondrial Proteome of Sensory Neurons From Diabetic Rats. 60. doi:10.2337/db10-0818.E.A.

Aley, K. O., Reichling, D. B., and Levine, J. D. (1996). Vincristine hyperalgesia in the rat: A model of painful vincristine neuropathy in humans. *Neuroscience*. doi:10.1016/0306-4522(96)00020-6.

Amir, R., Kocsis, J. D., and Devor, M. (2005). Multiple Interacting Sites of Ectopic Spike Electrogenesis in Primary Sensory Neurons. 25, 2576–2585. doi:10.1523/JNEUROSCI.4118-04.2005.

Andrade, P., Hoogland, G., Rosario, J. S. Del, Steinbusch, H. W., Visser-vandewalle, V., and Daemen, M. A. (2014). Tumor Necrosis Factor-α Inhibitors Alleviation of Experimentally Induced Neuropathic Pain is Associated With Modulation of TNF Receptor Expression. 1498, 1490–1498. doi:10.1002/jnr.23432.

Atzeni, F., Turiel, M., and Sarzi-puttinia, P. (2005). Autoimmunity and Anti-TNF-α Agents. 569, 559–569. doi:10.1196/annals.1361.100.

Austin, P. J., Kim, C. F., Perera, C. J., and Moalem-Taylor, G. (2012). Regulatory T cells attenuate neuropathic pain following peripheral nerve injury and experimental autoimmune neuritis. *Pain* 153, 1916–1931. doi:10.1016/j.pain.2012.06.005.

Avenali, L., Narayanan, P., Rouwette, T., Cervellini, I., Sereda, M., and Gomez-Varela, D. (2014). Annexin A2 Regulates TRPA1-Dependent Nociception. 34, 14506–14516. doi:10.1523/JNEUROSCI.1801-14.2014.

Balasubramanyan, S., Stemkowski, P. L., Stebbing, M. J., and Smith, P. A. (2006). Sciatic Chronic Constriction Injury Produces Cell-Type-Specific Changes in the Electrophysiological Properties of Rat Substantia Gelatinosa Neurons. *J. Neurophysiol.* doi:10.1152/jn.00087.2006.

Baloh, R. H. (2008). Mitochondrial Dynamics and Peripheral Neuropathy. 14. doi:10.1177/1073858407307354.

Bandell, M., Story, G. M., Hwang, S. W., Viswanath, V., Eid, S. R., Petrus, M. J., et al. (2004). Noxious Cold Ion Channel TRPA1 Is Activated by Pungent Compounds and Bradykinin. 41, 849–857.

Bareth, B., Nikolov, M., Lorenzi, I., Hildenbeutel, M., Mick, D. U., Helbig, C., et al. (2016). Oms1 associates with cytochrome c oxidase assembly intermediates to stabilize newly synthesized Cox1 . *Mol. Biol. Cell*. doi:10.1091/mbc.e15-12-0811.

Barrot, M. (2012). Tests and Models of Nociception and Pain in Rodents. *NSC* 211, 39–50. doi:10.1016/j.neuroscience.2011.12.041.

Basbaum, A. I., Bautista, D. M., Scherrer, G., and Julius, D. (2009). Cellular and Molecular Mechanisms of Pain. 267–284. doi:10.1016/j.cell.2009.09.028.

Bautista, D. M., Jordt, S., Nikai, T., Tsuruda, P. R., Read, A. J., Poblete, J., et al. (2006). TRPA1 Mediates the Inflammatory Actions of Environmental Irritants and Proalgesic Agents. 1269–1282. doi:10.1016/j.cell.2006.02.023.

Bautista, D. M., Movahed, P., Hinman, A., Axelsson, H. E., Sterner, O., Ho, E. D., et al. (2005). Pungent products from garlic activate the sensory ion channel TRPA1. 1–5.

Bautista, D. M., Pellegrino, M., and Tsunozaki, M. (2013). TRPA1 : A Gatekeeper for Inflammation. doi:10.1146/annurev-physiol-030212-183811.

Beggs, S., and Salter, M. W. (2007). Stereological and somatotopic analysis of the spinal microglial response to peripheral nerve injury. 21, 624–633. doi:10.1016/j.bbi.2006.10.017.

Bennett, D. L. H., and Woods, C. G. (2014). Painful and painless channelopathies. doi:10.1016/S1474-4422(14)70024-9.

Bennett, J. (1988). A peripheral mononeuropathy in rat that produces disorders of pain sensation like those seen in man. 33, 87–107.

Bostock, H., Campero, M., Serra, J., and Ochoa, J. L. (2005). Temperature-dependent double spikes in C-nociceptors of neuropathic pain patients. 2154–2163. doi:10.1093/brain/awh552.

Bourinet, E., Altier, C., Hildebrand, M. E., Trang, T., Salter, M. W., and Zamponi, G. W. (2014). Calcium-permeable ion channels in pain signaling. 81–140. doi:10.1152/physrev.00023.2013.

Breivik, H., Collett, B., Ventafridda, V., and Cohen, R. (2006). Survey of chronic pain in Europe : Prevalence , impact on daily life , and treatment. 10, 287–333. doi:10.1016/j.ejpain.2005.06.009.

Breivik, H., Eisenberg, E., and Brien, T. O. (2013). The individual and societal burden of chronic pain in Europe : the case for strategic prioritisation and action to improve knowledge and availability of appropriate care.

Caballero-Garrido, E., Pena-Philippides, J. C., Galochkina, Z., Erhardt, E., and Roitbak, T. (2017). Characterization of long-term gait deficits in mouse dMCAO , using the CatWalk system.

Campbell, J. N., and Meyer, R. A. (2006). Mechanisms of Neuropathic Pain. 77–92. doi:10.1016/j.neuron.2006.09.021.

Campbell, J. N., Raja, S. N., Meyer, R. A., and Mackinnon, S. E. (1988). Myelinated afferents signal the hyperalgesia associated with nerve injury. 32, 89–94.

Cannino, G., El-Khoury, R., Pirinen, M., Hutz, B., Rustin, P., Jacobs, H. T., et al. (2012). Glucose Modulates Respiratory Complex I Activity in Response to Acute Mitochondrial Dysfunction. 287, 38729–38740. doi:10.1074/jbc.M112.386060.

Cao, L., and Deleo, J. A. (2008). CNS-infiltrating CD4+ T lymphocytes contribute to murine spinal nerve transection-induced neuropathic pain. 448–458. doi:10.1002/eji.200737485.

Caterina, M. J., Leffler, A., Malmberg, A. B., Martin, W. J., Trafton, J., Koltzenburg, M., et al. (2000). Impaired Nociception and Pain Sensation in Mice Lacking the Capsaicin Receptor. 288, 306–314.

Caterina, M. J., Schumacher, M. A., Tominaga, M., Rosen, T. A., Levine, J. D., and Julius, D. (1997). The capsaicin receptor : a heat-activated ion channel in the pain pathway. 389.

Chen, G., Xie, R., Ji, R., Chen, G., Park, C., Xie, R., et al. (2015). Intrathecal bone marrow stromal cells inhibit neuropathic pain via TGF-β secretion. 125, 3226–3240. doi:10.1172/JCI80883DS1.

Clapham, D. E. (2003). TRP channels as cellular sensors. 426, 517–524.

Clark, A. K., and Malcangio, M. (2014). Fractalkine / CX3CR1 signaling during neuropathic pain. 8, 1–7. doi:10.3389/fncel.2014.00121.

Claros, M. G., and Vincens, P. (1996). Computational method to predict mitochondrially imported proteins and their targeting sequences. *Eur. J. Biochem.* doi:10.1111/j.1432-1033.1996.00779.x.

Cobos, E. J., Ghasemlou, N., Araldi, D., Segal, D., Duong, K., and Woolf, C. J. (2012). Inflammation-induced decrease in voluntary wheel running in mice : A nonreflexive test for evaluating inflammatory pain and analgesia. 153, 876–884. doi:10.1016/j.pain.2012.01.016.

Cobos, E. J., Nickerson, C. A., Gao, F., Rangachari, M., Woolf, C. J., Costigan, M., et al. (2018). Mechanistic Differences in Neuropathic Pain Modalities Revealed by Correlating Behavior with Global Expression Profiling. 1301–1312.

Cook, A. D., Lee, M., Saleh, R., Khiew, H., Christensen, A. D., Achuthan, A., et al. (2018). TNF and granulocyte macrophage-colony stimulating factor interdependence mediates inflammation via CCL17. 3, 1–18.

Costigan, M., Moss, A., Latremoliere, A., Johnston, C., Verma-Gandhu, M., Herbert, T. A., et al. (2009a). T-Cell Infiltration and Signaling in the Adult Dorsal Spinal Cord Is a Major Contributor to Neuropathic Pain-Like Hypersensitivity. 29, 14415–14422. doi:10.1523/JNEUROSCI.4569-09.2009.

Costigan, M., Scholz, J., and Woolf, C. J. (2009). Neuropathic Pain : A Maladaptive Response of the Nervous System to Damage. doi:10.1146/annurev.neuro.051508.135531.

Coull, J. A. M., Beggs, S., Boudreau, D., Boivin, D., Tsuda, M., Inoue, K., et al. (2005). BDNF from microglia causes the shift in neuronal anion gradient underlying neuropathic pain. 438, 1017–1021. doi:10.1038/nature04223.

Coulthard, P., Pleu, B. J., Brewster, M., Wilson, L., and Macfarlane, T. V (2002). Gait analysis as an objective measure in a chronic pain model. 116, 197–213.

Courteix, C. (1993). Streptozocin-induced diabetic rats : behavioural evidence for a model of chronic pain. 53, 81–88.

Cox, J. J., Reimann, F., Nicholas, A. K., Thornton, G., Roberts, E., Springell, K., et al. (2006). An SCN9A channelopathy causes congenital inability to experience pain. 444, 3–7. doi:10.1038/nature05413.

Dai, Y., Yamanaka, H., Noguchi, K., Dai, Y., Wang, S., Tominaga, M., et al. (2007). Sensitization of TRPA1 by PAR2 contributes to the sensation of inflammatory pain. doi:10.1172/JCI30951.known.

Deckers, M., Balleininger, M., Vukotic, M., Römpler, K., Bareth, B., Juris, L., et al. (2014). Aim24 stabilizes respiratory chain supercomplexes and is required for efficient respiration. *FEBS Lett.* doi:10.7554/eLife.01684.

Decosterd, I., and Woolf, C. J. (2000). Spared nerve injury : an animal model of persistent peripheral neuropathic pain. 87, 149–158.

Dengler, E. C., Alberti, L. A., Bowman, B. N., Kerwin, A. A., Wilkerson, J. L., Moezzi, D. R., et al. (2014). Improvement of spinal non-viral IL - 10 gene delivery by D-mannose as a transgene adjuvant to control chronic neuropathic pain. 1–21.

Descoeur, J., Pereira, V., Pizzoccaro, A., Francois, A., Ling, B., Courteix, C., et al. (2011). Oxaliplatin-induced cold hypersensitivity is due to remodelling of ion channel expression in nociceptors. 266–278. doi:10.1002/emmm.201100134.

Deumens, R., Jaken, R. J. P., Marcus, M. A. E., and Joosten, E. A. J. (2007). The CatWalk gait analysis in assessment of both dynamic and static gait changes after adult rat sciatic nerve resection. 164, 120–130. doi:10.1016/j.jneumeth.2007.04.009.

Dhaka, A., Viswanath, V., and Patapoutian, A. (2006). TRP Ion Channels and Temperature Sensation. doi:10.1146/annurev.neuro.29.051605.112958.

Dubin, A. E., and Patapoutian, A. (2010). Nociceptors: The sensors of the pain pathway. *J. Clin. Invest.* doi:10.1172/JCI42843.

Dubin, A. E., Schmidt, M., Mathur, J., Petrus, M. J., Xiao, B., and Coste, B. (2012). Inflammatory Signals Enhance Piezo2-Mediated Mechanosensitive Currents. 511–517.

Duchen, M. R. (2000). Mitochondria and calcium : from cell signalling to cell death. 57–68.

Ducreux, D., Attal, N., Parker, F., and Bouhassira, D. (2006). Mechanisms of central neuropathic pain: a combined psychophysical and fMRI study in syringomyelia. 963–976. doi:10.1093/brain/awl016.

Duggett, N. A., Griffiths, L. A., and Flatters, S. J. L. (2017). Paclitaxel-induced painful neuropathy is associated with changes in mitochondrial bioenergetics, glycolysis, and an energy deficit in dorsal root ganglia neurons. 158.

Dworkin, R. H., Backonja, M., Rowbotham, M. C., Allen, R. R., Argoff, C. R., Bennett, G. J., et al. (2003). Advances in Neuropathic Pain. *Arch. Neurol.* doi:10.1001/archneur.60.11.1524.

Ekstrand, M. I., Falkenberg, M., Rantanen, A., Park, C. B., Gaspari, M., Hultenby, K., et al. (2004). Mitochondrial transcription factor A regulates mtDNA copy number in mammals. 13, 935–944. doi:10.1093/hmg/ddh109.

Ellis, A., and Bennett, D. L. H. (2013). Neuroinflammation and the generation of neuropathic pain. 111, 26–37. doi:10.1093/bja/aet128.

Fernandes, E. S., Russell, F. A., Spina, D., Mcdougall, J. J., Graepel, R., Gentry, C., et al. (2011). A Distinct Role for Transient Receptor Potential Ankyrin 1 , in Addition to Transient Receptor Potential Vanilloid 1 , in Tumor Necrosis Factor α – Induced Inflammatory Hyperalgesia and Freund ' s Complete Adjuvant – Induced Monarthritis. 63, 819–829. doi:10.1002/art.30150.

Fernyhough, P. (2010). Mitochondrial stress and the pathogenesis of diabetic neuropathy. 5, 39–49.

Ferrick, D. A., Neilson, A., and Beeson, C. (2008). Advances in measuring cellular bioenergetics using

extracellular flux. 13. doi:10.1016/j.drudis.2007.12.008.

Fidanboylu, M., Griffiths, L. A., and Flatters, S. J. L. (2011). Global Inhibition of Reactive Oxygen Species (ROS) Inhibits Paclitaxel-Induced Painful Peripheral Neuropathy. 6. doi:10.1371/journal.pone.0025212.

Finnegan, T. F., Chen, S., and Pan, H. (2005). Effect of the μ Opioid on Excitatory and Inhibitory Synaptic Inputs to Periaqueductal Gray-Projecting Neurons in the Amygdala. 312, 441–448. doi:10.1124/jpet.104.074633.nucleus.

Flatters, S. J. L. (2015). "The contribution of mitochondria to sensory processing and pain," in *Progress in Molecular Biology and Translational Science* doi:10.1016/bs.pmbts.2014.12.004.

Fornoni, A., Ijaz, A., Tejada, T., and Lenz, O. (2008). Role of Inflammation in Diabetic Nephropathy. 7168, 10–17.

Fu, Y., Han, J., Ishola, T., Scerbo, M., Adwanikar, H., Ramsey, C., et al. (2008). Pain-related synaptic plasticity and behavior. 20, 1–20. doi:10.1186/1744-8069-4-26.

Fukuoka, T., Kobayashi, K., Yamanaka, H., Obata, K., Dai, Y., and Noguchi, K. (2008). Comparative study of the distribution of the α-subunits of voltage-gated sodium channels in normal and axotomized rat dorsal root ganglion neurons. *J. Comp. Neurol.* doi:10.1002/cne.21786.

Fünfschilling, U., Supplie, L. M., Mahad, D., Boretius, S., Saab, A. S., Edgar, J., et al. (2012). Glycolytic oligodendrocytes maintain myelin and long-term axonal integrity. *Nature*. doi:10.1038/nature11007.

Garami, A., Shimansky, Y. P., Pakai, E., Oliveira, D. L., Gavva, N. R., and Romanovsky, A. A. (2010). Contributions of Different Modes of TRPV1 Activation to TRPV1 Antagonist-Induced Hyperthermia. 30, 1435–1440. doi:10.1523/JNEUROSCI.5150-09.2010.

Gavva, N. R., Bannon, A. W., Surapaneni, S., Jr, D. N. H., Lehto, S. G., Gore, A., et al. (2007). The Vanilloid Receptor TRPV1 Is Tonically Activated In Vivo and Involved in Body Temperature Regulation. 27, 3366–3374. doi:10.1523/JNEUROSCI.4833-06.2007.

Gess, B., Ro, D., Fledrich, R., Sereda, M. W., Kleffner, I., Humberg, A., et al. (2011). Sodium-Dependent Vitamin C Transporter 2 Deficiency Causes Hypomyelination and Extracellular Matrix Defects in the Peripheral Nervous System. 31, 17180–17192. doi:10.1523/JNEUROSCI.3457-11.2011.

Gottschalk, A., and Ochroch, E. A. (2008). Clinical and Demographic Characteristics of Patients With Chronic Pain After Major Thoracotomy. 24, 708–716.

Grace, P. M., Hutchinson, M. R., Maier, S. F., and Watkins, L. R. (2014). Pathological pain and the neuroimmune interface. *Nat. Rev. Immunol.* doi:10.1038/nri3621.

Graeber, M. B., and Christie, M. J. (2012). Multiple mechanisms of microglia : A gatekeeper ' s contribution to pain states. *Exp. Neurol.* 234, 255–261. doi:10.1016/j.expneurol.2012.01.007.

Gregory, N. S., Harris, A. L., Robinson, C. R., Dougherty, P. M., Fuchs, P. N., and Sluka, K. A. (2013). An overview of animal models of pain: Disease models and outcome measures. *J. Pain*. doi:10.1016/j.jpain.2013.06.008.

Hains, B. C., and Waxman, S. G. (2007). Sodium channel expression and the molecular pathophysiology of pain after SCI. *Prog. Brain Res.* doi:10.1016/S0079-6123(06)61013-3.

Hall, D. D., Wu, Y., Domann, F. E., Spitz, D. R., and Anderson, M. E. (2014). Mitochondrial Calcium Uniporter Activity Is Dispensable for MDA-MB-231 Breast Carcinoma Cell Survival. 9. doi:10.1371/journal.pone.0096866.

Hehn, C. A. Von, Baron, R., and Woolf, C. J. (2012). Deconstructing the Neuropathic Pain Phenotype to Reveal Neural Mechanisms. *Neuron* 73, 638–652. doi:10.1016/j.neuron.2012.02.008.

Hervera, A., Virgiliis, F. De, Palmisano, I., Zhou, L., Tantardini, E., Kong, G., et al. (2018). Regeneration through the release of exosomal NADPH oxidase 2 complexes into injured axons. 20.

Honore, P., Chandran, P., Hernandez, G., Gauvin, D. M., Mikusa, J. P., Zhong, C., et al. (2009). Repeated dosing of ABT-102, a potent and selective TRPV1 antagonist, enhances TRPV1-mediated analgesic activity in rodents, but attenuates antagonist-induced hyperthermia. *Pain* 142, 27–35. doi:10.1016/j.pain.2008.11.004.

Hroudová, J., and Singh, N. (2014). Mitochondrial Dysfunctions in Neurodegenerative Diseases: Relevance to Alzheimer ' s Disease. 2014.

Hu, P., Bembrick, A. L., Keay, K. A., and Mclachlan, E. M. (2007). Immune cell involvement in dorsal root ganglia and spinal cord after chronic constriction or transection of the rat sciatic nerve. 21, 599–616. doi:10.1016/j.bbi.2006.10.013.

Hu, P., and McLachlan, E. M. (2002). Macrophage and lymphocyte invasion of dorsal root ganglia after peripheral nerve lesions in the rat. *Neuroscience*.

Hucho, T., and Levine, J. D. (2007). Signaling Pathways in Sensitization : Toward a Nociceptor Cell Biology. 365–376. doi:10.1016/j.neuron.2007.07.008.

Hung, C.-H., Wang, J. C.-F., and Strichartz, G. (2016). SPONTANEOUS CHRONIC PAIN AFTER EXPERIMENTAL THORACTOMY REVEALED BY CONDITIONED PLACE PREFERENCE: morphine differentiates tactile evoked pain from spontaneous pain. 16, 903–912. doi:10.1016/j.jpain.2015.06.006.SPONTANEOUS.

Huntjens, D. R. H., Spalding, D. J. M., Danhof, M., and Della, O. E. (2009). Differences in the sensitivity of behavioural measures of pain to the selectivity of cyclo-oxygenase inhibitors. *Eur. J. Pain* 13, 448–457. doi:10.1016/j.ejpain.2008.06.011.

Indo, Y. (2001). Molecular Basis of Congenital Insensitivity to Pain With Anhidrosis (CIPA): Mutations and Polymorphisms in TRKA (NTRK1) Gene Encoding the Receptor Tyrosine Kinase for Nerve Growth Factor. 471, 462–471.

Jaegle, M., Ghazvini, M., Mandemakers, W., Piirsoo, M., Driegen, S., Levavasseur, F., et al. (2003). The POU proteins Brn-2 and Oct-6 share important functions in Schwann cell development. *Genes Dev.*

Ji, R.-R., Berta, T., and Nedergaard, M. (2013). Glia and pain: Is chronic pain a gliopathy? 154, 1–46. doi:10.1016/j.pain.2013.06.022.Glia.

Ji, R. R., Chamessian, A., and Zhang, Y. Q. (2016). Pain regulation by non-neuronal cells and inflammation. *Science (80-.).* doi:10.1126/science.aaf8924.

Ji, R., Xu, Z., and Gao, Y. (2014). Emerging targets in neuroinflammation- driven chronic pain. 13, 533–548. doi:10.1038/nrd4334.

Ji, R., Xu, Z., Strichartz, G., and Serhan, C. N. (2011). Emerging roles of resolvins in the resolution of inflammation and pain. *Trends Neurosci.* 34, 599–609. doi:10.1016/j.tins.2011.08.005.

Jordt, S., Bautista, D. M., Chuang, H., Meng, I. D., and Julius, D. (2004). Mustard oils and cannabinoids excite sensory nerve fibres through the TRP channel ANKTM1. 427. doi:10.1038/nature02237.1.

Joseph, E. K., Chen, X., Khasar, S. G., and Levine, J. D. (2004). Novel mechanism of enhanced nociception in a model of AIDS therapy-induced painful peripheral neuropathy in the rat. 107, 147–158. doi:10.1016/j.pain.2003.10.010.

Joseph, E. K., Levine, J. D., and Francisco, S. (2009). Comparison of Oxaliplatin- and Cisplatin-Induced Painful Peripheral Neuropathy in the Rat. 10, 534–541. doi:10.1016/j.jpain.2008.12.003.

Julius, D. (2013). *TRP Channels and Pain*. doi:10.1146/annurev-cellbio-101011-155833.

Julius, D., and Basbaum, A. I. (2001). Molecular mechanisms of nociception. 413, 203–210.

Jung, H., Toth, P. T., White, F. A., and Miller, R. J. (2008). Monocyte chemoattractant protein-1 functions as a neuromodulator in dorsal root ganglia neurons. 254–263. doi:10.1111/j.1471-4159.2007.04969.x.

Kallenborn-Gerhardt, W., Schröder, K., Geisslinger, G., and Schmidtko, A. (2013). Pharmacology & Therapeutics NOXious signaling in pain processing. *Pharmacol. Ther.* 137, 309–317. doi:10.1016/j.pharmthera.2012.11.001.

Keller, A. F., Beggs, S., Salter, M. W., and Koninck, Y. De (2007). Transformation of the output of spinal lamina I neurons after nerve injury and microglia stimulation underlying neuropathic pain. 11, 1–11. doi:10.1186/1744-8069-3-27.

Keskinov, A. A., Tapias, V., Watkins, S. C., Ma, Y., Shurin, M. R., and Shurin, G. V. (2016). Impact of the sensory neurons on melanoma growth in vivo. *PLoS One*. doi:10.1371/journal.pone.0156095.

Khairatkar-joshi, N., and Szallasi, A. (2008). TRPV1 antagonists : the challenges for therapeutic targeting. doi:10.1016/j.molmed.2008.11.004.

Kiguchi, N., Kobayashi, Y., Saika, F., Sakaguchi, H., Maeda, T., and Kishioka, S. (2015). Peripheral interleukin-4 ameliorates inflammatory macrophage-dependent neuropathic pain. 156, 684–693.

Kiguchi, N., Maeda, T., Kobayashi, Y., Fukazawa, Y., and Kishioka, S. (2010). Macrophage inflammatory protein-1 a mediates the development of neuropathic pain following peripheral nerve injury through interleukin-1 β up-regulation. *Pain* 149, 305–315. doi:10.1016/j.pain.2010.02.025.

Kim, C. F., and Moalem-Taylor, G. (2011). Detailed characterization of neuro-immune responses following neuropathic injury in mice. *Brain Res.* 1405, 95–108. doi:10.1016/j.brainres.2011.06.022.

Kim, D., Kim, M. A., Cho, I., Kim, M. S., Lee, S., Jo, E., et al. (2007). A Critical Role of Toll-like Receptor 2 in Nerve Injury-induced Spinal Cord Glial Cell Activation and Pain Hypersensitivity. 282, 14975–14983. doi:10.1074/jbc.M607277200.

Kim, H. K., Park, S. K., Zhou, J., Taglialatela, G., Chung, K., Coggeshall, R. E., et al. (2004). Reactive oxygen species (ROS) play an important role in a rat model of neuropathic pain. 111, 116–124. doi:10.1016/j.pain.2004.06.008.

Kim, S. H., and Chung, J. M. (1992). An experimental model for peripheral neuropathy produced by segmental spinal nerve ligation in the rat. *Pain*.

Kirillova, I., Rausch, V. H., Tode, J., Baron, R., and Jänig, W. (2011). Mechano- and thermosensitivity of injured muscle afferents. 2058–2073. doi:10.1152/jn.00938.2010.

Kobayashi, Y., Kiguchi, N., Fukazawa, Y., Saika, F., Maeda, T., and Kishioka, S. (2015). Macrophage-T Cell Interactions Mediate Neuropathic Pain through the Glucocorticoid-induced Tumor Necrosis Factor Ligand System. 290, 12603–12613. doi:10.1074/jbc.M115.636506.

Kollarik, M., Ru, F., and Brozmanova, M. (2010). Vagal afferent nerves with the properties of nociceptors. *Auton. Neurosci. Basic Clin.* doi:10.1016/j.autneu.2009.08.001.

Koltzenburg, M. (1998). Painful neuropathies. *Curr. Opin. Neurol.* doi:10.1097/00019052-199810000-00014.

Kumar, V., and Sharma, A. (2010). Neutrophils : Cinderella of innate immune system. *Int. Immunopharmacol.* 10, 1325–1334. doi:10.1016/j.intimp.2010.08.012.

Kwan, K. Y., Allchorne, A. J., Vollrath, M. A., Christensen, A. P., Zhang, D., Woolf, C. J., et al. (2006). TRPA1 Contributes to Cold, Mechanical, and Chemical Nociception but Is Not Essential for Hair-Cell Transduction. 1, 277–289. doi:10.1016/j.neuron.2006.03.042.

Laing, R. J., and Dhaka, A. (2016). ThermoTRPs and Pain. doi:10.1177/1073858414567884.

Lakso, M., Pichel, J. G., Gormant, J. R., Sauer, B., Ii, Y. O. O., Lee, E., et al. (1996). Efficient in vivo manipulation of mouse zygote stage genomic sequences at the. 93, 5860–5865.

Larsson, N.-G., Wang, J., Wilhelmsson, H., Oldfors, A., Rustin, P., Lewandoski, M., et al. (1998). Mitochondrial transcription factor A is necessary for mtDNA maintenance and embryogenesis in mice. 18, 231–236.

Latham, J. R., Pathirathna, S., Jagodic, M. M., Choe, W. J., Levin, M. E., Nelson, M. T., et al. (2009). Selective T-Type Calcium Channel Blockade Alleviates Hyperalgesia in ob / ob Mice. 58. doi:10.2337/db08-1763.

Latremoliere, A., and Woolf, C. J. (2009). Central Sensitization: A Generator of Pain Hypersensitivity by Central Neural Plasticity. *J. Pain*. doi:10.1016/j.jpain.2009.06.012.

Leger, T., Grist, J., Acquisto, F. D., Clark, A. K., and Malcangio, M. (2011). Glatiramer acetate attenuates neuropathic allodynia through modulation of adaptive immune cells. *J. Neuroimmunol.* 234, 19–26. doi:10.1016/j.jneuroim.2011.01.005.

Levin, M. E., Jin, J. G., Ji, R., Tong, J., Pomonis, J. D., Lavery, D. J., et al. (2008). Complement activation in the peripheral nervous system following the spinal nerve ligation model of neuropathic pain q. 137, 182–201. doi:10.1016/j.pain.2007.11.005.

Lim, T. K. Y., Rone, M. B., Lee, S., Antel, J. P., and Zhang, J. (2015). Mitochondrial and bioenergetic dysfunction in trauma-induced painful peripheral neuropathy. 1–9. doi:10.1186/s12990-015-0057-7.

Ling, B., Coudor, M., Balayssac, D., and Eschalier, A. (2007). Behavioral and immunohistological assessment of painful neuropathy induced by a single oxaliplatin injection in the rat. 234, 176–184. doi:10.1016/j.tox.2007.02.013.

Liou, J., Liu, F., Ph, D., Mao, C., and Ph, D. (2011). Inflammation Confers Dual Effects on Nociceptive

Processing in Chronic Neuropathic Pain Model.

Liu, Y., Beyer, A., and Aebersold, R. (2016). Review On the Dependency of Cellular Protein Levels on mRNA Abundance. 535–550.

Luis-Rodríguez, D., Martínez-Castelao, A., Górriz, J. L., Álvaro, F. De, and Navarro-González, J. F. (2012). Pathophysiological role and therapeutic implications of inflammation in diabetic nephropathy. 3, 7–18. doi:10.4239/wjd.v3.i1.7.

Macpherson, L. J., Dubin, A. E., Evans, M. J., Marr, F., Schultz, P. G., Cravatt, B. F., et al. (2007). Noxious compounds activate TRPA1 ion channels through covalent modification of cysteines. 445, 541–545. doi:10.1038/nature05544.

Macpherson, L. J., Geierstanger, B. H., Viswanath, V., Bandell, M., Eid, S. R., Hwang, S., et al. (2005). The Pungency of Garlic : Activation of TRPA1 and TRPV1 in Response to Allicin. 15, 929–934. doi:10.1016/j.cub.2005.04.018.

Maguire, M. F., Ravenscroft, A., Beggs, D., and Duffy, J. P. (2006). A questionnaire study investigating the prevalence of the neuropathic component of chronic pain after thoracic surgery. 29, 800–805. doi:10.1016/j.ejcts.2006.02.002.

Mali, P., Esvelt, K. M., and Church, G. M. (2013). Cas9 as a versatile tool for engineering biology. *Nat. Methods*. doi:10.1038/nmeth.2649.

Mapplebeck, J. C. S., Beggs, S., and Salter, M. W. (2016). Sex differences in pain: a tale of two immune cells. 157, 2–6.

Marchand, F., Perretti, M., and Mcmahon, S. B. (2005). Role of the Immune System in Chronic Pain. 6, 521–532. doi:10.1038/nrn1700.

McGaraughty, S., Chu, K. L., Perner, R. J., Didomenico, S., Kort, M. E., and Kym, P. R. (2010). TRPA1 modulation of spontaneous and mechanically evoked firing of spinal neurons in uninjured, osteoarthritic , and inflamed rats. 1–11.

Melzack, R., and Casey, K. L. (1968). Sensory, Motivational, and Central Control Determinants of Pain: A New Conceptual Model.

Melzack, R., and Wall, P. D. (1965). Pain Mechanisms : A New Theory. 150, 971–979.

Meng, J., Wang, J., Steinhoff, M., and Dolly, J. O. (2016). TNF α induces co-trafficking of vesicles to the plasmalemma via mediated fusion. 1–15. doi:10.1038/srep21226.

Meyer, M., Hrabé, M., Angelis, D., Wurst, W., Kühn, R., and Allele, K. O. K. I. (2010). Gene targeting by homologous recombination in mouse zygotes mediated by zinc-finger nucleases. 107, 1–5. doi:10.1073/pnas.1009424107.

Mick, D. U., Dennerlein, S., Wiese, H., Reinhold, R., Pacheu-grau, D., Lorenzi, I., et al. (2012). MITRAC Links Mitochondrial Protein Translocation to Respiratory-Chain Assembly and Translational Regulation. 1.

Micó, J. A., Ardid, D., Berrocoso, E., and Eschalier, A. (2006). Antidepressants and pain. *Trends Pharmacol. Sci.* doi:10.1016/j.tips.2006.05.004.

Milligan, E. D., and Watkins, L. R. (2009). Pathological and protective roles of glia in chronic pain. 10. doi:10.1038/nrn2533.

Minett, M. S., Quick, K., and Wood, J. N. (2011). Behavioral Measures of Pain Thresholds. 1, 383–412. doi:10.1002/9780470942390.mo110116.

Mishra, S. K., Tisel, S. M., Orestes, P., Bhangoo, S. K., and Hoon, M. A. (2011). TRPV1-lineage neurons are required for thermal sensation. 30, 582–593. doi:10.1038/emboj.2010.325.

Moalem, G., and Tracey, D. J. (2006). Immune and inflammatory mechanisms in neuropathic pain. 51. doi:10.1016/j.brainresrev.2005.11.004.

Moalem, G., Xu, K., and Yu, L. (2004). T Lymphocytes play a Role in Neuropathic Pain Follwing Peripheral Nerve Injury in Rats. 129, 767–777. doi:10.1016/j.neuroscience.2004.08.035.

Mogil, J. S., Graham, A. C., Ritchie, J., Hughes, S. F., Austin, J., Schorscher-, A., et al. (2010). Hypolocomotion , asymmetrically directed behaviors (licking , lifting , flinching , and shaking) and dynamic weight bearing (gait) changes are not measures of neuropathic pain in mice. 1–15.

Möller, K. Ä., Kinert, S., Storkson, R., and Berge, O.-G. (2012). Gait Analysis in Rats with Single Joint Inflammation : Influence of Experimental Factors. 7. doi:10.1371/journal.pone.0046129.

Morin, N., Owolabi, S. A., Harty, M. W., Papa, E. F., Jr, T. F. T., Shaw, S. K., et al. (2007). Neutrophils

invade lumbar dorsal root ganglia after chronic constriction injury of the sciatic nerve. 184, 164–171. doi:10.1016/j.jneuroim.2006.12.009.

Mossmann, D., Meisinger, C., and Vögtle, F. (2012). Processing of mitochondrial presequences. *BBA - Gene Regul. Mech.* 1819, 1098–1106. doi:10.1016/j.bbagrm.2011.11.007.

Nagata, K., Duggan, A., Kumar, G., and Garci, J. (2005). Nociceptor and Hair Cell Transducer Properties of TRPA1, a Channel for Pain and Hearing. 25, 4052–4061. doi:10.1523/JNEUROSCI.0013-05.2005.

Narayanan, P., Sondermann, J., Rouwette, T., Karaca, S., Urlaub, H., Gomez-Varela, D., et al. (2016). Native Piezo2 Interactomics Identifies Pericentrin as a Novel Regulator of Piezo2 in Somatosensory Neurons. doi:10.1021/acs.jproteome.6b00235.

Nassini, R., Materazzi, S., Benemei, S., and Geppetti, P. (2014). The TRPA1 channel in inflammatory and Neuropathic pain and migraine. *Rev. Physiol. Biochem. Pharmacol.* doi:10.1007/112_2014_18.

Nathan, C. F. (1987). Secretory Products of Macrophages. 79, 319–326.

Nicholls, D. G. (2006). Simultaneous Monitoring of Ionophore- and Inhibitor-mediated Plasma and Mitochondrial Membrane Potential Changes in Cultured Neurons: doi:10.1074/jbc.M510916200.

Nicholls, D. G., and Budd, S. L. (2000). Mitochondria and Neuronal Survival. 80, 315–360.

Nishida, K., Kuchiiwa, S., Oiso, S., Futagawa, T., Masuda, S., Takeda, Y., et al. (2008). Up-regulation of matrix metalloproteinase-3 in the dorsal root ganglion of rats with paclitaxel-induced neuropathy. doi:10.1111/j.1349-7006.2008.00877.x.

Noack, M., and Miossec, P. (2017). Selected cytokine pathways in rheumatoid arthritis. 365–383. doi:10.1007/s00281-017-0619-z.

Obata, K., Katsura, H., Mizushima, T., Yamanaka, H., Kobayashi, K., Dai, Y., et al. (2005). TRPA1 induced in sensory neurons contributes to cold hyperalgesia after inflammation and nerve injury. 115, 2393–2401. doi:10.1172/JCI25437.They.

Obrosova, I. G., Ilnytska, O., Lyzogubov, V. V, Pavlov, I. A., Mashtalir, N., Nadler, J. L., et al. (2007). Effects of “Healthy” Diet and Aldose Reductase Inhibition. 56. doi:10.2337/db06-1176.DRG.

Old, E. A., Clark, A. K., and Malcangio, M. (2015). The Role of Glia in the Spinal Cord in Neuropathic and Inflammatory Pain. 145–170. doi:10.1007/978-3-662-46450-2.

Osio, M., Muscia, F., Zampini, L., Nascimbene, C., Mailland, E., Cargnel, A., et al. (2006). Acetyl-l-carnitine in the treatment of painful antiretroviral toxic neuropathy in human immunodeficiency virus patients : an open label study. 76, 72–76.

Pagliarini, D. J., Calvo, S. E., Chang, B., Sheth, S. A., Vafai, S. B., Ong, S., et al. (2008). A Mitochondrial Protein Compendium Elucidates Complex I Disease Biology. 112–123. doi:10.1016/j.cell.2008.06.016.

Palmer, M. T., and Weaver, C. T. (2009). Autoimmunity : increasing suspects in the CD4+ T cell lineup. *Nat. Immunol.* 11, 36–40. doi:10.1038/ni.1802.

Parvathy, S. S., and Masocha, W. (2013). Gait analysis of C57BL / 6 mice with complete Freund ’ s adjuvant-induced arthritis using the CatWalk system.

Patapoutian, A., Tate, S., and Woolf, C. J. (2009). Transient receptor potential channels : targeting pain at the source. 8. doi:10.1038/nrd2757.

Pedersen, L. H., Scheel-kru, J., and Blackburn-munro, G. (2007). Amygdala GABA-A receptor involvement in mediating sensory-discriminative and affective-motivational pain responses in a rat model of peripheral nerve injury. 127, 17–26. doi:10.1016/j.pain.2006.06.036.

Perkins, N. M., and Tracey, D. J. (2000). Hyperalgesia due to Nerve Injry: Role of Neutrophils. 101.

Peters, C. M., Jimenez-andrade, J. M., Jonas, B. M., Sevcik, M. A., Koewler, N. J., Ghilardi, J. R., et al. (2007). Intravenous paclitaxel administration in the rat induces a peripheral sensory neuropathy characterized by macrophage infiltration and injury to sensory neurons and their supporting cells. 203, 42–54. doi:10.1016/j.expneurol.2006.07.022.

Petrus, M., Peier, A. M., Bandell, M., Hwang, S. W., Huynh, T., Olney, N., et al. (2007). A role of TRPA1 in mechanical hyperalgesia is revealed by pharmacological inhibition. 8, 1–8. doi:10.1186/1744-8069-3-40.

Piesla, M. J., Leventhal, L., Strassle, B. W., Harrison, J. E., Cummons, T. A., Lu, P., et al. (2009). Abnormal gait , due to inflammation but not nerve injury , reflects enhanced nociception in preclinical pain models. *Brain Res.* 1295, 89–98. doi:10.1016/j.brainres.2009.07.091.

Pinto, M., Pickrell, A. M., and Moraes, C. T. (2012). Regional susceptibilities to mitochondrial dysfunctions in the CNS. 393, 275–281. doi:10.1515/hsz-2011-0236.

Pitzer, C., Kuner, R., and Tappe-theodor, A. (2016a). Voluntary and evoked behavioral correlates in inflammatory pain conditions under different social housing conditions. 1, 1–12.

Pitzer, C., Kuner, R., and Tappe-theodor, A. (2016). Voluntary and evoked behavioral correlates in neuropathic pain states under different social housing conditions. 12, 1–15. doi:10.1177/1744806916656635.

Plun-Favreau, H., Burchell, V. S., Holmström, K. M., Yao, Z., Deas, E., Cain, K., et al. (2012). HtrA2 deficiency causes mitochondrial uncoupling through the F 1F0-ATP synthase and consequent ATP depletion. *Cell Death Dis.* doi:10.1038/cddis.2012.77.

Prato, V., Taberner, F. J., Hockley, J. R. F., Callejo, G., Arcourt, A., Tazir, B., et al. (2017). Functional and Molecular Characterization of Mechanoinsensitive “Silent” Nociceptors. 3102–3115.

Puntel, R. L., Roos, D. H., Lopes, R., and Rocha, J. B. T. (2013). Mitochondrial electron transfer chain complexes inhibition by different organochalcogens. *Toxicol. Vitr.* 27, 59–70. doi:10.1016/j.tiv.2012.10.011.

Raouf, R., Quick, K., and Wood, J. N. (2010). Pain as a channelopathy. 120. doi:10.1172/JCI43158.to.

Reichl, S., Segelcke, D., Keller, V., Jonas, R., Boecker, A., Wenk, M., et al. (2016). Activation of glial glutamate transporter via MAPK p38 prevents enhanced and long-lasting non-evoked resting pain after surgical incision in rats. 105, 607–617.

Reinders, J., Zahedi, P., Pfanner, N., Meisinger, C., and Sickmann, A. (2006). Toward the Complete Yeast Mitochondrial Proteome : Multidimensional Separation Techniques for Mitochondrial Proteomics research articles. 1543–1554.

Ren, K., and Dubner, R. (2010). Interactions between the immune and nervous systems in pain. *Nat. Med.* 16, 1267–1276. doi:10.1038/nm.2234.

Richards, N., and McMahon, S. B. (2013). Targeting novel peripheral mediators for the treatment of chronic pain. 111, 46–51. doi:10.1093/bja/aet216.

Richner, M., Bjerrum, O. J., Nykjaer, A., and Vaegter, C. B. (2011). The Spared Nerve Injury (SNI) Model of Induced Mechanical Allodynia in Mice. 3–5. doi:10.3791/3092.

Rivero, A., Mora, C., Muros, M., and Garc, J. (2009). Pathogenic perspectives for the role of inflammation in diabetic nephropathy. 492, 479–492. doi:10.1042/CS20080394.

Rouwette, T., Sondermann, J., Avenali, L., Gomez-Varela, D., and Schmidt, M. (2016). Standardized Profiling of The Membrane- Enriched Proteome of Mouse Dorsal Root Ganglia (DRG) Provides Novel Insights Into Chronic Pain. 2152–2168. doi:10.1074/mcp.M116.058966.

Salat, K., Moniczewski, A., and Librowski, T. (2013). Transient Receptor Potential Channels - Emerging Novel Drug Targets for the Treatment of Pain. doi:10.2174/09298673113209990107.

Schmidt, M., Dubin, A. E., Petrus, M. J., Earley, T. J., and Patapoutian, A. (2009). Nociceptive Signals Induce Trafficking of TRPA1 to the Plasma Membrane. doi:10.1016/j.neuron.2009.09.030.

Schmidt, O., Pfanner, N., and Meisinger, C. (2010). Mitochondrial protein import: from proteomics to functional mechanisms. *Nat. Publ. Gr.* 11, 655–667. doi:10.1038/nrm2959.

Scholz, J., and Woolf, C. J. (2007). The neuropathic pain triad : neurons, immune cells and glia. 10, 1361–1368. doi:10.1038/nn1992.

Schuh, C. D., Pierre, S., Weigert, A., Weichand, B., Altenrath, K., Schreiber, Y., et al. (2014). Prostacyclin mediates neuropathic pain through interleukin 1β-expressing resident macrophages. *Pain*. doi:10.1016/j.pain.2013.12.006.

Schwanhäusser, B., Busse, D., Li, N., Dittmar, G., Schuchhardt, J., Wolf, J., et al. (2011). Global quantification of mammalian gene expression control. *Nature*. doi:10.1038/nature10098.

Schwartz, E. S., Kim, H. Y., Wang, J., Lee, I., Klann, E., Chung, J. M., et al. (2009). Persistent Pain Is Dependent on Spinal Mitochondrial Antioxidant Levels. 29, 159–168. doi:10.1523/JNEUROSCI.3792-08.2009.

Seltzer, Z., Dubner, R., and Shir, Y. (1990). A novel behavioral model of neuropathic pain disorders

produced in rats by partial sciatic nerve injury. *Pain*. doi:10.1016/0304-3959(90)91074-S.

Sharma, K., Schmitt, S., Bergner, C. G., Tyanova, S., Kannaiyan, N., Manrique-hoyos, N., et al. (2015). Cell type – and brain region – resolved mouse brain proteome. 18. doi:10.1038/nn.4160.

Sheets, P. L., Heers, C., Stoehr, T., and Cummins, T. R. (2008). Differential Block of Sensory Neuronal Voltage-Gated Sodium Channels by Lacosamide [(2 R) -2- (Acetylamino) - N -benzyl-3-. doi:10.1124/jpet.107.133413.

Shishkin, V., Potapenko, E., Kostyuk, E., Girnyk, O., Voitenko, N., and Kostyuk, P. (2002). Role of mitochondria in intracellular calcium signaling in primary and secondary sensory neurones of rats. 32, 121–130. doi:10.1016/S0143-4160(02)00095-7.

Sickmann, A., Reinders, J., Wagner, Y., Joppich, C., Zahedi, R., Meyer, H. E., et al. (2003). The proteome of Saccharomyces cerevisiae mitochondria. *Proc. Natl. Acad. Sci.* doi:10.1073/pnas.2135385100.

Siemens, J., Zhou, S., Piskorowski, R., Nikai, T., Lumpkin, E. A., Basbaum, A. I., et al. (2006). Spider toxins activate the capsaicin receptor to produce inflammatory pain. *Nature*. doi:10.1038/nature05285.

Silva, J. P., Köhler, M., Graff, C., Oldfors, A., Magnuson, M. A., Berggren, P., et al. (2000). Impaired insulin secretion and β -cell loss in tissue-specific knockout mice with mitochondrial diabetes. 26, 336–340.

Simonetti, M., Hagenston, A. M., Vardeh, D., Freitag, H. E., Mauceri, D., Lu, J., et al. (2013). Nuclear Calcium Signaling in Spinal Neurons Drives a Genomic Program Required for Persistent Inflammatory Pain. *Neuron* 77, 43–57. doi:10.1016/j.neuron.2012.10.037.

Smith, F. M., Haskelberg, H., and Tracey, D. J. (2008). Role of Histamine H 3 and H 4 Receptors in Mechanical Hyperalgesia following Peripheral Nerve Injury. 317–325. doi:10.1159/000125048.

Sondermann, J. R., Barry, A. M., Jahn, O., Michel, N., Abdelaziz, R., Gomez-Varela, D., et al. (2018). Vti1b promotes TRPV1 sensitization during inflammatory pain. 00.

Sörensen, L., Ekstrand, M., Silva, J. P., Lindquist, E., Xu, B., Rustin, P., et al. (2001). Late-Onset Corticohippocampal Neurodepletion Attributable to Catastrophic Failure of Oxidative Phosphorylation in MILON Mice Lene So. 21, 8082–8090.

Sorge, R. E., Mapplebeck, J. C. S., Rosen, S., Beggs, S., Taves, S., Alexander, J. K., et al. (2015). Different immune cells mediate mechanical pain hypersensitivity in male and female mice. 18, 3–5. doi:10.1038/nn.4053.

Sousa-Valente, J., Andreou, A. P., Urban, L., and Nagy, I. (2014). Transient receptor potential ion channels in primary sensory neurons as targets for novel analgesics. doi:10.1111/bph.12532.

Steglitz, J., Buscemi, J., and Ferguson, M. J. (2012). The future of pain research, education, and treatment: 8–10. doi:10.1007/s13142-012-0110-2.

Stehling, O., and Lill, R. (2013). The Role of Mitochondria in Cellular Iron – Sulfur Processes , and Diseases.

Stevens, B., Tanner, S., and Fields, R. D. (1998). Control of Myelination by Specific Patterns of Neural Impulses. c, 9303–9311.

Story, G. M., Peier, A. M., Reeve, A. J., Eid, S. R., Mosbacher, J., Hricik, T. R., et al. (2003). ANKTM1, a TRP-like Channel Expressed in Nociceptive Neurons, Is Activated by Cold Temperatures. 112, 819–829.

Streit, W. J. (2002). Microglia as Neuroprotective, Immunocompetent Cells of the CNS. 139, 133–139. doi:10.1002/glia.10154.

Sun, J. H., Yang, B., Donnelly, D. F., Ma, C., and LaMotte, R. H. (2006). MCP-1 Enhances Excitability of Nociceptive Neurons in Chronically Compressed Dorsal Root Ganglia. *J. Neurophysiol.* doi:10.1152/jn.00222.2006.

Ta, L. E., Low, P. A., and Windebank, A. J. (2009). Mice with cisplatin and oxaliplatin-induced painful neuropathy develop distinct early responses to thermal stimuli. 11, 1–11. doi:10.1186/1744-8069-5-9.

Talavera, K., Nilius, B., and Voets, T. (2008). Neuronal TRP channels: thermometers , pathfinders and life-savers. 287–295. doi:10.1016/j.tins.2008.03.002.

Tanga, F. Y., Nutile-mcmenemy, N., and Deleo, J. A. (2005). The CNS role of Toll-like receptor 4 in

innate neuroimmunity and painful neuropathy. 2005.

Taylor-Clark, T. E., McAlexander, M. A., Nassenstein, C., Sheardown, S. A., Wilson, S., Thornton, J., et al. (2008). Relative contributions of TRPA1 and TRPV1 channels in the activation of vagal bronchopulmonary C-fibres by the endogenous autacoid 4-oxononenal. *J. Physiol.* doi:10.1113/jphysiol.2008.153585.

Taylor, A. B., Smith, B. S., Kitada, S., Kojima, K., Miyaura, H., Otwinowski, Z., et al. (2001). Crystal Structures of Mitochondrial Processing Peptidase Reveal the Mode for Specific Cleavage of Import Signal Sequences. 9, 615–625.

Todd, A. J. (2010). Neuronal circuitry for pain processing in the dorsal horn. 11. doi:10.1038/nrn2947.

Tominaga, M., Caterina, M. J., Malmberg, A. B., Rosen, T. A., Gilbert, H., Skinner, K., et al. (1998). The Cloned Capsaicin Receptor Integrates Multiple Pain-Producing Stimuli. 21, 531–543.

Torsney, C., and Macdermott, A. B. (2006). Disinhibition Opens the Gate to Pathological Pain Signaling in Superficial Neurokinin 1 Receptor-Expressing Neurons in Rat Spinal Cord. 26, 1833–1843. doi:10.1523/JNEUROSCI.4584-05.2006.

Trevisani, M., Siemens, J., Materazzi, S., Bautista, D. M., Nassini, R., Campi, B., et al. (2007). 4-Hydroxynonenal, an endogenous aldehyde, causes pain and neurogenic inflammation through activation of the irritant receptor TRPA1. *Proc. Natl. Acad. Sci.* doi:10.1073/pnas.0705923104.

Tsuda, M., Inoue, K., and Salter, M. W. (2005). Neuropathic pain and spinal microglia : a big problem from molecules in 'small' glia. 28. doi:10.1016/j.tins.2004.12.002.

Twillman, R. K. (2007). Mental Disorders in Chronic Pain Patients Mental Disorders. 0288. doi:10.1080/J354v21n04.

Üçeyler, N., and Sommer, C. (2008). Status of Immune Mediators in Painful Neuropathies.

Urban, R., Scherrer, G., Goulding, E. H., Tecott, L. H., and Basbaum, A. I. (2011). Behavioral indices of ongoing pain are largely unchanged in male mice with tissue or nerve injury-induced mechanical hypersensitivity. *Pain* 152, 990–1000. doi:10.1016/j.pain.2010.12.003.

Usoskin, D., Furlan, A., Islam, S., Abdo, H., Lönnerberg, P., Lou, D., et al. (2015). Unbiased classification of sensory neuron types by large-scale single-cell RNA sequencing. 18. doi:10.1038/nn.3881.

Valko, M., Leibfritz, D., Moncol, J., Cronin, M. T. D., Mazur, M., and Telser, J. (2007). Free radicals and antioxidants in normal physiological functions and human disease. 39, 44–84. doi:10.1016/j.biocel.2006.07.001.

Vay, L., Gu, C., and Mcnaughton, P. A. (2012). The thermo-TRP ion channel family: properties and therapeutic implications. doi:10.1111/j.1476-5381.2011.01601.x.

Viader, A., Golden, J. P., Baloh, R. H., Schmidt, R. E., Hunter, D. A., and Milbrandt, J. (2011). Schwann Cell Mitochondrial Metabolism Supports Long-Term Axonal Survival and Peripheral Nerve Function. 31, 10128–10140. doi:10.1523/JNEUROSCI.0884-11.2011.

Vögtle, F. N., Wortelkamp, S., Zahedi, R. P., Becker, D., Leidhold, C., Gevaert, K., et al. (2009). Global Analysis of the Mitochondrial N-Proteome Identifies a Processing Peptidase Critical for Protein Stability. *Cell*. doi:10.1016/j.cell.2009.07.045.

Vrinten, D. H., and Hamers, F. F. T. (2003). 'CatWalk' automated quantitative gait analysis as a novel method to assess mechanical allodynia in the rat; a comparison with von Frey testing. 102, 203–209.

Wang, J., Wilhelmsson, H., Graff, C., Li, H., Oldfors, A., Rustin, P., et al. (1999). Dilated cardiomyopathy and atrioventricular conduction blocks induced by heart-specific inactivation of mitochondrial DNA gene expression. 21, 133–137.

Wang, S., Dai, Y., Fukuoka, T., Yamanaka, H., Kobayashi, K., Obata, K., et al. (2008). Phospholipase C and protein kinase A mediate bradykinin sensitization of TRPA1: a molecular mechanism of inflammatory pain. doi:10.1093/brain/awn060.

Watkins, L. R., and Maier, S. F. (2015). Beyond Neurons: Evidence That Immune and Glial Cells Contribute to Pathological Pain States. *Physiol. Rev.* doi:10.1152/physrev.00011.2002.

Wildgaard, K., Ravn, J., and Kehlet, H. (2009). Chronic post-thoracotomy pain : a critical review of pathogenic mechanisms and strategies for prevention §. 36. doi:10.1016/j.ejcts.2009.02.005.

Willemen, H. L. D. M., Kavelaars, A., Prado, J., and Maas, M. (2018). Identification of FAM173B as a

protein methyltransferase promoting chronic pain. 1–30.

Wittig, I., Braun, H., and Scha, H. (2006). Blue native PAGE. doi:10.1038/nprot.2006.62.

Wittig, I., Karas, M., and Schägger, H. (2007). High Resolution Clear Native Electrophoresis for In-gel Functional Assays and Fluorescence Studies of Membrane Protein Complexes. *Mol. Cell. Proteomics*. doi:10.1074/mcp.M700076-MCP200.

Wong, G. Y., and Gavva, N. R. (2008). Therapeutic potential of vanilloid receptor TRPV1 agonists and antagonists as analgesics : Recent advances and setbacks. *Brain Res. Rev.* 60, 267–277. doi:10.1016/j.brainresrev.2008.12.006.

Wood, J. N. (2006). Ion Channels in Analgesia Research. 329–358.

Woolf, C. J. (1983). Evidence for a central component of post-injury pain hypersensitivity. *Nature*. doi:10.1038/306686a0.

Woolf, C. J. (2007). Central sensitization: uncovering the relation between pain and plasticity. *Anesthesiology*. doi:10.1097/01.anes.0000264769.87038.55.

Woolf, C. J., and Ma, Q. (2007). Nociceptors — Noxious Stimulus Detectors. 353–364. doi:10.1016/j.neuron.2007.07.016.

Woolf, C. J., and Mannion, R. J. (1999). Neuropathic pain: aetiology, symptoms, mechanisms, and management. 353, 1959–1964.

Woolf, C. J., and Salter, M. W. (2000). Neuronal Plasticity: Increasing the Gain in Pain. 288, 1765–1769.

Woolf, C. J., Shortland, P., and Coggeshall, R. E. (1992). Peripheral nerve injury triggers central sprouting of myelinated afferents. *Nature*. doi:10.1038/355075a0.

Wredenberg, A., Wibom, R., Wilhelmsson, H., Graff, C., Wiener, H. H., Burden, S. J., et al. (2002). Increased mitochondrial mass in mitochondrial myopathy mice.

Wu, G., Ringkamp, M., Murinson, B. B., Pogatzki, E. M., Hartke, T. V, Weerahandi, H. M., et al. (2002). Degeneration of Myelinated Efferent Fibers Induces Spontaneous Activity in Uninjured C-Fiber Afferents. 22, 7746–7753.

Xu, Z. Z., Kim, Y. H., Bang, S., Zhang, Y., Berta, T., Wang, F., et al. (2015). Inhibition of mechanical allodynia in neuropathic pain by TLR5-mediated A-fiber blockade. *Nat. Med.* doi:10.1038/nm.3978.

Zelenka, M., Schäfers, M., and Sommer, C. (2005). Intraneural injection of interleukin-1β and tumor necrosis factor-alpha into rat sciatic nerve at physiological doses induces signs of neuropathic pain. *Pain*. doi:10.1016/j.pain.2005.04.018.

Zhang, X., Wu, Z., Hayashi, Y., Okada, R., and Nakanishi, H. (2014). Peripheral Role of Cathepsin S in Th1 Cell-Dependent Transition of Nerve Injury-Induced Acute Pain to a Chronic Pain State. 34, 3013–3022. doi:10.1523/JNEUROSCI.3681-13.2014.

Zhao, X., Li, X., Liu, X., Wang, C., Zhou, D., Ma, Q., et al. (2015). Antinociceptive effects of fisetin against diabetic neuropathic pain in mice : Engagement of antioxidant mechanisms and spinal GABA A receptors. 102, 286–297.

Zhu, X., Cao, S., Zhu, M., Liu, J., Chen, J., and Gao, Y. (2014). Contribution of Chemokine CCL2/CCR2 Signaling in the Dorsal Root Ganglion and Spinal Cord to the Maintenance of Neuropathic Pain in a Rat Model of Lumbar Disc Herniation. *J. Pain* 15, 516–526. doi:10.1016/j.jpain.2014.01.492.

Zuo, Y., Perkins, N. M., Tracey, D. J., and Geczy, C. L. (2003). Inflammation and hyperalgesia induced by nerve injury in the rat : a key role of mast cells. 105, 467–479. doi:10.1016/S0304-3959(03)00261-6.

Zurborg, S., Piszczek, A., Martínez, C., Hublitz, P., Banchaabouchi, M. Al, Moreira, P., et al. (2011). Generation and characterization of an Advillin -Cre driver mouse line. 1–10.

CURRICULUM VITAE

MEIKE HÜTTE

Jüdenstraße 13a, 37073 Göttingen, Germany
Phone: (+49) 176-21650916
E-Mail: meike_huette@gmx.net

Date of Birth: 16/02/1990
Place of Birth: Holzminden, Germany

WORK EXPERIENCE

11/2015 to date

PHD STUDENT
Max Planck Institute of Experimental Medicine, Göttingen, Germany
Department: Somatosensory Signaling and Systems Biology

- Investigation of Molecular Mechanisms of Chronic Pain (Characterization of Novel Proteins Specific for Chronic Pain)
- Writing of Publications (List of Publications Attached)
- Presentation of Research Findings on International Conferences
- Training and Supervision of Students and Technicians
- Tutor for General Sensory Physiology & Somatic Senses

01-04/2015

RESEARCH INTERNSHIP
Nuffield Department of Clinical Neurosciences, Oxford, UK
Department: Neural Injury

- Characterization of Transduction Efficiency and Specificity of a Serotype of Adeno-associated Virus (AAV)

10-12/2014

University Medical Center, Göttingen, Germany
Department: Molecular Psychiatry

- Behavioral Examination of Mouse Models of Alzheimer´s Disease

08-10/2014

University Medical Center, Göttingen, Germany
Department: Neurology

- Investigation of α-Synuclein Aggregation in the A53T Mouse Model

07-08/2014

Schwann Schleiden Research Institute, Göttingen, Germany
Department: Molecular Neurobiology

- Effect Analysis of L-DOPA Treatment on Dopaminergic and Serotoninergic Neurons in *Drosophila melanogaster*

05/2014

Institute of Multiple Sclerosis Research, Göttingen, Germany
Department: Neuroimmunology

- Distribution Study of Inflammatory and Homeostatic T-cells in an EAE (Experimental Autoimmune Encephalomyelitis) Rat Model

04-09/2013 & 01-05/2014

RESEARCH ASSISTANT
Max Planck Institute of Experimental Medicine, Göttingen, Germany
Department: Clinical Neurosciences

- Investigation of EPO Effects on Oligodendrocyte Differentiation

EDUCATION AND TRAINING

11/2015 to date	**DOCTORAL STUDIES** **Max Planck Institute of Experimental Medicine, Göttingen, Germany** **Department: Somatosensory Signaling and Systems Biology** Thesis: „Exploring the Function of a Novel Chronic Pain Player“ (Supervisor: Prof. Dr. Manuela Schmidt) Intended Degree: Dr. rer. nat. (expected June 2019)
10/2013-05/2015	**MASTER'S PROGRAM „DEVELOPMENTAL, NEURAL AND BEHAVIORAL BIOLOGY“** **Georg-August-University Göttingen, Germany** Thesis: „Analysis of Tg4-42 Mice with Regard to Memory Deficits and Gene Expression“ (Supervisor: Prof. Dr. Oliver Wirths, Grade: 1.8) Degree: Master of Science, Overall Grade: 1.8
10/2009-09/2013	**BACHELOR'S PROGRAM „BIOLOGY“** **Georg-August-University Göttingen, Germany** Thesis: „EPO Effects on the Oligodendrocyte Differentiation in the NG2-CreERT2:R26R-td-tomato-mEGFP Mouse Model“ (Supervisor: Prof. Dr. Dr. Hannelore Ehrenreich, Grade: 1.3) Degree: Bachelor of Science, Overall Grade: 2.3
06/2009	**HIGH-SCHOOL DIPLOMA** **Paul-Gerhardt-School, Dassel, Germany**

MEMBERSHIPS AND STIPENDS

11/2015 to date	**Graduate School GGNB** (Göttingen Graduate School for Neurosciences, Biophysics and Molecular Biosciences)
01/2017-01/2018	**GGNB Junior Group Stipend**
09/2018	**GGNB Travel Grant for the Poster** „Mitochondrial Dysfunction in Chronic Pain-New Insights from Uncharacterized Mitochondrial Proteins“ (World Congress on Pain 2018, Boston)
10/2017	**GGNB Travel Grant for the Poster** „Proteomics-ein vielversprechender Weg zur Charakterisierung neuer „Schmerzkandidaten““ (German Pain Congress 2017, Mannheim, Germany)

PERSONAL SKILLS AND QUALIFICATIONS

Languages	German (Mother Tongue), English (Proficient User), Spanish (Basic User)
Computer Skills	Microsoft Office Tools, Graph Pad Prism, Image J

Additional Qualifications GMP Course-Good Manufacturing Practice (18/09/2017-22/09/2017)

Göttingen, April 2019

LIST OF PUBLICATIONS

Original Articles

Mtmr2 and PI(3,5)P2 interdependently control Piezo2-mediated mechanotransduction in peripheral sensory neurons. Narayanan P, **Hütte M**, Kudryasheva G, Francisco T, Lechner S, Rehlfelft F, Gomez-Varela D, Schmidt M. eLife 2018;7:e32346 doi: 10.7554/eLife.32346.

Publication about PhD Project will follow.